Addis Ababa University

College of Technology and Built Environment

School of Electrical and Computer Engineering

Frequency Regulation in Ethiopian Power Grid with Solar PV and Hybrid Energy Storage

By Melat Bogale Ergete

A thesis submitted to the Graduate School of Electrical and Computer Engineering in partial fulfillment of the requirements for the Degree of Master of Science (M.Sc.) in Electrical Engineering (Electrical Power Engineering).

December 12, 2025

Addis Ababa, Ethiopia

Addis Ababa University

College of Technology and Built Environment

School of Electrical and Computer Engineering

Approved by Examining Committee

Dean, school of Graduate Studies	Signature	Date
Advisor		
Amare Assefa		
Internal Examiner		
Dr. Dawit Habtu		
External Examiner		
Mr. Alula Mebratu		

Declaration

I hereby declare that this thesis, entitled *"***Frequency Regulation in Ethiopian Power Grid with Solar PV and Hybrid Energy Storage**,*"* is my original work and has not been submitted previously, in whole or in part, for the award of any degree or diploma at any other institution. Every source of information used has been properly credited.

Name: Melat Bogale

Signature: _____

Place: Addis Ababa University College of Technology and Built Environment School of Electrical and Computer Engineering

Date of submission: _____

This thesis has been submitted for examination with my approval as a university advisor.

Mr. Amare Assefa _____

Advisor's Name Signature

Acknowledgments

First, I want to express my deepest gratitude to **God**. His guidance, strength, and blessings have carried me through every stage of this work. I truly could not have reached this point without His presence in my life.

I am also sincerely grateful to my **advisor Mr. Amare Assefa**. Thank you for your patience, your encouragement, and the countless ways you have supported me throughout this journey. Your guidance did not only help me complete this thesis, but also helped me grow as a person and as a researcher.

To my **family**, my heartfelt thanks. Your love, understanding, and constant support have meant everything to me. You believed in me even on days I doubted myself, and for that, I am forever grateful.

Abstract

The growing use of renewable energy is a central pathway for reducing greenhouse gas emissions and supporting sustainable power system development. Ethiopia's power system, which already relies heavily on hydropower and planning in integrating photovoltaic (PV) generation, is moving toward a renewable-dominated grid. While this transition brings clear environmental and economic benefits, it also introduces new technical challenges. In particular, the replacement of conventional synchronous generators with inverter-based renewable resources has reduced system inertia, making the grid more vulnerable to frequency instability during disturbances and interconnection events.

This research examines frequency control enhancement strategies for the Ethio–Sudan power interconnection, modeled as a two-area power system. The study focuses on improving inertial, primary, and secondary frequency responses under different PV penetration levels and load disturbance scenarios. To address the challenges associated with reduced inertia, a hybrid energy storage system (HESS), combining a supercapacitor and a battery energy storage system, is proposed and installed in the low-inertia area of the interconnected network.

The supercapacitor and battery is designed to respond rapidly to disturbances, providing fast inertial and primary frequency support respectively. This significantly limits the rate of change of frequency (RoCoF) and reduces the depth of the frequency nadir or the peak frequency immediately after a disturbance. The battery energy storage system operates in coordination with the filtered area control error(ACE) method to support secondary frequency control, enabling smooth frequency recovery and reducing steady-state frequency deviations. In addition, a contingency-based sizing approach for the HESS is developed to ensure that operational limits and system frequency performance requirements are satisfied.

The effectiveness of the proposed strategy is demonstrated through detailed MATLAB/Simulink simulations of the Ethio–Sudan interconnected system under sudden load changes and varying levels of PV penetration. Simulation results clearly show that the inclusion of the hybrid energy storage system(HESS) leads to substantial improvements in RoCoF reduction, frequency nadir and peak enhancement, oscillation damping, and settling time when compared to cases without energy

storage. Overall, this study demonstrates that coordinated hybrid energy storage control can effectively compensate for inertia loss in renewable-rich interconnected power systems.

Contents

List of Figures

List of Tables

Acronyms

PV	Photovoltaic
LFC	Load Frequency Control
RES	Renewable Energy Sources
PFR	Primary Frequency Response
IR	Inertial Response
ESS	Energy Storage System
AGC	Automatic Generation Control
RMS	Root Mean Square
SC	Supercapacitor
BESS	Battery Energy Storage System
SESS	Supercapacitor Energy Storage System
HESS	Hybrid Energy Storage System
ACE	Area Control Error
RoCoF	Rate of Change of Frequency
SoC	State of Charge
VDC	Virtual Droop Control
VIC	Virtual Inertia Control
VNIC	Virtual Negative Inertia Control
IFR	Inertial Frequency Regulation

1 Introduction

1.1 Background

As the global energy sector increasingly transitions towards sustainable, low-carbon technologies, solar photovoltaic (PV) systems have emerged as a key component of modern energy solutions. Their rapid adoption has been driven by both environmental imperatives and the significant decline in solar technology costs. Ethiopia, with its abundant hydropower potential, maintains a predominantly hydro-dominated electricity grid, making it one of the few nations that rely heavily on renewable hydropower for energy generation.

However, integrating solar PV a non-synchronous and variable energy source into this hydro centric grid introduces operational challenges, particularly in the domain of frequency regulation. Frequency stability in power systems is a fundamental requirement to ensure reliable and uninterrupted electricity supply. It is achieved through three sequential layers of response: Inertial Response (IR), Primary Frequency Response (PFR), and Secondary Frequency Response (SFR).

Traditionally, hydropower plants support frequency regulation due to their mechanical inertia and fast-acting governor systems. The system inertia provided by large rotating masses inherently resists frequency deviations following disturbances such as sudden load changes or generation losses. However, solar PV systems lack physical inertia, and their growing penetration diminishes the overall system inertia, thus increasing the vulnerability of the grid to rapid frequency deviations. This necessitates the deployment of alternative mechanisms to maintain frequency stability and prevent system collapse.

1.2 Statement of the Problem

The increasing integration of photovoltaic (PV) generation into modern power systems is widely recognized as a key pathway toward reducing greenhouse gas emissions and achieving sustainable energy development. For countries like Ethiopia, this transition is especially important, as the national grid is already dominated by renewable hydropower and is rapidly expanding its PV capacity. While this shift offers substantial environmental and economic advantages, it also

introduces serious operational challenges, particularly in maintaining frequency stability under disturbances.

Traditionally, power system frequency stability has relied on the natural rotational inertia of synchronous generators, such as hydropower units. This inherent inertia slows down frequency changes following sudden load variations or generation outages, allowing sufficient time for governor and secondary control actions to respond. In the Ethiopian power system, hydropower plants have historically played a central role in providing this inertial and primary frequency support. However, the growing replacement of synchronous generators with inverter-based PV systems, which contribute little or no physical inertia, is progressively reducing the overall system inertia.

As a result, the power system becomes more vulnerable to high rates of change of frequency (RoCoF) and deeper frequency nadirs and higher frequency peaks immediately after disturbances. These faster and more severe frequency deviations place significant stress on conventional control mechanisms. Hydropower governors and turbines, although reliable, are constrained by mechanical response limits and ramp-rate restrictions, making them insufficiently fast to counteract sudden power imbalances in a low-inertia environment. If left unaddressed, these limitations increase the risk of under-frequency load shedding (UFLS), reduced power quality, and, in extreme cases, widespread system instability or blackouts.

Despite the growing urgency of this issue, there remains a lack of practical and well-coordinated solutions tailored to renewable-dominated, hydropower-based grids such as Ethiopia's. In particular, there is a need for fast-acting frequency support mechanisms that can complement existing hydropower controls without compromising long-term system operation.

To address this challenge, this research investigates the application of a Hybrid Energy Storage System (HESS) that combines supercapacitors and battery energy storage systems for frequency regulation. Supercapacitors are capable of delivering or absorbing power within milliseconds, making them well suited for arresting rapid frequency changes and limiting RoCoF immediately after a disturbance. Batteries, on the other hand, can provide sustained power support to assist in frequency recovery and secondary control. By coordinating these two technologies, the proposed

HESS aims to bridge the dynamic gap between fast inertial response and longer-term frequency restoration.

This study evaluates the effectiveness of the proposed HESS in enhancing frequency stability in the Ethiopian power grid under varying PV penetration levels and load disturbance scenarios. By focusing on a hydropower-dominated, low-inertia system, the research seeks to provide practical insights into how advanced energy storage solutions can strengthen frequency resilience and support the reliable operation of renewable-rich power systems.

1.3 Objective of the Research

1.3.1 General Objective:

- To investigate and develop an integrated frequency regulation framework utilizing solar PV and a supercapacitor-battery hybrid energy storage system (HESS) to support Inertial Response (IR), Primary Frequency Response (PFR), and Secondary Frequency Response (SFR) in Ethiopia's hydro-dominated power grid.

1.3.2 Specific Objectives:

- To design and size a hybrid energy storage system combining supercapacitors and batteries suitable for multi-timescale frequency support.
- To develop a coordinated control strategy that integrates solar PV, HESS, and hydropower units to provide hierarchical frequency responses.
- To model and simulate the performance of the integrated system under disturbance using realistic Ethiopian grid data.
- To analyze the comparative benefits of the HESS approach over conventional frequency regulation methods in a hydro-dominated grid.

1.4 Significance of the Study

The following is a list of this thesis's contributions:

- A hybrid energy storage system (HESS) utilizing paired energy storage plans is deployed instead of a singular energy storage type. The benefits of several energy storage devices can be combined by the HESS. In order to improve inertial responsiveness, a supercapacitor with a high energy density is employed. It is confirmed that the battery with sufficient power density can support the enhancement in primary frequency control.

- A multi-area interconnected model makes use of HESS. Compared to employing a single area model, research projects founded on the multi-area model are more close to real world and significant.

- A practical control technique is suggested for the HESS, under short-term system contingencies. Through both simulation findings and mathematical techniques, the efficacy of Hybrid energy storage system for improving primary frequency control performance and inertial response is confirmed.

- In addition to the previously described control techniques, a filtered ACE method is employed to enhance the secondary frequency control performance using the battery. Furthermore, the requirement for power system operation requirements is taken into consideration while determining the HESS size.

2 Literature Review

Several approaches have been put forth to effectively control system frequency, particularly in order to reduce the exacerbated frequency fluctuations brought on by greater RES penetration. Load frequency control (LFC), the most widely used technique, may guarantee power system frequency stability following load disturbances. Numerous researchers have examined the LFC issues.

2.1 Energy Storage System

The use of energy storage systems (ESS) has become increasingly necessary in recent years. ESS can often be thought of as an energy buffer that can release stored energy when needed and store redundant energy when power generation surpasses load demand. Additionally, because of its relatively small time constant, ESS can respond to rapid power swings in comparison to traditional devices, making it suitable for a variety of control objectives. For example, ESSs can enable frequency management and peak shaving by offering active power compensation. Furthermore, the original core system structure need not be altered in order to integrate ESSs into power systems.

As a result, using ESSs is yet another sensible way to enhance LFC performance. Table 1. 1 lists common types of ESSs [1]. The choice of ESS type is contingent upon its intended use, as the attributes of various ESS types differ from one another [2].

Energy Storage Systems		
Mechanical	Kinetic	Flywheels
	Gravity	Pumped-Hydro
Electrochemical	Hydrogen	Fuel Cells + Electrolyser
	Batteries	Li-Ion, Lead Acid, NaNiCl, NiCd, NaS, NiMh and so on
	Flow Batteries	PSBr, ZnBr, Vanadium
Electromagnetic	Magnetic	SMES
	Electric	Capacitors
Thermodynamic	Heat	Thermo-Electric
	Pressure	CAES
	Pressure + Heat	Adiabatic-CAES

Table 1 *Typical Types of ESS [1]*

Reference [1] presents that in response to growing challenges posed by the volatility of renewable energy sources (RESs), an integrated strategy for hybrid energy storage systems (HESSs) that bolsters primary frequency regulation (PFR) in regional power grids is proposed. The authors design a control framework that deploys battery energy storage systems (BESS) to absorb high-frequency deviations using virtual inertia and adaptive droop control, while pumped hydroelectric energy storage (PHES) addresses the residual load. A novel self-recovery mechanism restores the BESS's state of charge (SOC) during stable periods, enabling sustained frequency support. Simulated under diverse disturbance conditions using the RT 1000 real-time platform, their model demonstrates enhanced frequency stability and dynamic response capabilities.

Reference [2] presented that as renewable energy sources (RESs) increasingly reshape the dynamics of modern power systems, challenges such as reduced system inertia and volatile frequency/voltage fluctuations have grown more pronounced. To enhance frequency stability in such environments—particularly in the Egyptian Power System (EPS) Magdy et al. (2019) introduce an optimized coordinated control approach integrating Superconducting Magnetic Energy Storage (SMES) into the secondary frequency control framework, namely Load Frequency

Control (LFC). This strategy employs a PI controller finely tuned using the Particle Swarm Optimization (PSO) algorithm to counteract frequency deviations amidst varied system contingencies. The EPS model incorporates nonlinear conventional generation units alongside RESs, including wind and solar power. Simulations conducted using Matlab/Simulink® demonstrate the proposed system's resilience in maintaining frequency stability under high renewable penetration.

Reference [5] presented that to mitigate frequency fluctuations caused by load disturbances in multi-area interconnected power systems, propose a sophisticated sliding mode control strategy that integrates interval observers and disturbance reconstruction. Their approach uses a hybrid energy storage system (HESS) comprising a battery and a supercapacitor to enhance load frequency control (LFC) performance. The interval observers track system state bounds in real time across different areas, enabling accurate reconstruction of load disturbances. This feeds into a tailored sliding mode controller, which effectively manages energy consumption and storage to stabilize grid frequency. Simulation results confirm the strategy's ability to suppress both frequency and tie-line power fluctuations, improving overall system reliability and stability.

Reference [6] presented that to ensure stable electricity supply in remote, islanded communities presents growing technical difficulties because of the variability of renewable energy sources (RESs) and the absence of system inertia from replacing conventional synchronous generators with inverter-based alternatives. Akram, Shah, and Mithulananthan (2019) address this issue by examining a hybrid energy storage system (HESS) composed of battery energy storage and supercapacitors for frequency regulation (FR) in microgrids facing demand and supply uncertainties. Using simulations in MATLAB/Simulink®, the study evaluates how this HESS mitigates frequency instability caused by intermittent solar and wind generation. The results reveal that the combination of fast-response supercapacitors and robust batteries enables effective FR, improving overall system stability in isolated grids.

Reference [7] present a novel control methodology for enhancing the performance and resilience of hybrid power systems composed of diverse generation sources such as wind turbines, solar photovoltaics, diesel engines, fuel cells, and aqua electrolyzers alongside energy storage devices including batteries, flywheels, and ultra-capacitors. The authors introduce a fractional order (FO) fuzzy control scheme, whose parameters are fine-tuned using a particle swarm optimization (PSO)

algorithm enhanced with two chaotic maps. Compared to classical PID and integer-order fuzzy PID controllers, the FO fuzzy controller delivers improved control across both linear and nonlinear system behaviors and demonstrates superior robustness against parameter variations and operational constraints. This robustness is particularly beneficial in hybrid systems where components are intermittently active or operate across varied output levels.

Reference [8] present a state reconstruction-based strategy to enhance the dynamic performance of hybrid wind-storage power plants participating in primary frequency regulation. The study addresses the complexities of coordinating wind generation with energy storage systems particularly in balancing frequency modulation efficiency during fluctuating load conditions. By dynamically evaluating the energy storage system's state of charge (SOC), the proposed framework restructures its frequency support role and computes wind power's active reserve requirements. Both components are then equipped with adaptive virtual inertia controls—SOC-dependent for storage, and kinetic energy-based for wind power. These parallel controls enable rapid, reliable active power support, responsive to frequency disturbance types and real-time system conditions. Simulation results affirm the strategy's effectiveness in maintaining grid stability under load fluctuations.

Reference [9] presents that in response to the increasing integration of renewable energy sources, a frequency control strategy tailored for multi-area hybrid power systems proposed. By leveraging both Load Frequency Control (LFC) and Battery Energy Storage Systems (BESS), the authors introduce a method that decomposes area control error and active power disturbances into low- and high-frequency components. This enables a dual-layered regulation approach: a sliding mode algorithm addresses low-frequency deviations via LFC, while a disturbance observer fine-tunes BESS response for high-frequency disturbances. Notably, this strategy enhances control accuracy and reduces the required battery capacity. Validated through real-time digital simulation, the framework demonstrates improved frequency regulation and operational efficiency.

2.2 Battery – Supercapacitor Hybrid Energy Storage System

Among the most often used energy storage tools in the market is the battery. Electrochemical energy is the form in which the energy is kept. To obtain the required voltage and capacity, a group of many cells can be connected either in series or parallel.

Each cell is made up of one electrolyte and two electrodes, as shown in Fig. 2.1. The electrons move through the external circuit, and the electrolyte can act as a channel of ion exchange between these two electrodes.

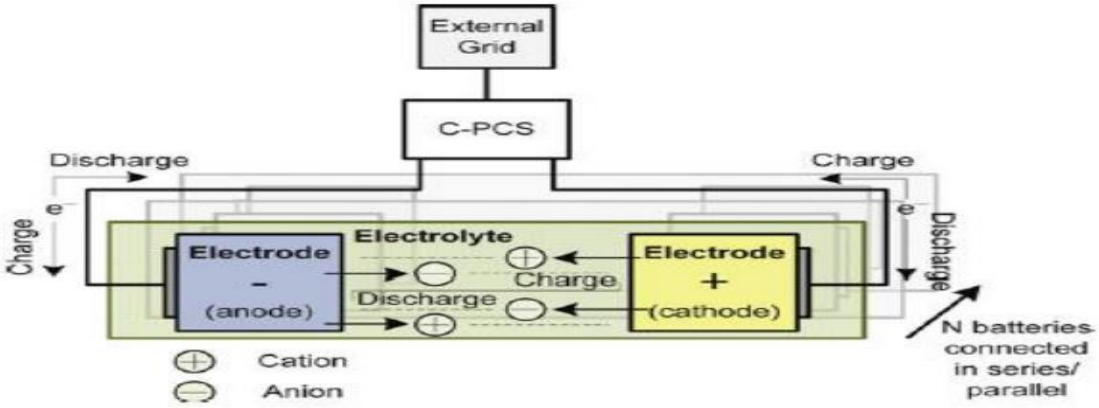

Figure 2.1 *Battery Energy Storage System Operation Theory [10]*

The efficiency of employing a BESS to enhance Load Frequency Control dynamics is demonstrated in [11], [12]. [13] shows that because the BESS can adjust for abrupt changes in load, it is efficient in lowering frequency and tie-power peak deviations. It is also possible to lower the steady-state values of time error and unintentional interchange. In [14], the impacts of BESS are examined while taking governor dead band and generation rate limits into account. By employing area control error (ACE) as the feedback signal the BESS can further enhance LFC. A typical two area interconnected power system and conventional controllers with the BESS are compared qualitatively and quantitatively in [15], demonstrating how the BESS improves system dynamic performance.

Supercapacitors are sometimes referred to as double-layer capacitors or ultracapacitors. Electrochemical cells are the foundation of supercapacitors. Each cell is made up of two electrodes: the porous membrane and the electrolyte, as seen in Fig. 2.2. The contact between two electrodes and the electrolyte surface is where the electrostatic store charge reaction takes place. Due to the two boundaries (electrolyte-negative electrode and positive electrode –electrolyte), this structure can be thought of as two capacitors. Additionally, the supercapacitor stores electrochemical energy, which is proportional to the capacitor and the square of the voltage between the electrochemical cell's terminals. The parallel and series connection of many cells allows the supercapacitor to reach the required voltage and capacity while maintaining a low cell voltage. Supercapacitors have an energy density that is approximately 100 times greater than that of conventional capacitors [16].

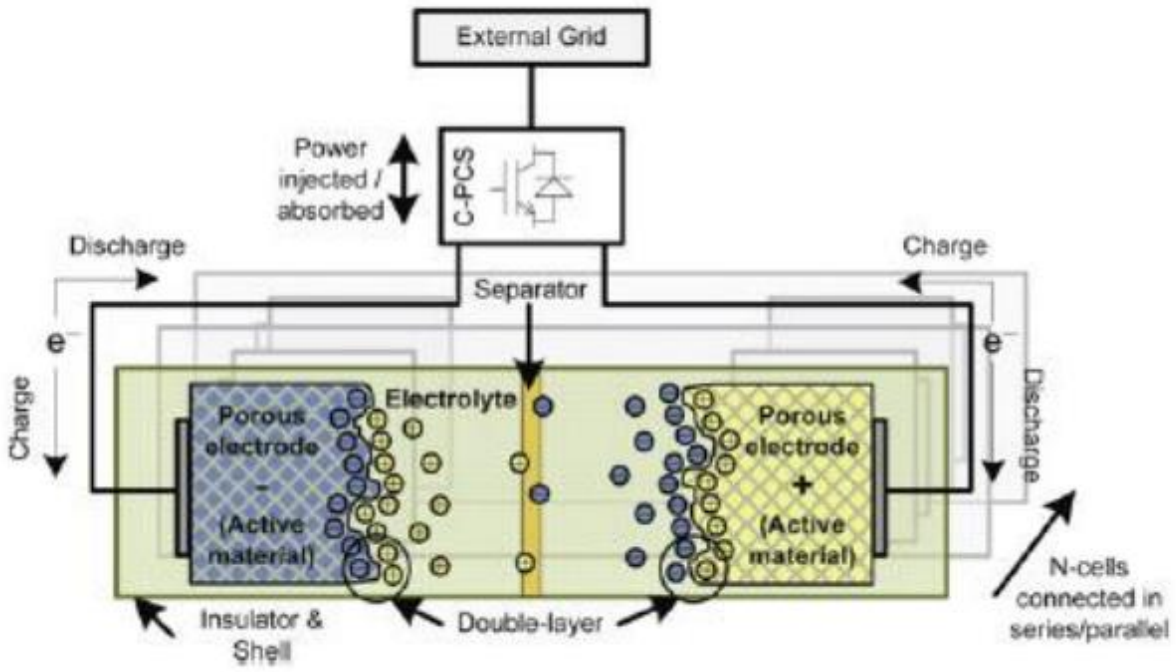

Figure 2.2 *Supercapacitor Energy Storage System Operation Theory [10]*

A Supercapacitor bank controlled by fuzzy-logic for LFC enhancement in an interconnected power system is suggested in [17]. The outcomes of the simulation demonstrate how successful this

approach is. The frequency deviation and tie-line power deviation are shown to significantly decrease when the supercapacitor and GA tuned algorithm are used together, as suggested in [18].

In conclusion, an energy storage system that combines batteries with supercapacitors can significantly enhance the system's dynamic performance. In comparison to a battery, a supercapacitor typically has a much shorter charging and discharging time (less than 1 million hm) [10] and a power density that is approximately ten times greater [16]. However, the energy density of the supercapacitor is very low. These characteristics show that the supercapacitor is proper for short-term, high-density energy discharging or charging scenarios. The Li-ion battery, which has a high energy density of around 170–300 Wh/l, is the most widely used battery [17]. Because of this feature, batteries are often utilized in scenarios where a long-term power exchange is required at a relatively low intensity.

3 Mathematical Description and Fundamental Principles

This topic presents the fundamentals of control of frequency, such as the association between frequency control and active power, the formation of a frequency control model and the different control stages. The application of the conventional Load Frequency Control approach in a power system model that is interconnected has been examined after the introduction of the basic principles of Automatic Generation Control (AGC) and primary frequency control in a power system that is isolated.

3.1 Frequency and Active Power Control

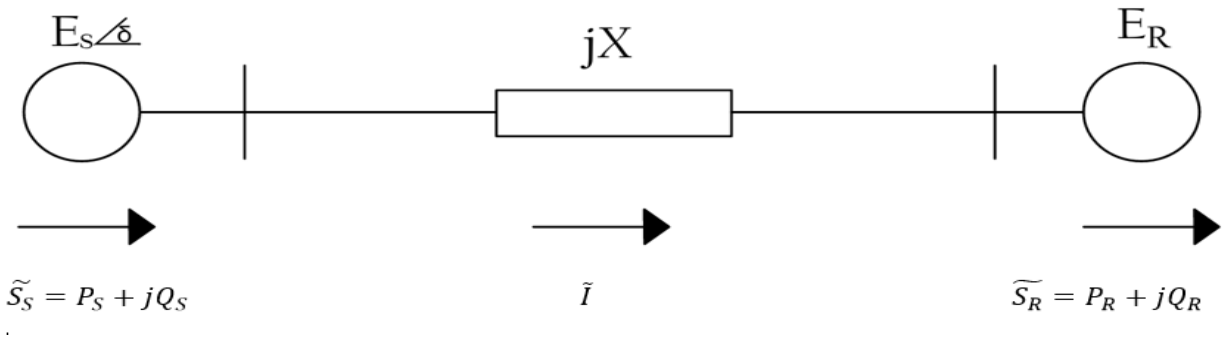

Figure 3.1 *Power System Equivalent Diagram*

Figure. 3.1 shows an equivalent schematic of two distinct power system regions connected by a transmission line. The impedance (Z) in this context is regarded as purely inductive, since it is mostly inductive. Consequently, the following formula can be used to determine the complex power ($\tilde{S}_R$) expected at the receiving end:

$$\tilde{S}_R = P_R + jQ_R = \widetilde{E_R}\tilde{I}^* = E_R[\frac{E_S Cos\delta + jE_S\, Sin\delta - E_R}{jX}]^* \qquad (3.1)$$

Thus, the subsequent equations can be derived:

$$P_R = \frac{E_S E_R \, Sin\delta}{X} \qquad (3.2)$$

$$Q_R = \frac{E_S E_R Cos\delta - E_R^2}{X} \qquad (3.3)$$

Where E_R and E_S are the root-mean-square (RMS) voltage values at the receiving and sending ends respectively, δ is the voltage angle difference between the transmitting and receiving ends. One can compute the transmitted active and reactive power as follows:

$$P_S = \frac{E_S E_R Sin\delta}{X} \qquad (3.4)$$

$$Q_S = \frac{E_S^2 - E_S E_R Cos\delta}{X} \qquad (3.5)$$

According to equations (3.2) – (3.5), the reactive power is controlled by the voltage magnitude difference, whereas by altering the angle difference δ, the transferred active power can be controlled.

$$\Delta\delta = 2\pi \int \Delta f dt \qquad (3.6)$$

Furthermore, the frequency can be changed to regulate the active power since the integration of frequency (Δf) equals the angle difference ($\Delta\delta$). The control issue of active and reactive power can be examined independently since they will affect frequency and voltage, respectively. Since the goal of this study is to improve frequency performance, the regulatory model only takes active power into account.

3.2 Various Frequency Control Stages

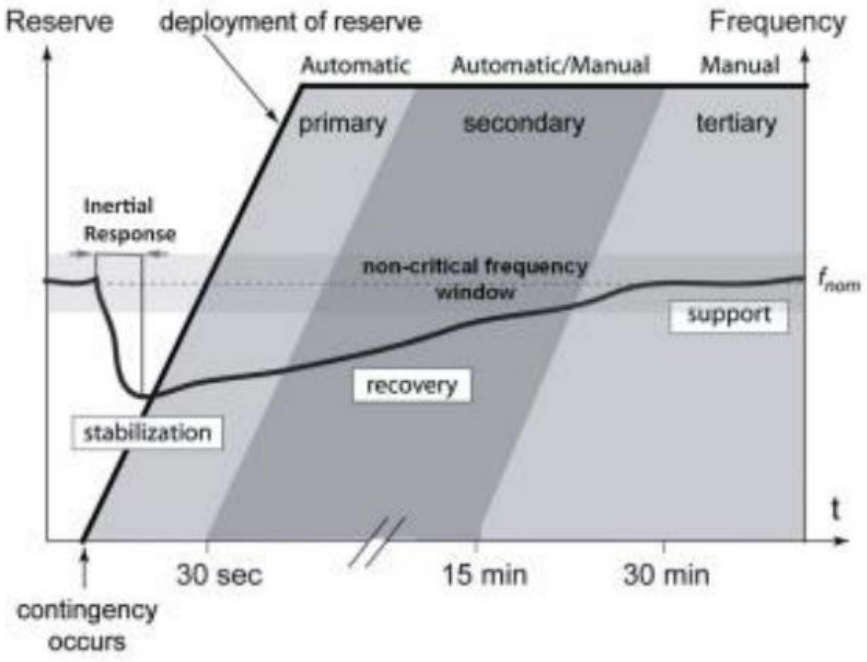

Figure 3.2 *Stages of Frequency Control [19]*

Fig. 3.2 illustrates the frequency control phases following a system disturbance. In order to withstand the frequency shift, the turbines will release their stored kinetic energy during the first stage, known as the inertial reaction (IR). The inertia constant H is the index that can characterize such an effect. With the help of the speed governors of the generating units, the frequency variation is reduced to a steady-state value during the second step, known as the Primary frequency response (PFR). The associated disturbance and system properties determine the frequency deviation. The frequency deviation is then eliminated to zero by secondary control, and all generations are rescheduled by tertiary control.

3.3 Isolated Power System Frequency Control

3.3.1 Key Components of the Frequency Regulation Model

A. Dynamic system model

It is assumed that there is strong enough interconnection between the power system and all of the control components to allow for a single frequency to be used for the analysis. Assuming this, the difference between the power generation ΔP_G and the load variation ΔP_L can be used to represent the instantaneous power disturbance.

As mentioned in [21][20], the following strategies will be used to lessen this power disturbance:

1. By converting the excess power into kinetic energy (E_k), which is stored in reserve in the system's spinning mass:

$$\frac{\mathrm{d}}{\mathrm{dt}}E_k = \frac{\mathrm{d}}{\mathrm{dt}}\left[E_K^*\left(\frac{\mathrm{f}}{f^*}\right)^2\right] \cong \frac{\mathrm{d}}{\mathrm{dt}}\left[E_K^*\left(1+2\frac{\Delta \mathrm{f}}{f^*}\right)\right] \cong 2\frac{E_K^*}{f^*}\frac{\mathrm{d}}{\mathrm{dt}}(\Delta f) \qquad (3.7)$$

2. By the load consumptions that rely on frequency:
   When D is the load-damping constant, all load speeds or frequencies will rise by
   $D \triangleq \partial PD/\partial f$ MW/Hz.
3. By transferring the excess power to a neighboring system that is connected, where ΔP_{tie} is the total amount of power that is transferred out of this region.

The following equation can be obtained from 1-3:

$$\Delta P_G - \Delta P_L = 2\frac{E_K^*}{f^*}\frac{\mathrm{d}}{\mathrm{dt}}(\Delta f) + D\Delta f + \Delta P_{tie} \qquad (3.8)$$

Both side of the equation can then be divided by the nominal power (S_b) to normalize (3.8):

$$\Delta P_G - \Delta P_L = 2\frac{\mathrm{H}}{f^*}\frac{\mathrm{d}}{\mathrm{dt}}(\Delta f) + D\Delta f + \Delta P_{tie} \qquad (3.9)$$

where $H = E^*_k / S_b$ is the inertia constant H.

Equation (3.9) is transformed using Laplace transforms into:

$$[\Delta P_G(s) - \Delta P_L(s) - \Delta P_{tie}(s)] \frac{1}{2\mathrm{Hs+D}} = \Delta F(s) \qquad (3.10)$$

Where M = 2H, (3.10) can be expressed as:

$$[\Delta P_G(s) - \Delta P_L(s) - \Delta P_{tie}(s)] \frac{1}{\mathrm{Ms+D}} = \Delta F(s) \qquad (3.11)$$

Thus, the system's transfer function can be described as follows:

$$G(S) = \frac{1}{\mathrm{Ms+D}} \qquad (3.12)$$

The frequency regulation is the main focus of this research, and the contributions of each generator are combined. The transmission line and inter-machine effects are not taken into account in this research to prevent needless complexity.

In (3.12), D stands for the overall power system damping ratio. Furthermore, the weighted average value of the inertia of each generator is used to compute the overall power system inertia, or H_{sys}.

$$H_{sys} = \frac{\sum_{i=1}^{n} H_i S_i}{\sum_{i=1}^{n} S_i} \qquad (3.13)$$

where S_i is the rated power generator i and H_i is the inertia constant generator i.

The number of generators and their individual power contributions to the grid determine how the system inertia constant, or H_{sys}, varies during the day. As PV penetration increases, system inertia fluctuates more, especially during the day when PV penetration is at its highest during peak sun hours. The H_{sys} at any given moment can be linearized for simplicity's sake [21].

$$H_{sys} = H_0(1-\propto) \qquad (3.14)$$

where α is the degree of PV penetration, which ranges from 0 to 1, and H_o is the system's inertia constant when there is no PV penetration at that moment.

B. Speed governor with droop control model

The turbine, controller, and valve/gate typically make up a synchronous generator. There will be an error signal produced and sent proportionately to the valve or gate if there is a difference between the reference and actual speeds. The turbine's output power will then be altered by adjusting the valve/gate position until the error signal is removed. It is possible to return the system frequency to the set point. However, when two or more generators are linked, the governors cannot be used. All of the generators will experience speed control issues if their reference speeds are not set to the same value. The well-known droop control, whose control diagram is displayed in Fig. 3.3 [40] [22], has been widely used to address this problem by adjusting the rotation speed in accordance with the delivered power.

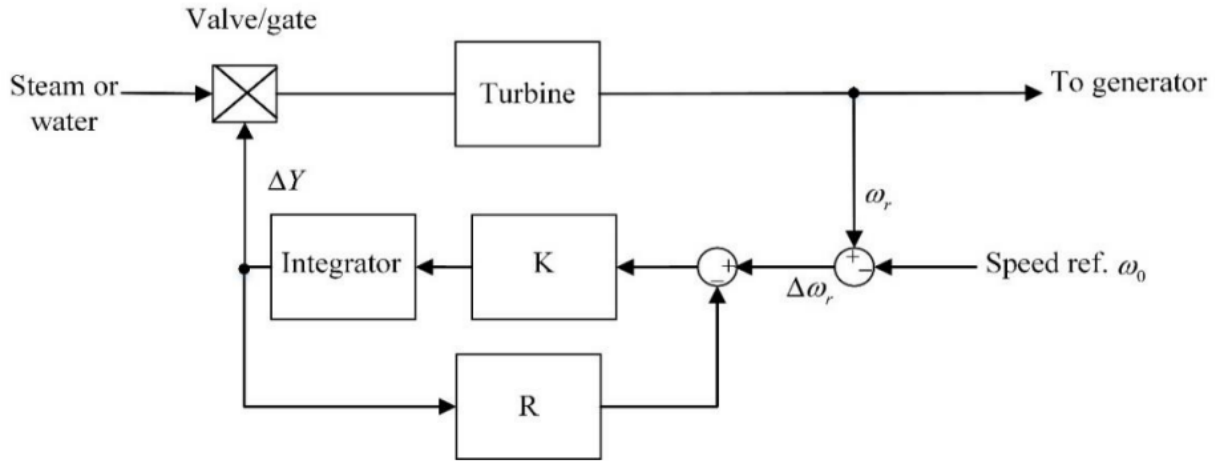

(a) Governor With Steady-State Feedback Control

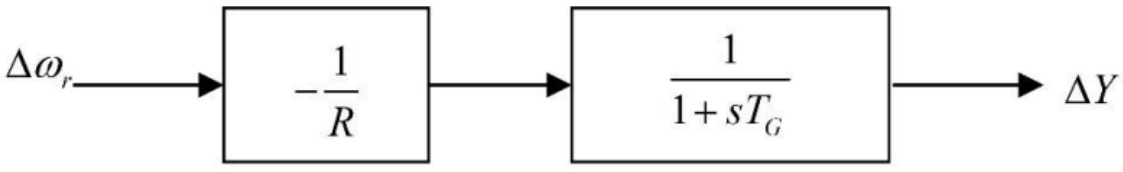

$$T_G = \frac{1}{KR}$$

(b) Simplified Block Diagram

Figure 3.3 *Block Structure With Steady-State Control Loop [22]*

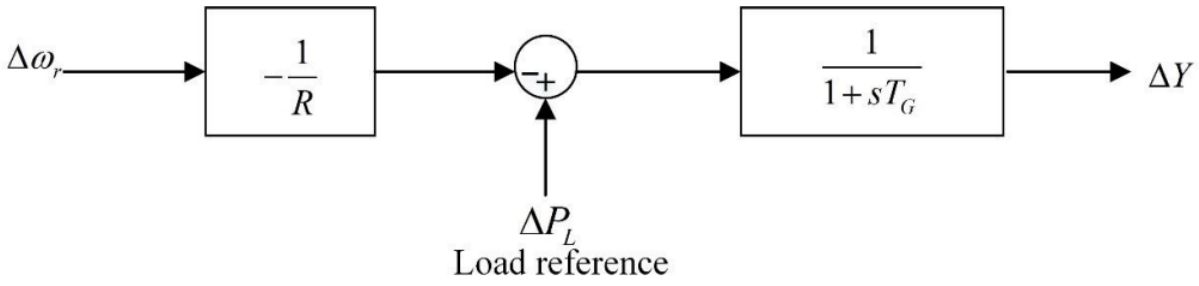

Figure 3.4 *Generation Control's Simplified Block Structure*

As was indicated in the preceding section, altering the generator's output power can alter the relationship between the load and generator speed. This can be accomplished by using the technique, which provides a load reference, as illustrated in Fig. 3. 4.

In reality, when two or more generators work together to supply power to the system, the speed droop coefficient which is impacted by the load reference determines each generator's output power change value.

3.3.2. Primary Frequency Control

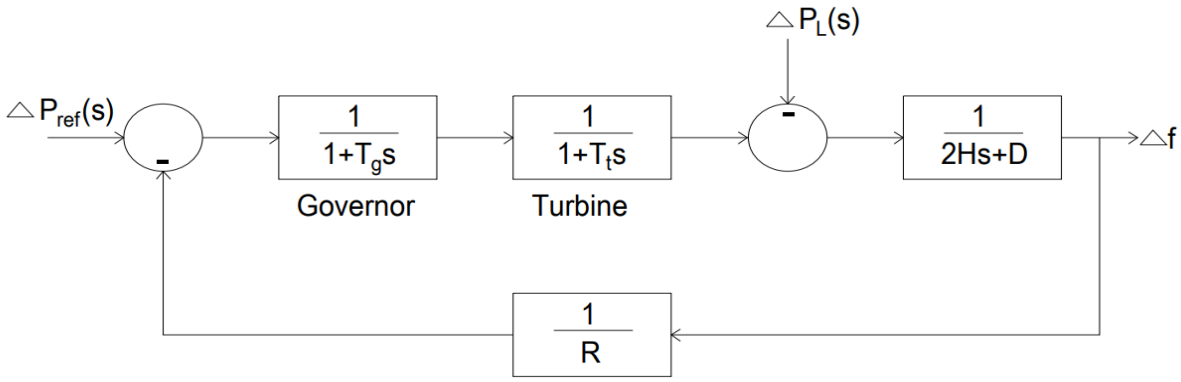

Figure 3.5 *Droop Control's Basic Diagram [41].*

Fig. 3.5 depicts the fundamental primary frequency control model, sometimes referred to as droop control. The dynamic system model, the turbine model, and the speed governor with droop control make up the entire model.

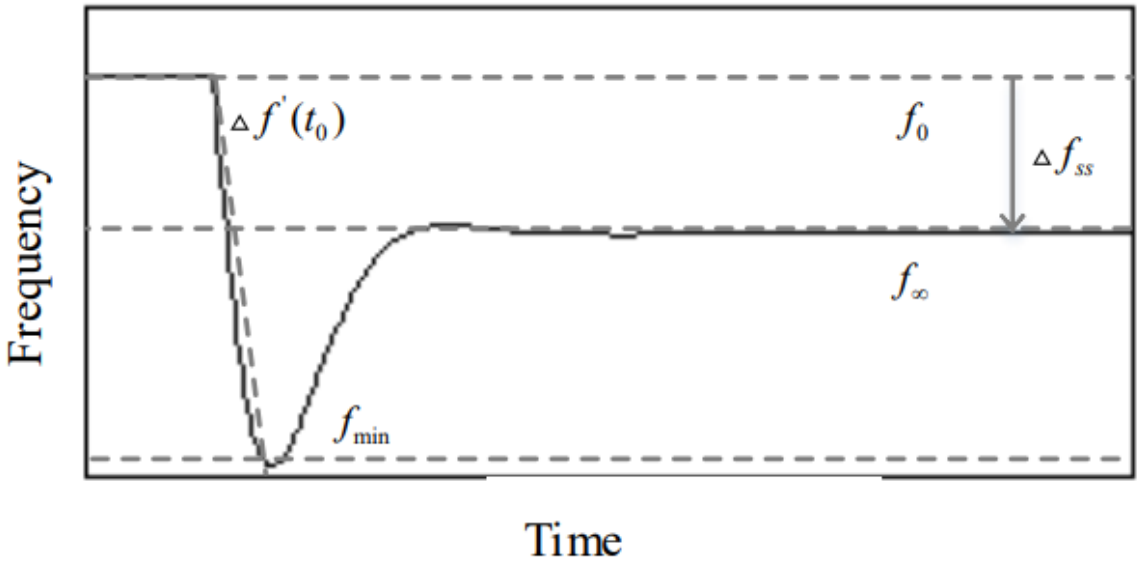

Figure 3.6 *Droop Control's Typical Frequency Response*

Fig. 3.6 shows an isolated power system's normal frequency response and controlled only by droop. Since some rotational energy has been used to correct for the power imbalance, the system frequency will decrease if there is a disturbance brought on by the imbalanced power. The rate of change of frequency (RoCoF) at t_0 can be written as follows [23], assuming that the system stays stable following such a disturbance:

$$\frac{d(\Delta f)}{dt}(t_0) = f_0 \frac{P_G(t_0) - P_L(t_0)}{2E_{Keq}} = f_0 \frac{\Delta P^{pu}(t)}{2H_{eq}} = f_0 \frac{\Delta P^{pu}(t)}{M_{eq}} \qquad (3.15)$$

where $P_L(t_0)$ is the load demand and $P_G(t_0)$ is the power generation. At the frequency setpoint f_0, E_{keq} is the kinetic energy contained in the generator's rotating mass.

Primary frequency control is the second phase of frequency regulation. By modifying the speed governor, all of the generators within that area will cooperate.

The following equation can be used to characterize such a process:

$$\frac{\Delta P}{S_b} = -\frac{1}{R}\frac{\Delta f(t)}{f_0} \qquad (3.16)$$

where the power change in this region is denoted by ΔP. The permanent droop is denoted by R.

After a while, the frequency will decrease to the nadir f_{min}. Numerous factors, including loads, dynamic response characteristics of the generating units, system inertia and power variation etc., might affect the frequency nadir, claims [40]. Figure 3. 7 displays the system block used for frequency control analysis. The nth generating unit is denoted by ΔP_{mn}.

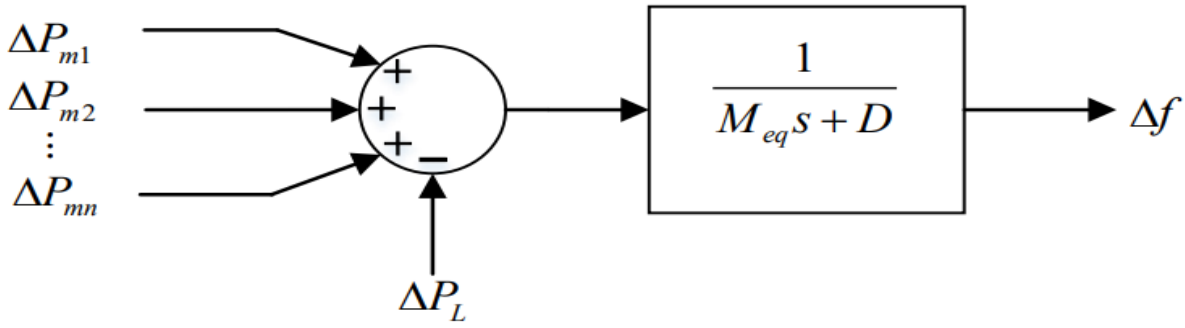

Figure 3.7 *System Block Diagram for Investigation Of LFC*

However, it is expected that after this disturbance, the system is stable, meaning that the frequency regulation requirements can be met by the primary frequency control. Depending on the power imbalance and system parameters, the frequency can be tuned to a constant value f_∞ in the steady state.

$$\Delta f_\infty = \frac{\Delta P}{\left(\frac{1}{R_1}+\frac{1}{R_2}+\cdots+\frac{1}{R_n}\right)+D} = \frac{\Delta P}{\frac{1}{R_{eq}}+D} \qquad (3.17)$$

$$R_{eq} = \frac{1}{\left(\frac{1}{R_1}+\frac{1}{R_2}+\cdots+\frac{1}{R_n}\right)} \qquad (3.18)$$

where R_{eq} stands for the total impact of the generating units' droop constants. The load-damping ratio, or D can be thought of as each loads frequency characteristic.

For additional regulation, secondary frequency control or the automatic generation control (AGC) or which can remove the frequency variation brought on by primary frequency response is also incorporated into the real power system.

3.3.3. Fundamental AGC

To remove the frequency error in AGC, a proportional integral (PI) controller is used. The response speed can be increased when there is a frequency error by using the proportional controller to generate an output that is proportionate to the original signal, e(t). Equation (3.19) is used to express such a relationship. It should be noted that proper tuning of the proportional gain is required. While a small proportional gain could impair dynamic performance, a big proportional gain could cause system instability.

$$P_{out} = K_p * e(t) \qquad (3.19)$$

The integral controller will keep operating until the error signal is removed as long as it is not 0. The relationship between the integral controller's input and output is explained by equation (3.20).

$$I_{out} = K_i \int_0^t e(\tau) d\tau \qquad (3.20)$$

AGC control typically consists of two components. The turbine's speed governor provides the PFR, which is the first component. The second component, the integral controller, is utilized to remove the steady-state inaccuracy and enhance the system's dynamic response. Fig. 3. 8 displays the AGC control simulation model.

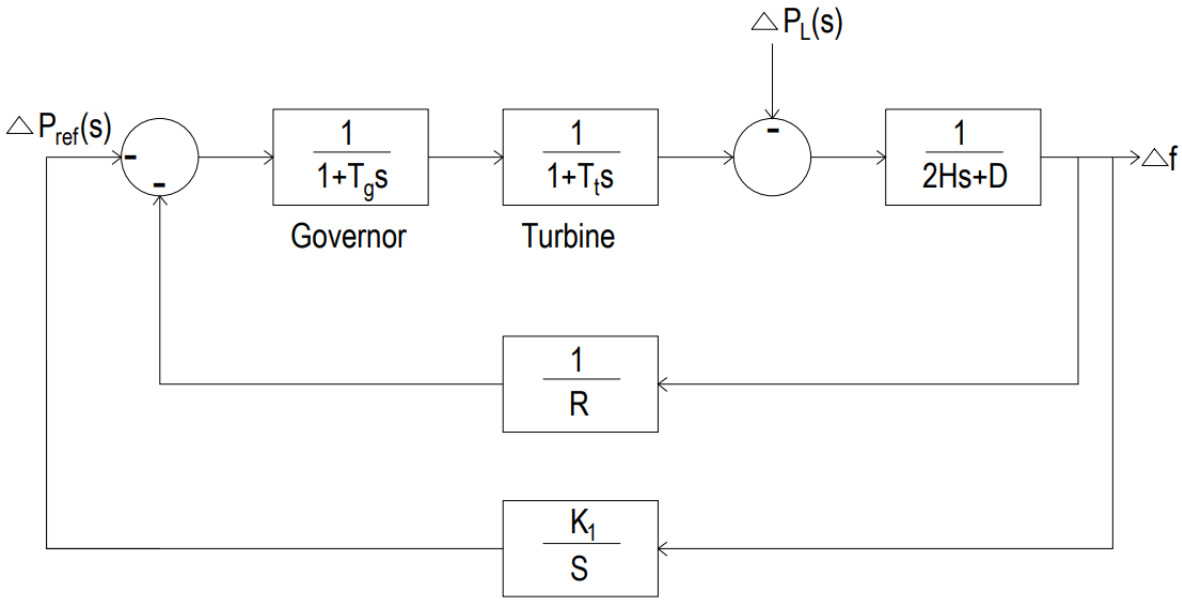

Figure 3.8 *AGC Control's Simulation Model [41].*

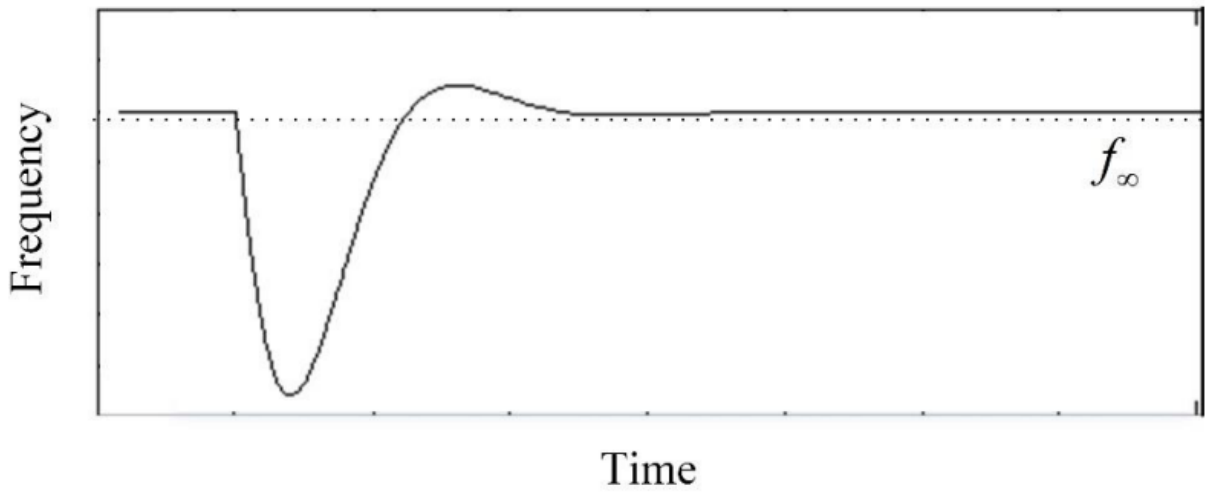

Figure 3.9 *AGC Control's Frequency Response*

Only a portion of the generating units in this power system are able to give both secondary control and droop control at the same time; the remaining units can only do droop control. Compared to the widely used model, where all of the generators can provide both supplementary control and droop control, this model is more realistic [24]. The elimination of steady-state error is evident

from the frequency response of AGC control, which is essential for system performance and stability.

3.4 Conventional LFC in Multi – Area Power System

The tie-line bias control method is the most often utilized load frequency control technique for multi-area interconnected power systems. This method's block diagram can be found in Fig. 3. 10 [25]. Tie-line bias control seeks to maintain tie-line power within a predetermined range and restrict frequency deviation within an acceptable range. Power changes or load disturbances in the system can be tracked by a well-designed LFC model. In addition to enhancing the system's dynamic response and stability, this control technique can raise the standard of electricity.

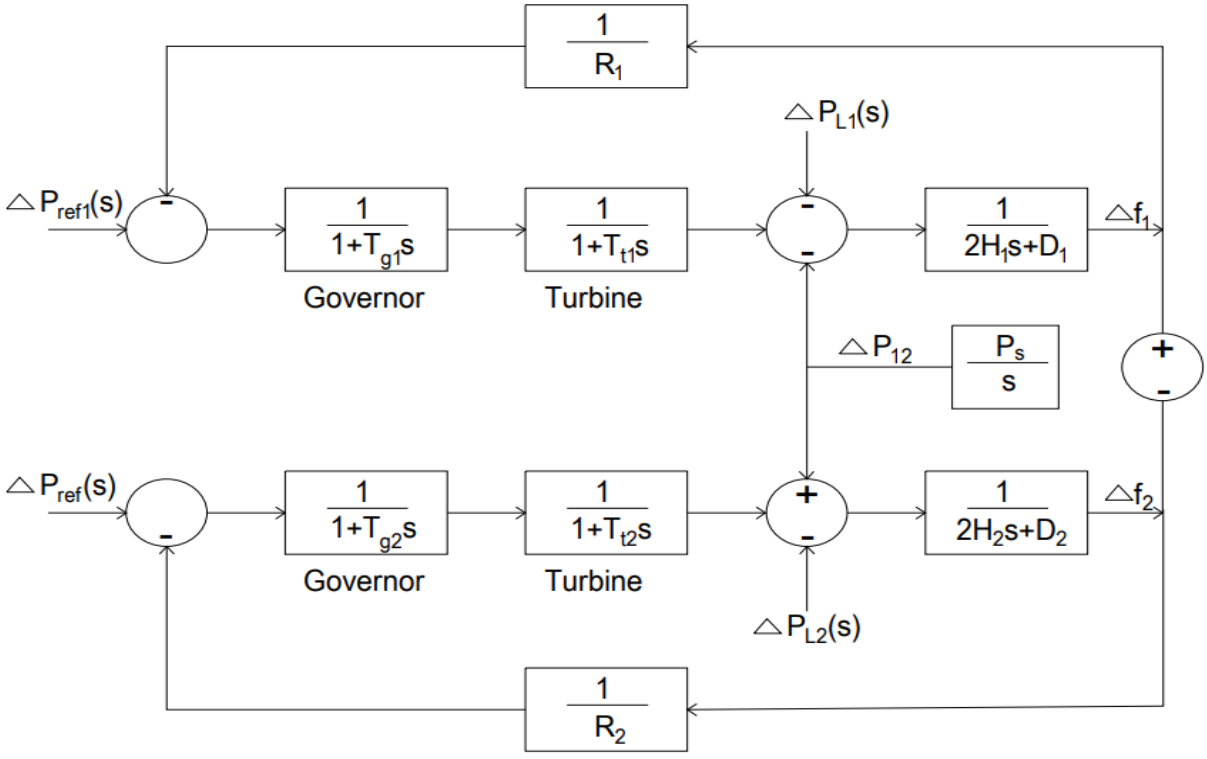

Figure 3.10 *Multi –Area Power System's LFC Block Diagram [41].*

Both bias and droop control are used in this multi-area system to accomplish LFC. The speed governor of the generating units is used to achieve droop control. The two goals of interconnected power systems for which bias control is suggested are as follows:

1. Following this control procedure, the frequency deviation should reach zero.
2. It is important to keep the power transferred across the tie-line constant;

Area control error (ACE_i, i=1, 2…n), which is the control signal of the bias control, is computed as follows:

$$ACE_i = B_i \Delta f_i + \Delta P_{tie} \qquad (3.21)$$

where B_i is the corresponding area's bias factor. The frequency deviation is represented by Δf_i, and the power exchange across the tie-line is represented by $\Delta P_{tie,\,i}$.

This error signal is then eliminated using an integral controller with a proportional gain, K_i. Equation (3.21) indicates that ACE_i can only become zero when both Δf_i and $\Delta P_{tie,i}$ equal zero. This results in the accomplishment of the two control goals previously stated.

In addition, choosing K_i can enhance the dynamic response of the system. The bias factor selection B_i can affect system performance as well. It must be used to lessen the impact of disturbances inside its own area. For instance, if B_i is selected incorrectly, a load disturbance in area 1 will result in control activities in area 2, however the area 2 controllers will respond by attempting to remove this change. The system control scheme deteriorates as a result of these acts.

3.4.1 The Tie-line Model

Tie-lines are used to connect several areas in multi-area power networks. The existence of power exchange between various regions is the primary distinction among the multi-area model and one area model.

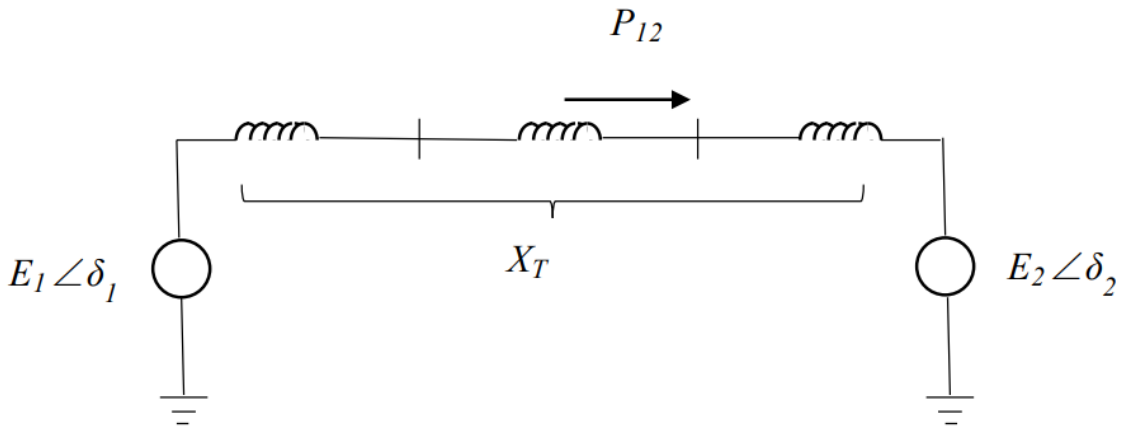

Figure 3.11 *Power Exchange Between Two Terminals*

The flow of power among the two interconnected areas is as follows, derived from Fig. 3.11 and the analysis in [26]:

$$P_{12} = \frac{E_1 E_2}{X_T} Sin(\delta_1 - \delta_2) \qquad (3.22)$$

where the terminal voltages are denoted by E_1 and E_2. X_T is the line's reactance, while δ_1 and δ_2 are the voltage angles.

It is impossible to maintain the equilibrium between generation and demand when the load disturbance happens. Consequently, the initial value δ_{i0} (i=1, 2) will be subject to a voltage phase angle difference $\Delta\delta_i$ (i=1, 2). The power exchange value ΔP_{12} variation can be calculated by:

$$\Delta P_{12} = \frac{E_1 E_2}{X_T} Cos(\delta_{10} - \delta_{20})(\Delta\delta_1 - \Delta\delta_2) \qquad (3.23)$$

Δf_i (i=1, 2) and $\Delta\delta_i$ (i=1, 2) are related in the following way:

$$\Delta\delta_i = 2\pi \int \Delta f_i dt \qquad (3.24)$$

Equations (3.23) and (3.24), when combined, yield the following equation:

$$\Delta P_{12} = 2\pi T_{12}(\int \Delta f_1 dt - \int \Delta f_2 dt) \qquad (3.25)$$

in which,

$$T_{12} = \frac{E_1 E_2}{X_T} Cos(\delta_{10} - \delta_{20}) \qquad (3.26)$$

The power flow computation can determine these two regions' electrical connection, which is represented by T_{12}. For power system planning and optimization, which often takes place prior to the simulation processes, power flow calculations are frequently utilized. Nonetheless, this research's primary goal is to observe and enhance an interconnected power system model's frequency response performance. Consequently, an equal value T_{12} = 0.05 is employed for simulation in accordance with [8,27,33].

3.4.2 Frequency Bias Control Factor

The frequency deviation Δf following a load disturbance ΔP_{L1} in an interconnected power system model with just droop control must meet the following requirements [24]:

$$\Delta f \left(\frac{1}{R_1} + D_1\right) = -\Delta P_{12} - \Delta p_{L1} \qquad (3.27)$$

$$\Delta f \left(\frac{1}{R_2} + D_2\right) = \Delta P_{12} \qquad (3.28)$$

The steady-state frequency deviation can therefore be computed as follows:

$$\Delta f = \frac{-\Delta p_{L1}}{\left(\frac{1}{R_1}+D_1\right)+\left(\frac{1}{R_2}+D_2\right)} = \frac{-\Delta p_{L1}}{\beta_1+\beta_2} \qquad (3.29)$$

where the composite frequency response characteristics are represented by β_1 and β_2.

The following equation represents the power exchange between these two areas:

$$\Delta p_{12} = \frac{-\Delta p_{L1}\left(\frac{1}{R_2}+D_2\right)}{\left(\frac{1}{R_1}+D_1\right)+\left(\frac{1}{R_2}+D_2\right)} = \frac{-\Delta p_{L1}\beta_2}{\beta_1+\beta_2} \quad (3.30)$$

Tie-line bias control is used to remove the frequency deviation. Area control error (ACE) is the name of the control signal. Area 1's error signal in the event of a load disruption is:

$$ACE_1 = \Delta P_{12} + B_1\Delta f \quad (3.31)$$

Similarly, for area 2,

$$ACE_2 = -\Delta P_{12} + B_2\Delta f \quad (3.32)$$

where the bias factors are represented by B_1 and B_2.

The performance of secondary control greatly depends on the value of ACE. Equations (3.29) and (3.30) indicate that the relevant frequency response characteristic β has the best bias factor value.

Given that the ACE signal can be set to 0 using the integral controller in supplementary control, it can be inferred from [19], [30], [27]-[29] that the steady-state has little influence on the choice of the bias factor. Using the subsequent formula:

$$ACE_1 = A_1\Delta P_{12} + B_1\Delta f \quad (3.33)$$

For this equation to be proved, ΔP_{12} and Δf must both be zero for any $A_1 \neq 0$ and $B_1 \neq 0$. In the event that area 1 experiences a load disturbance, the droop control will reduce the frequency deviation. The secondary control which is triggered after the primary control then starts to exertion to remove this deviance. The bias factors' values have an impact on this stage's dynamic performance. This issue is demonstrated using many sets of B_1 and B_2 values.

For these two areas, it is expected that all other parameters and conditions are the same.

1) The following equations can be obtained if the parameters are set as $B_1 = \beta_1$ and $B_2 = \beta_2$:

$$ACE_1 = \Delta P_{12} + B_1 \Delta f_R = \frac{-\Delta P_{L1}\beta_2}{\beta_1+\beta_2} + \frac{-\Delta P_{L1}\beta_1}{\beta_1+\beta_2} = -\Delta P_{L1} \qquad (3.34)$$

And

$$ACE_2 = -\Delta P_{12} + \beta_2 \Delta f_R = \frac{\Delta P_{L1}\beta_2}{\beta_1+\beta_2} + \frac{-\Delta P_{L1}\beta_2}{\beta_1+\beta_2} = 0 \qquad (3.35)$$

This disruption is not visible for the analogous control in the second area, and it is suggested that only region 1's supplementary control would react to this variation. only region 1's supplemental control.

2) ACE_1 and ACE_2 become: if the parameters $B_1 = 2\beta_1$ and $B_2 = \beta_2$ are selected.

$$ACE_1 = \Delta P_{12} + B_1 \Delta f_R = \frac{-\Delta P_{L1}}{\beta_1+\beta_2}(\beta_1 + 2\beta_2) = -\Delta P_{L1}\,(1 - \frac{1}{\beta_2}) \qquad (3.36)$$

In the same way, for area 2:

$$ACE_2 = -\Delta P_{12} + B_2 \Delta f_R = \frac{-\Delta P_{L1}}{\beta_2} \qquad (3.37)$$

It is evident from these calculations that the supplementary control in these two areas will react and modify the frequency difference twice as quickly as the condition 1 adjusting speed. The generation that area 2 picks up, however, will later reflect back as ACE_2 and be retracted in the steady state.

3) First, the response speed will be slower if B_1 and B_2 are set smaller than β_1 and β_2. Additionally, area 2's primary and supplementary controls will be turned on. This operation

will take longer to recover from because the response speed is slower than under the previous conditions. Actually, this kind of behavior degrades the frequency control mechanism.

Apart from the previously discussed circumstances, excessive control operations may also affect system stability if the bias factor values are excessively high. A strategy that chooses $B = 0.5\beta$ in [25] has not yet gained acceptance. Setting $B = 0.5\beta$ is shown to be acceptable and rational in [29].

4 Hybrid Energy Storage System-Based Frequency Regulation

This topic examines the use of hybrid energy storage systems (HESS) to increase Secondary frequency response, primary frequency response (PFR) and inertial response (IR) in the presence of system contingencies. The ethio – Sudan power exchange is represented in two-area interconnected power system model employed in this research is first described, along with its structure. Following that, a few frequency characteristics that are utilized to describe the dynamic performance of the system are shown. A workable control plan for the HESS is then suggested. Additionally, the requirement for power system operation requirements is taken into consideration while determining HESS sizes. Both mathematical techniques and simulation data are used to confirm the effectiveness of this control and sizing procedure.

4.1 Ethio–Sudan Power Interconnection in the East Africa Power Pool

The Ethio–Sudan Power Interconnection is a critical infrastructure project that strengthens regional energy cooperation under the East Africa Power Pool (EAPP) framework. Commissioned in 2013, the 500 kV transmission line connects Ethiopia's robust hydropower-based grid to Sudan’s electricity network, enabling cross-border electricity trade and grid stability between the two countries.

This interconnection allows Ethiopia to export surplus electricity mainly from its renewable hydropower sources to Sudan, contributing to economic integration, improved energy access, and reduced dependence on fossil fuels in the region. The project aligns with EAPP’s broader goal of developing a unified, reliable, and sustainable power grid across East Africa by facilitating cross-border power exchange, enhancing energy security, and optimizing resource utilization.

Overall, the Ethio–Sudan interconnection is a foundational step toward achieving a more interconnected and energy-resilient East Africa.

4.2 Frequency Standards in Ethiopian Power System

All synchronous electric power system components use frequency as a common metric, and it is widely recognized as a measure of the system's ability to control disturbances and balance supply and demand. The frequency of the East African Power Pool (EAPP) Interconnected Transmission System is normally adjusted between 49.5 Hz and 50.5 Hz and maintained at 50 Hz (±1%) during normal operation. The frequency spectrum may be expanded to 49.0 Hz to 51.0 Hz (±2%) in the case of a system disruption, such as a change in the load on the Ethiopian grid. When a heavy load is suddenly disconnected or a major generating unit or transmission equipment fails, the maximum frequency band increases to 48.75 Hz to 51.25 Hz (±2.5%). The frequency may fall below 47.5 Hz or rise over 51.5 Hz (±5%) for up to 20 s under extreme situations where several contingencies happen at once, necessitating quick action to restore system stability. As indicated in Table 3.1, the frequency restrictions are derived from the Ethiopian National Electricity Transmission Grid Code Draft report.

Frequency Excursions (HZ)			
Description	Ethiopia	Sudan	Integrated System
Normal system performance state	49.95 – 50.05	-	49.50 - 50.50
Disturbed System Conditions	49.00 – 51.50	-	49.00 – 51.00
Maximum allowable band during system disturbance	49.00 – 49.50	-	48.75 – 51.25
Extreme system fault scenarios	>48.50 <52.50	-	>47.50 <51.50

Table 2 *Frequency Standards in Ethiopian Power System.*

Stages	Stage 1(49 Hz)	Stage 2(48.8 Hz)	Stage 3(48.6 Hz)	Stage 4(48.4 Hz)	Stage 5(48.2 Hz)	Stage 6(48 Hz)	Stage 7(47.75 Hz)	Grand total
	TD=200ms	TD=200ms	TD=200ms	TD=200ms	TD=200ms	TD=200ms	TD=200ms	
Total sheded loads	152.345985MW	82.14305MW	122.458945MW	267.223763MW	326.24716MW	410.4711MW	364.06MW	1724.95MW

Table 3 *Under Frequency Load Shedding Lines and Stages in Ethiopian Power System.*

4.3 Simulation Model of an Interconnected Power System

The industry frequently uses the multi-area model because of its ability to adjust to different outside situations. Each generating unit's position in such a model is determined by factors like cost effect and distance to the primary load demand. The tie-lines connect the different areas.

Figure 4. 1 shows the simulation model of ethio - sudan linked power system that was used for this research. This chapter's primary goal is to examine the system frequency response to contingencies. The system contingencies in this model are a step-up and step-down load disturbance.

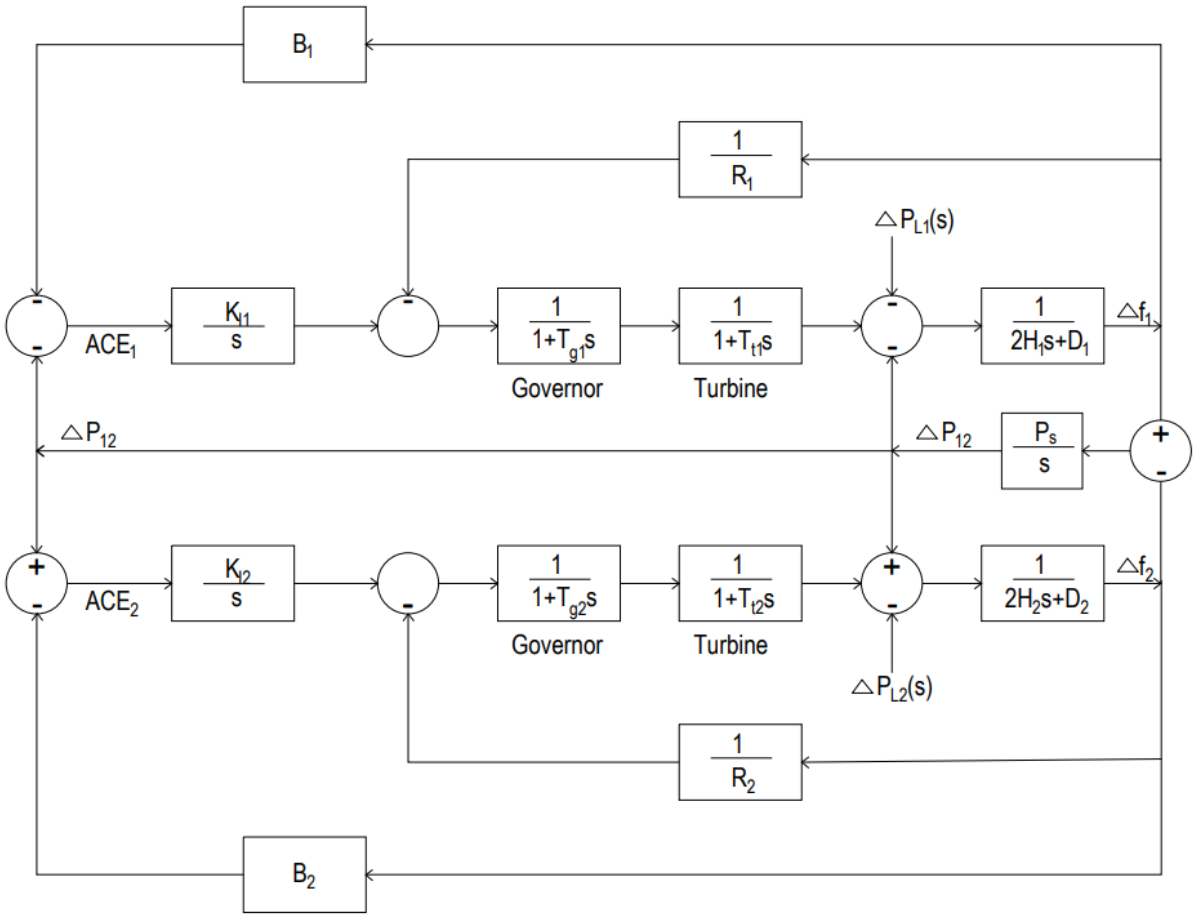

Figure 4.1 *Interconnected Power System Simulation Model [41].*

The integral controller's output signal, u(t), for the tie-line bias control can be computed as follows:

$$U(t) = -K_i \int ACE_i(t)dt \quad (4.1)$$

where $ACE_i = B_i\Delta f_i + \Delta P_{12}$ (i=1, 2) is the area control error and K_i (i=1, 2) is the integral controller's proportional gain. The bias factor is called B_i.

It is clear that the dynamic performance of the system will be affected by the value of K_i. The integral squared error (ISE) approach [34], which can be defined as follows, can be used to optimize the values of K_i (i=1, 2).

$$J = \int_0^\infty (ACE_1^2 + ACE_2^2)dt \quad (4.2)$$

Since J includes Δf_1, Δf_2, and ΔP_{12}, lowering J can result in a more stable power exchange and a reduced frequency deviation, which will optimize the dynamic responsiveness of the system. It is evident from Figure 4.2 that J has the lowest point, which matches the ideal values of K_1 and K_2.

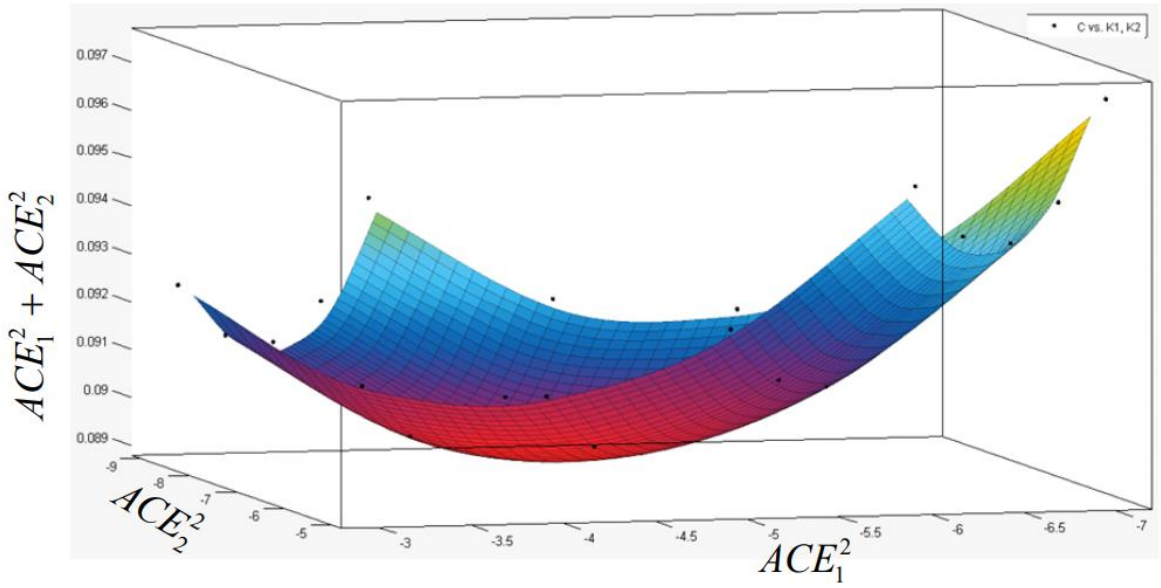

Figure 4.2 *Response of the Performance Index* ***J*** *to Variations in ACE_1 and ACE_2*

4.3.1 Grid Frequency Characteristics

The rate of change of frequency (RoCoF, df/dt) and the lowest point of the frequency change (the frequency nadir) are two identical metrics that can be used to characterize the system frequency response. In addition, the load damping ratio D, the droop coefficient R_i, the inertia constant H, and the power/frequency characteristic λ can all be included when talking about frequency characteristics.

The definition of an isolated area's inertia constant H, as determined by the analysis in [31], is [32]:

$$H = \frac{E_K}{S_B} = \frac{1}{2}\frac{J\omega^2}{S_b} \qquad (4.3)$$

where E_k is the rotor's stored kinetic energy, S_b is the system's rated power and ω is the rotational speed. Moreover, equation (3.13) can be used to determine the equivalent system inertia constant H_{sys} for a power system with multiple areas.

Eqn. (3.15) states that the link between H_{sys} and RoCoF can be expressed as follows:

$$\frac{2H_{sys}}{f_0}\frac{df}{dt} = \frac{P_G - P_L}{S_b} = \frac{\Delta P_b}{S_b} \qquad (4.4)$$

where ΔP_b is the power shortfall brought on by an imbalance between load demand (P_L) and power generation (P_G).

Equation (4.4) shows that the inertia coefficient H affects the system dynamics. This equation suggests that since a lesser RoCoF and frequency deviation value are obtained, when H is greater and can enhance frequency performance.

Since the steady-state frequency deviation Δf_{SS} is computed as follows:

$\Delta f_{SS} = -\Delta P_L/(1/R_1+D_1+1/R_2+D_2)$, the load damping ratio D is another crucial component that can also affect the system frequency performance in addition to H. This equation shows that a higher D results in a lower frequency deviation and a smaller Δf_{SS}.

Apart from the H and D discussion, the droop coefficient R_i (i =1, 2) is an additional parameter that can be described as follows [33]:

$$R_i = \frac{\frac{\Delta f}{f_0}}{\frac{\Delta P_i}{S_i}} \qquad (4.5)$$

The system frequency characteristic λ_i (i = 1, 2) is illustrated as follows [34] based on the definition of R:

$$\lambda_i = -\frac{\Delta P}{\Delta f_{ss}} = \sum_{i=1}^{n} \frac{1}{R_i} \frac{S_i}{f_0} \qquad (4.6)$$

where S_i (i=1, 2) is the rated power and ΔP is the change in load demand.

4.4 The Hybrid Energy Storage System

Concerns about the energy and environment scarcity have led to a steady increase in the use of renewable energy in contemporary power systems. The H_{sys} will be reduced based on equation (3.13), as renewable energy hardly affects system inertia. Under severe disturbance, such a decline will impair the system's dynamic performance and possibly jeopardize its stability. This issue can be resolved with the installation of an Energy Storage System (ESS), which is essentially an energy buffer. When power generation surpasses the demand for the load, ESS can store redundant energy and release it when required.

Since hybrid energy storage systems (HESSs) can combine the benefits of various energy storage devices, they have recently attracted more study attention. Two distinct kinds of energy storage devices are often combined to form a HESS. While one of them has a high power density, the other has a high energy density [19]. The battery is one of the most widely used energy storage technologies, as was covered in the first chapter. However, because of its low power density, the battery by itself would not be the optimum option for frequency regulation given the need for quick response after load disturbances. The supercapacitor can be used to achieve inertial response because of its great power density. PFR and SFR can cover frequency deviation that surpass

frequency restrictions if the battery capacity is chosen appropriately. In order to improve system dynamics, a HESS including a supercapacitor and a battery is used in this research for LFC. The power system's block diagram looks like this after the HESS is implemented:

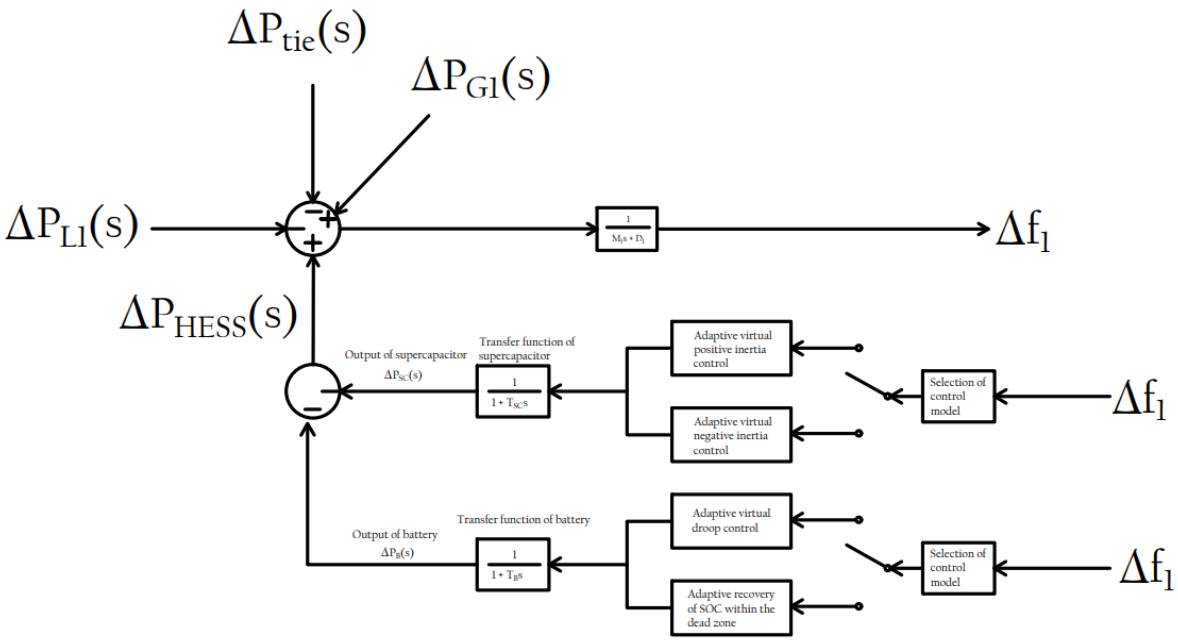

Figure 4.3 *Power System Structure*

.4.5 HESS Based Primary Frequency Response Control Model

In this section, a dynamic model is built to show how a hybrid energy storage system (HESS) supports a regional grid's primary frequency response. It then takes a closer look at the theory behind virtual droop and inertia controls weighing the pros and cons of VDC, VIC, and VNIC.

4.5.1 Primary Frequency Regulation Model.

By using the regional equivalent method, it is translated each individual component into its transfer function equivalent. Figure 4.3 displays the PFR model.

4.5.2 Control Strategies

When frequency fluctuations occur within the grid, the regulation signal is processed by the unit's governor and prime mover. This triggers a change in the turbine's water inlet flow, which ultimately adjusts the mechanical power output [23]. To help stabilize these deviations, Energy Storage Systems (ESS) can be programmed to mimic the control characteristics of traditional hydro units, as expressed in Equation (4.7).

$$\begin{aligned} \Delta f(s) &= \frac{\Delta P_G(s)+\Delta P_E(s)-\Delta P_L-\Delta P_{tie}(s)}{2Hs+D} \\ \Delta P_G(s) &= -K_G \Delta f(s) G_g(s) \\ G_g(s) &= \frac{1}{R(1+T_g s)(1+T_T s)} \\ \Delta P_E(s) &= \Delta P_{KE}(s) + \Delta P_{ME}(s) \end{aligned} \tag{4.7}$$

In this framework, Gg(s) defines the transfer function for the hydro power unit, while $\Delta P_E(s)$ denotes the power contribution from the energy storage system. The specific outputs for the virtual droop and virtual inertia controls $\Delta P_{ME}(s)$ and $\Delta P_{KE}(s)$, respectively, are determined by Equation (4.8). Because the logic behind virtual negative inertia control (VNIC) mirrors that of VIC but acts in the opposite direction, it is treated as a derivative of the same analysis rather than a separate case.

$$\begin{aligned} \Delta P_{ME}(s) &= -M_E s \Delta f(s) G_E(s) \\ \Delta P_{KE}(s) &= -K_E \Delta f(s) G_E(s) \\ s\Delta f(s) &= d\Delta f(s)/dt \end{aligned} \tag{4.8}$$

In this formulation, the term Δf(s) denotes the Rate of Change of Frequency (RoCoF), which captures the speed of the grid's response to a disturbance. The parameters M_E and K_E represent the coefficients for the Virtual Inertia Control (VIC) and Virtual Droop Control (VDC), respectively. By substituting the control laws from Equation (4.8) into the system model in Equation (4.7), we derive the following transfer functions:

$$\Delta f_{ME}(s) = \frac{-\Delta P_L(s) - \Delta P_{tie}(s)}{2Hs + D - K_G G_g(s) - M_E s G_E(s)}$$
$$\Delta f_{KE}(s) = \frac{-\Delta P_L(s) - \Delta P_{tie}(s)}{2Hs + D - K_G G_g(s) - K_E G_E(s)} \quad (4.9)$$

By examining both the rate of change of frequency (RoCoF), and the resulting quasi-steady-state deviation Δf_{qs}, we can evaluate the performance of the Virtual Droop Control (VDC) as follows:

$$RoCoF = \lim_{s\to\infty} s\ .[s.\Delta f_{KE}(s)] = \frac{-\Delta P_L - \Delta P_{tie}}{2H}$$
$$\Delta f_{qs} = \lim_{s\to 0} s\,.\Delta f_{KE}(s) = \frac{-\Delta P_L - \Delta P_{tie}}{D + K_G + K_E} \quad (4.10)$$

Equation (4.10) demonstrates that while Virtual Droop Control (VDC) is highly effective at minimizing the steady-state frequency deviation, it does not influence the rate of change of frequency (RoCoF).

To address this early transient phase, we evaluate how Virtual Inertia Control (VIC) affects both the RoCoF, and the subsequent quasi-steady-state deviation Δf_{qs}, as shown in the following derivation:

$$RoCoF = \lim_{s\to\infty} s\ .[s.\Delta f_{KE}(s)] = \frac{-\Delta P_L - \Delta P_{tie}}{2H + M_E}$$
$$\Delta f_{qs} = \lim_{s\to 0} s\,.\Delta f_{KE}(s) = \frac{-\Delta P_L - \Delta P_{tie}}{D + K_G} \quad (4.11)$$

According to Equation (4.11), Virtual Inertia Control (VIC) primarily influences the rate of change of frequency (RoCoF) without altering the final steady-state deviation. While positive inertia control effectively limits the speed of the initial frequency drop, it can inadvertently slow down the recovery process. To counter this, Virtual Negative Inertia Control (VNIC) is introduced during the recovery phase to accelerate the restoration of the grid frequency. By strategically coordinating VIC and VNIC, the energy storage system (ESS) can be more effectively utilized across the entire frequency regulation window.

4.6 ESS Control Strategies

4.6.1 Coordinated Control Strategy Based on Supercapacitor-Battery HESS

Previous analysis indicates that Virtual Droop Control (VDC) provides a sustained power output across the frequency regulation cycle to eliminate frequency deviations. In contrast, Virtual Inertia Control (VIC) must act rapidly during the initial frequency drop to suppress sudden changes, while Virtual Negative Inertia Control (VNIC) is essential for supporting the recovery phase. Given that each control method serves a distinct purpose, achieving optimal grid stability requires their seamless coordination throughout the entire disturbance event. While some studies have integrated VIC, VNIC, and VDC into single storage units or utilized hybrid energy storage systems (HESS) with basic droop control, there remains a gap in existing literature. Specifically, many current approaches, such as those in Reference [16], successfully coordinate these strategies within a single device but fail to align the unique response requirements of VIC and VDC with the specific physical characteristics of the storage media.

Battery Energy Storage Systems (BESS) are currently the most prevalent storage solution, valued for their high energy density and cost-effectiveness, despite limitations in power density and cycle life. Conversely, Supercapacitor Energy Storage Systems (SESS) offer exceptional power density and longevity, though their high cost and limited capacity often restrict their use in Inertial Frequency Regulation (IFR). By aligning these distinct physical characteristics with specific control objectives, a more robust system emerges: the SESS is utilized for its rapid response to handle inertial signals (VIC), while the BESS leverages its high energy capacity to manage virtual droop control (VDC) across the full regulation cycle.

To achieve an optimal alignment between storage technologies and control objectives, this topic introduces a coordinated framework for HESS driven primary frequency regulation (PFR). Within this architecture, the BESS utilizes Virtual Droop Control (VDC) once the frequency deviation exceeds the established dead zone to ensure long-term stabilization. Simultaneously, the SESS manages transient events based on the grid's state. During the deterioration phase defined by $[d\Delta f/dt] \cdot \Delta f > 0$ the SESS applies Virtual Inertia Control (VIC) to arrest the decline. Conversely,

during the recovery phase [dΔf /dt] . Δf < 0, the SESS switches to Virtual Negative Inertia Control (VNIC) to accelerate the return to nominal frequency.

To further capitalize on the rapid response and durability of the Supercapacitor Energy Storage System (SESS), its frequency dead zone (Δf_{SC}^{d}) is configured to be narrower than that of the battery (BESS). This hierarchy ensures that the SESS is the first responder to frequency fluctuations, often initiating restoration before the BESS dead zone is even reached. By prioritizing the SESS in this manner, it significantly decreases the charge-discharge cycles imposed on the BESS, thereby extending its operational lifespan. Furthermore, the BESS dead zone (Δf_{B}^{d}) is set smaller than that of the Hydro Power Unit (HPU) to shield the mechanical generators from frequent start-stop stresses and unnecessary wear.

To better accommodate the varying demands placed on the system by different load types and temporal shifts, we implement a time-varying dynamic dead zone for the energy storage components. By transitioning from a fixed to a flexible threshold, the system improves its responsiveness to real-time grid needs; the specific expression for this dynamic behavior is provided in Equation (4.12).

$$Dead\ Zone(t, \Delta f) = K_1(\Delta f) k_2(t) f_G^d \qquad (4.12)$$

In this model, K_1 serves as a dynamic load adjustment coefficient, while K_2 acts as a time-based parameter that distinguishes between peak and off-peak operational demands and f_G^d is the hydro power unit's dead zone.

The design logic for K_1 is inherently adaptive: during periods of minor, high-frequency fluctuations, a wider dead zone is utilized to prevent unnecessary mechanical wear and 'chatter' from ineffective cycling. Conversely, when the system faces significant, low-frequency disturbances, the dead zone is narrowed to prioritize a swift and robust frequency regulation response. The mathematical definition of K_1 is detailed in Equation (4.13).

$$K_1(f) = \begin{cases} K_{1\min} + \frac{\Delta f_{th}}{|\Delta f|}(K_{1\max} - K_{1\min}) & |\Delta f| \geq \Delta f_{th}, \\ K_{1\max} & |\Delta f| < \Delta f_{th} \end{cases} \qquad (4.13)$$

The load adjustment coefficient k_1 is bounded by specific upper and lower limits to ensure stable operation. For the SESS, these limits are set between a minimum (k_1) of 0.55 and a maximum (k_1) of 0.60, while the BESS utilizes a higher range between 0.75 and 0.80. Additionally, it is defined Δf_{th} as a critical threshold for frequency deviation; any fluctuation exceeding this reference value is categorized as a significant load disturbance, triggering a more aggressive control response. In this study, Δf_{th} is set to 0.05 Hz.

The design principle for the time-adjustment coefficient, K_2, accounts for the heightened grid stress typical of peak electricity hours specifically between 18:00 and 22:00. During this window, simultaneous residential and commercial demand creates a landscape of frequent, low-magnitude fluctuations. By strategically widening the dead zone during these peak periods, the system can overlook minor disturbances that fall within safety margins. This approach prevents the unnecessary and rapid switching of storage devices, thereby preserving their operational life. The mathematical derivation for K_2 is provided in Equation (4.14).

$$K_2(t) = \begin{cases} 1.1 & 18{:}00 < t < 22{:}00 \\ 1 & elsetimeperiods \end{cases} \tag{4.14}$$

4.6.2 SOC Feedback Based Adaptive Droop Coefficient

Traditional primary frequency regulation often relies on a 'Fixed-K' approach, where virtual droop coefficients remain constant regardless of the system's state. While this method performs reliably during initial frequency fluctuations, it ignores the State of Charge (SOC), frequently pushing the battery toward harmful overcharging or deep discharging both of which drastically shorten its operational life. To bridge the gap between grid stability and battery health, this paper adopts an adaptive virtual droop coefficient that is sensitive to the SOC. Under this scheme, the ESS provides maximum power support when its energy levels are optimal. However, as the SOC approaches its upper or lower limits, the system intelligently scales back its power output to balance frequency

needs with safety. If the SOC crosses a critical threshold, the system halts operation entirely to prevent catastrophic over-discharging or overcharging.

To manage power output constraints effectively, many researchers traditionally rely on the logistic function [43–45]. According to Reference [46], the engineering convenience and viability of future hardware implementation should be taken into account while designing output limits for ESS. As noted in, complex mathematical operations particularly exponential functions can place a heavy computational burden on embedded systems. In contrast, algebraic S-curves provide a more efficient alternative, offering the high speed and precision required for demanding applications like robotics. Furthermore, research in trajectory planning for automated machinery confirms that algebraic S-curves allow for a better balance between motion smoothness and computational overhead.

Equations $(4.15)\ and\ (4.16)$ display the virtual droop coefficient based on the algebraic S-curve. When Δf is greater than zero,

$$K_c = \begin{cases} K_{max} & SOC \le SOC_{high} \\ K_{max} X \left[1 - \left(3 \left(\frac{SOC - SOC_{high}}{SOC_{max} - SOC_{high}} \right)^2 - 2 \left(\frac{SOC - SOC_{high}}{SOC_{max} - SOC_{high}} \right)^3 \right) \right] & SOC_{high} < SOC < SOC_{max} \\ 0 & SOC \ge SOC_{max} \end{cases} \quad (4.15)$$

When $\Delta f < 0$

$$K_d = \begin{cases} 0 & SOC \le SOC_{min} \\ K_{max} X \left[\left(3 \left(\frac{SOC - SOC_{min}}{SOC_{low} - SOC_{min}} \right)^2 - 2 \left(\frac{SOC - SOC_{min}}{SOC_{low} - SOC_{min}} \right)^3 \right) \right] & SOC_{min} < SOC < SOC_{low} \\ K_{max} & SOC \ge SOC_{low} \end{cases} \quad (4.16)$$

where K_d and K_c stand for the virtual droop coefficient during the ESS's discharging and charging, respectively. SOC represents the ESS's measured SOC. The maximum, minimum, high and low SOC levels are represented by SOC_{max}, SOC_{min}, SOC_{high} and SOC_{low} respectively, and they change depending on the kind of ESS.

With SOC_{min} = 0.1, SOC_{max} = 0.9, SOC_{low} = 0.45 and SOC_{high} = 0.55, and, the virtual droop coefficients for SESS discharging and charging are K_{SCd} and K_{SCc} respectively. It should be

mentioned that VDC is not used by the SESS in the suggested control technique. Nonetheless, its virtual inertia control coefficient is constructed using the notion of the virtual droop control coefficient. The virtual droop coefficients for BESS discharging and charging are K_{Bd} and K_{Bc}, with $SOC_{min} = 0.2$, $SOC_{max} = 0.8$, $SOC_{low} = 0.45$ and $SOC_{high} = 0.55$.

Figure 4.4 illustrates the relationship between the SOC and virtual droop coefficient using the SESS as an example.

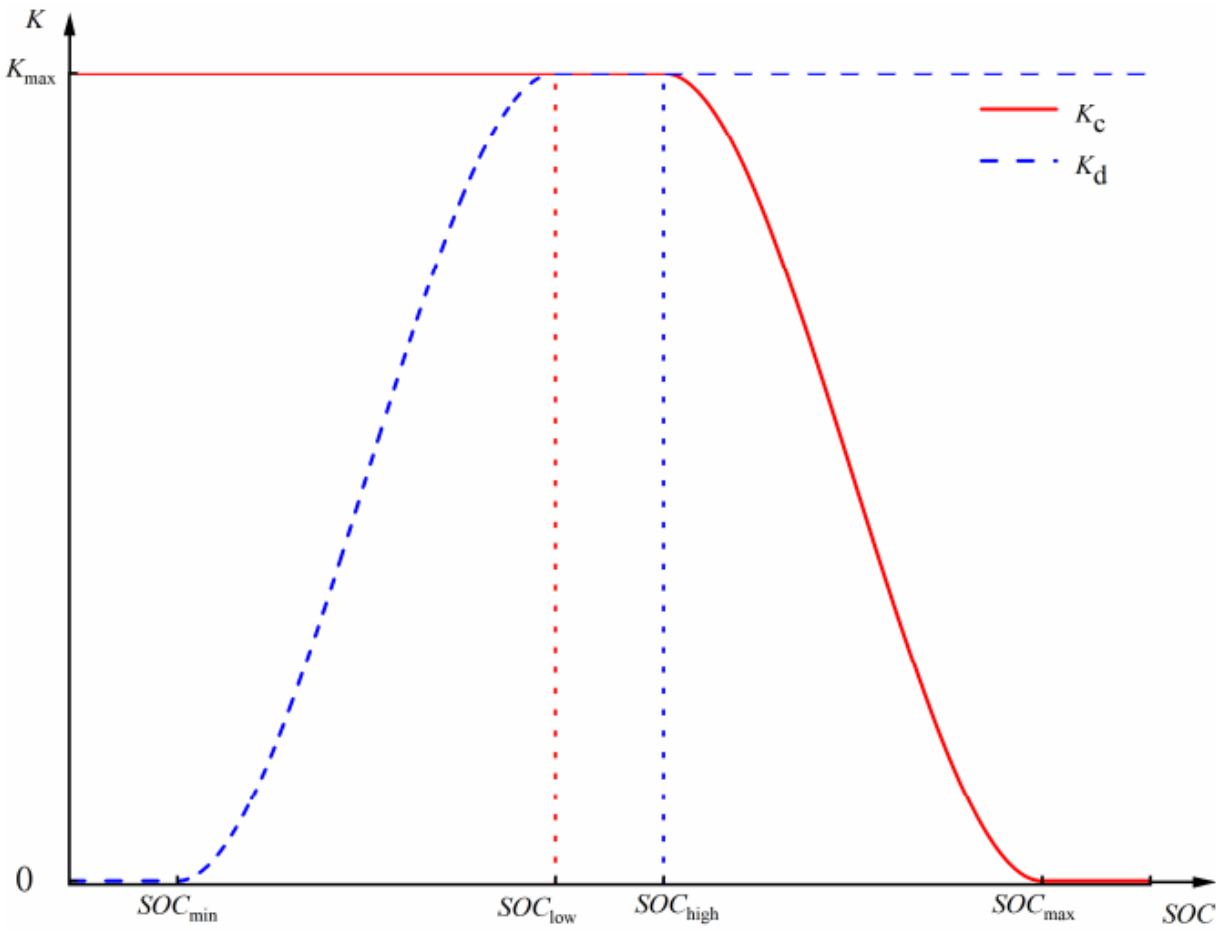

Figure 4.4. *SOC and the VDC Coefficient Relationship.*

4.6.3 SOC and Disturbance Type Based Adaptive Inertia Coefficient

Equation (4.17) expresses the virtual inertia control coefficient, or MEP.

$$M_{EP} = \begin{cases} \alpha\beta\gamma K_{SCc}, \Delta f \geq 0 \\ \alpha\beta\gamma K_{SCc}, \Delta f < 0 \end{cases} \quad (4.17)$$

Where the output adjustment factor is represented by α. A suitable value of α should be adjusted to provide comparable outputs of VDC and VIC because the magnitudes of the Δf and RoCoF differ significantly. In this research, α is selected to be 0.5 [50–52].

β represents the load adjustment factor, which varies with the kind of load. As studied in [50], the RoCoF is quit minor under load fluctuation; mitigating frequency deviation can be assisted by a moderate increase in the inertia coefficient. β is set to 1 in this research.
The direction adjustment factor is denoted by γ.

Sensitivity curves for various ME values are shown in Reference [54], which discovers that the sensitivity shifts from negative to positive before tending toward zero. Additional sensitivity study on ME shows that VIC is only useful prior to the frequency deviation peaking. Following that, frequency recovery is suppressed; the suppression intensifies with a higher ME.

In order to control the direction of power production, γ is introduced. The system is in a frequency deterioration phase when $d\Delta f/dt \cdot \Delta f > 0$, indicating that the frequency deviation and its RoCoF have the same direction; γ takes a positive value, suggesting that VIC is applied to alleviate frequency deterioration. The system is in a frequency recovery phase when $d\Delta f/dt \cdot \Delta f \leq 0$, the frequency deviation and its RoCoF are opposite, and γ becomes negative, indicating the employment of VNIC to support frequency recovery.

4.6.4 SOC Recovery Within the BESS Frequency Regulation Dead Zone

According to earlier studies, the BESS's SOC frequently finds it difficult to maintain stability amid significant system disruptions [17]. Consequently, an adaptive recovery mechanism is included within the BESS's dead zone in addition to the adaptive BESS output during the frequency regulation phase. The recovery demand coefficient is determined using the SOC within the dead

zone, where grid frequency stays within permissible bounds. A recovery constraint coefficient is calculated taking into account the grid's tolerance capacity in order to avoid excessive charging or discharging power during recovery, which could push the frequency outside the dead zone once more. Both the recovery demand coefficient and the recovery constraint coefficient are used to calculate the SOC recovery coefficient. Conversely, SESS does not need an extra SOC recovery mechanism because it can successfully maintain its SOC across a variety of operating situations.

4.6.5 SOC Based Determination Recovery Demand Coefficient

Using the charging recovery demand coefficient Kc1 as an example, when SOC < SOCmin, the SOC is abnormally low, which could shorten the BESS's lifespan. In these circumstances, Kc1 achieves its maximum value and the BESS charges at maximum power. Kc1 stays reasonably high when SOC_{min} < SOC < SOC_{low}, but it falls as SOC rises. The SOC is deemed to be within a safe range in the range SOC_{low} < SOC < SOC_{high}, and recovery is not necessary. The SOC is already high when SOC > SOC_{high}, and more charging may make the situation worse. K_{c1} is therefore set to 0 if SOC > SOC_{low}. Equations (4.18) and (4.19) provide the precise expressions for the charging and discharging recovery demand coefficients K_{c1} and K_{d1}.

$$K_{c1} = \begin{cases} K_{max} & SOC \le SOC_{min} \\ K_{max} X \left[1 - \left(3\left(\frac{SOC - SOC_{min}}{SOC_{low} - SOC_{min}}\right)^2 - 2\left(\frac{SOC - SOC_{min}}{SOC_{low} - SOC_{min}}\right)^3\right)\right] & SOC_{min} < SOC < SOC_{low} \\ 0 & SOC \ge SOC_{low} \end{cases} \quad (4.18)$$

$$K_{d1} = \begin{cases} 0 & SOC \le SOC_{high} \\ K_{max} X \left[\left(3\left(\frac{SOC - SOC_{high}}{SOC_{max} - SOC_{high}}\right)^2 - 2\left(\frac{SOC - SOC_{high}}{SOC_{max} - SOC_{high}}\right)^3\right)\right] & SOC_{high} < SOC < SOC_{max} \\ K_{max} & SOC \ge SOC_{max} \end{cases} \quad (4.19)$$

Figure 4.5 shows the recovery demand coefficients for charge and discharge.

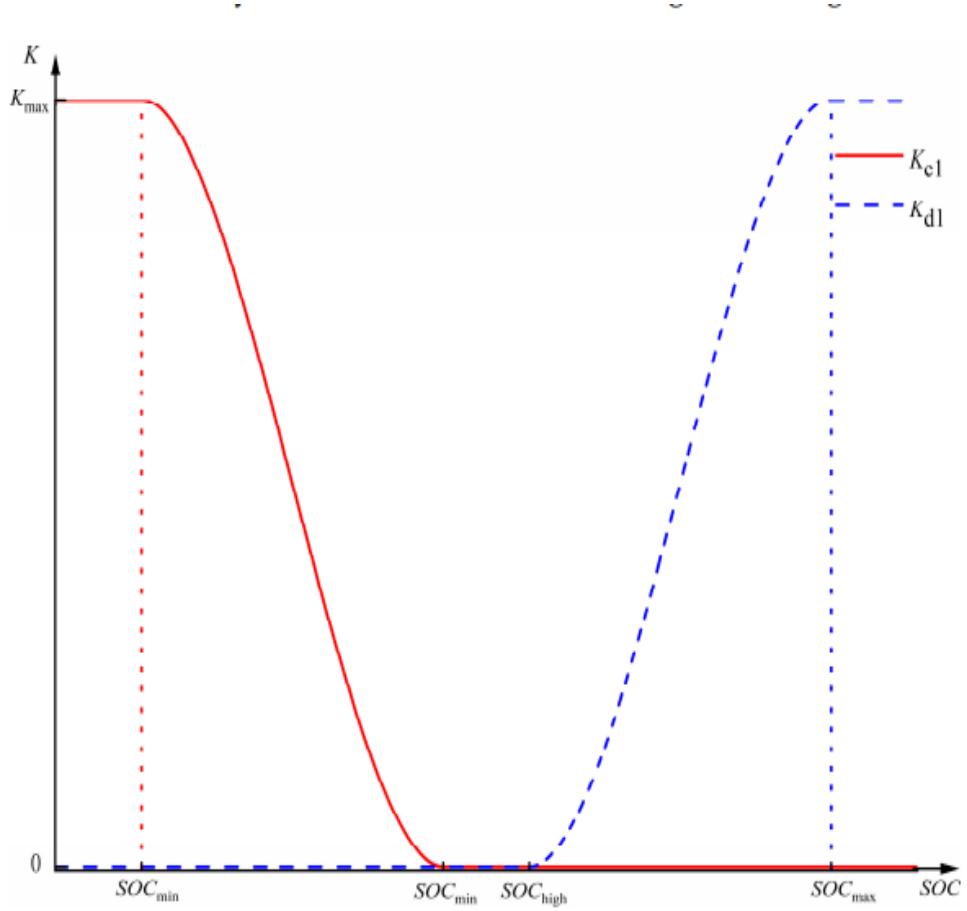

Figure 4.5 *Charge/Discharge Recovery Coefficient of Demand*

4.6.6 Δf Based Recovery Constraint Coefficient

The Δf is divided into six states: Δf_d, Δf_{high}, Δf_{low}, $-\Delta f_{high}$, $-\Delta f_{low}$, $-\Delta f_d$. The higher value, lower value, and upper dead zone limit of the Δf are represented by Δf_{high}, Δf_{low}, and Δf_d, respectively.

The logic is as follows, using the charging recovery constraint coefficient Kc_2 as an example: when Δf is less than −Δf high, the grid frequency is in a dangerous situation with a risk of leaving the dead zone, and the BESS discharge is necessary to correct the FD; therefore, Kc_2 is set to 0. When Δf lies between $-\Delta f_{high}$ and $-\Delta f_{low}$, the grid frequency is relatively safe, and Kc_2 increases as the absolute value of the Δf decreases. The frequency is within

a safe range when Δf is between $-\Delta f_{low}$ and Δf_{low}. The grid needs BESS charging when Δf is higher than Δf_{low}. Consequently, Kc_2 reaches its maximum value when $\Delta f > -\Delta f_{low}$. Equations (4.20) and (4.21) provide the precise formulations for the charge/discharge recovery constraint coefficients Kc_2 and Kd_2, which are derived using a cosine function.

$$K_{c2} = \begin{cases} 0 & -f_d < f < -f_{high} \\ K_{max} X \dfrac{1-\cos\left(\pi \dfrac{f-(-f_{high})}{-f_{low}-(-f_{high})}\right)}{2} & -f_{high} \le f \le -f_{low} \\ K_{max} & -f_{low} < f < f_d \end{cases} \quad (4.20)$$

$$K_{d2} = \begin{cases} K_{max} & -f_d < f < f_{low} \\ K_{max} X \dfrac{1+\cos\left(\pi \dfrac{f-f_{low}}{f_{high}-f_{low}}\right)}{2} & f_{low} \le f \le f_{high} \\ 0 & f_{high} < f < f_d \end{cases} \quad (4.21)$$

Figure 4.6 shows the recovery constraint coefficients for charge and discharge.

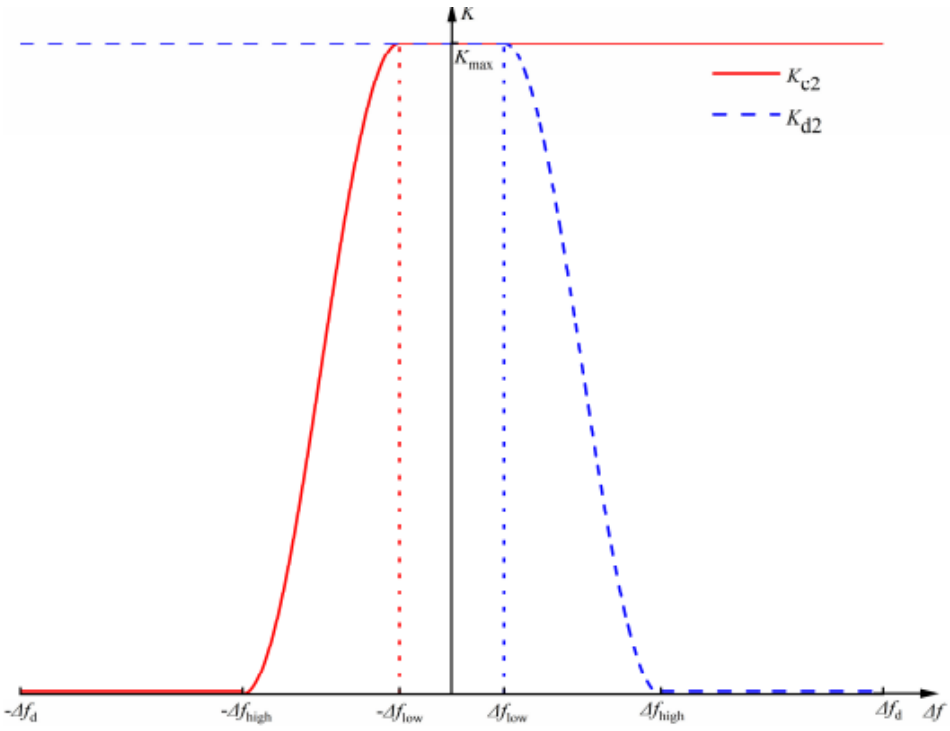

Figure 4.6 *Charge/Discharge Recovery Coefficient of Restriction*

4.6.6.1 Recovery Coefficient Determination

The majority of research chose the smaller value between the recovery demand coefficient and the recovery constraint coefficient as the SOC recovery coefficient of the BESS in order to balance the SOC recovery demand of the BESS with the grid's Δf constraint [55–57]. Nevertheless, this method causes sudden variations in BESS output during recovery, which disrupts the system in a secondary way. Furthermore, choosing the minimum value makes the technique unduly conservative by placing undue limitations on recovery power. Equation (4.22) expresses the demand-constraint dynamically coupled recovery coefficient, which is used to achieve smoother power output during battery recovery.

$$K_{requ} = \begin{cases} a.K_{c1} + (1-a)K_{c2} & S \le SOC_{low} \\ 0 & SOC_{low} < S < SOC_{high} \\ a.K_{d1} + (1-a)K_{d2} & S \ge SOC_{high} \end{cases} \quad (4.22)$$

Equation (4.23) determines the value of a,

$$a = \frac{1}{1+e^{-K_1(SOC-0.5)}} X \left(1-\frac{|\Delta f|}{\Delta f_d}\right)^{k_2} \quad (4.23)$$

where the tuning factors k_1 and k_2 are utilized to adjust a's magnitude.

Prioritizing the SOC recovery demand, an approaches 1 when the frequency stays within a safe range but the SOC deviates significantly from 0.5. A trends toward 0, giving frequency limitations priority, when the SOC is near 0.5 but the Δf is going to cross the dead zone. The weight of a, which ranges from 0 to 1 in intermediate states, is based on the variations of Δf and SOC.

Equation (4.24), expresses the BESS recovery output P_{requ} within the dead zone.

$$\Delta P_{requ} = -K_{requ}|\Delta f| \quad (4.24)$$

4.6.7 Comprehensive Control Strategy

By taking into account the features of SESS and BESS, flexibly implementing the three control strategies, and incorporating adaptive control rules based on SOC and load type, this work proposes a comprehensive control approach for HESS to take part in PFR. Figure 4.7 shows the particular control technique.

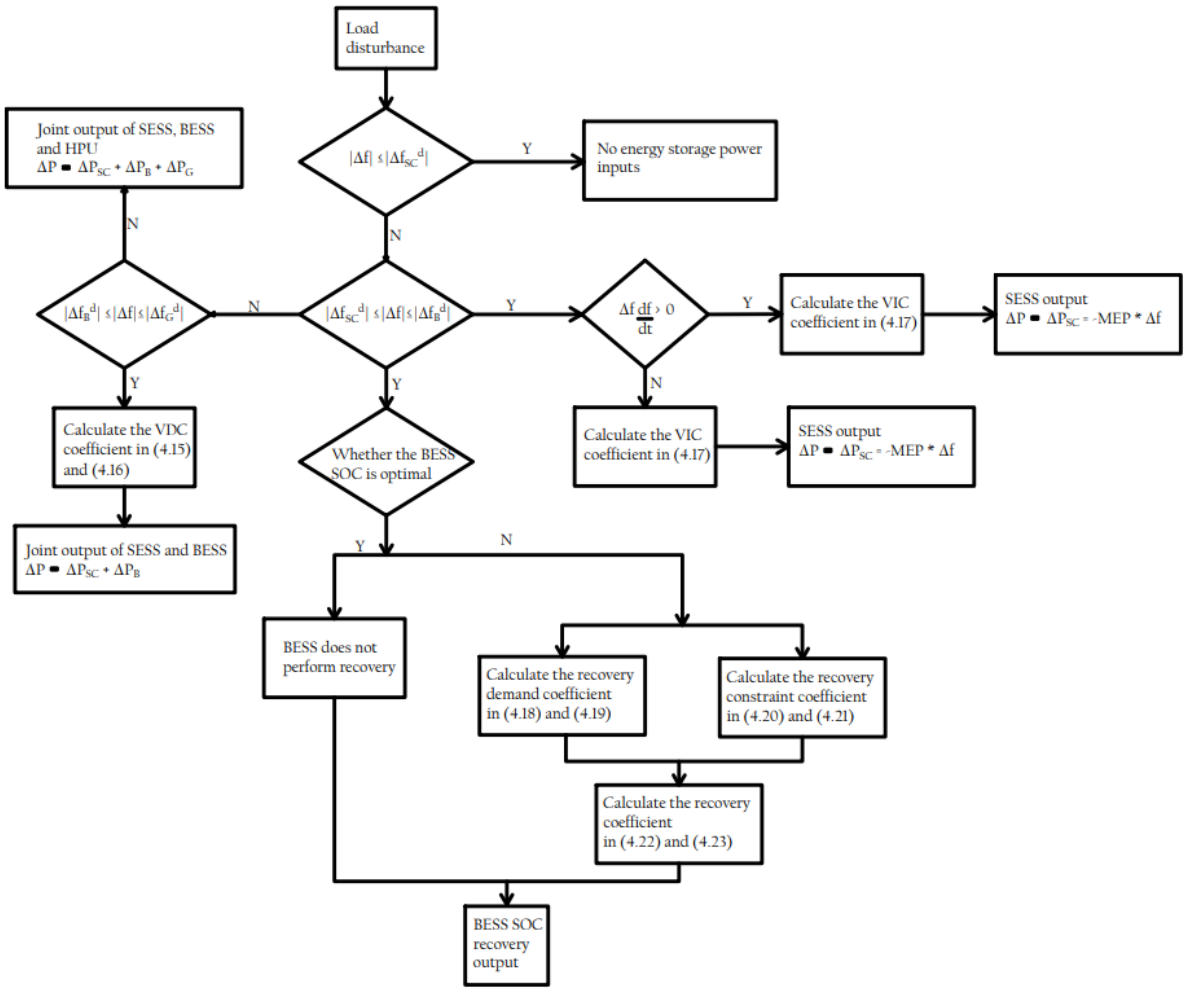

Figure 4.7 *HESS Engaging in PFR of the Power Grid Using a Comprehensive Control Mechanism*

The following results from assuming that $\Delta f > 0$, which means that the BESS must absorb power for frequency regulation:

1. There is no need for frequency regulation when $\Delta f < \Delta f_{SC}^{d}$ because the Δ is within a safe range.
2. The BESS determines whether to restore its SOC depending on its present condition, while the SESS is used for frequency management when $\Delta^{fSCd} \ll \Delta f \ll \Delta f_{B}^{d}$.

The following guidelines apply to the SESS's involvement in grid frequency regulation:

a) When RoCoF > 0, a worsening frequency condition is indicated because the Δf and RoCoF are pointing in the same direction. Based on (4.17), the SESS calculates the VIC coefficient and uses adaptive VIC to reduce frequency deterioration.
b) When RoCoF $\ll$ 0, a frequency recovery phase is indicated since the Δf and its RoCoF are pointing in opposite directions. To expedite frequency recovery, the SESS uses adaptive VNIC and calculates the VNIC coefficient using (4.17).

The following guidelines control BESS SOC recovery in the dead zone:

a) The recovery of SOC is considered superfluous when the BESS's SOC is in a suitable state.
b) The recovery demand coefficient is determined using (4.18) and (4.19) when the BESS's SOC is suboptimal, and the recovery constraint coefficient is computed using (4.20) and (4.21). Equations (4.22) and (4.23) determine the recovery coefficient by taking into account both the recovery demand and recovery constraint. The recovery coefficient is then utilized to compute the BESS's SOC recovery power output.

3. The SESS and BESS work together to regulate frequency for $\Delta f_{B}^{d} \ll \Delta f \ll \Delta f_{G}^{d}$. The BESS uses VDC to participate in grid frequency regulation; (4.15) and (4.16) are used to calculate the VDC coefficient. Depending on the product of the Δf and its rate of change, the SESS continues to apply either positive or negative inertia control.
4. When $\Delta f > \Delta f_{G}^{d}$, the HESS works with the Hydro Power Units to provide power since the FD is large.

The aforementioned procedure demonstrates how the suggested comprehensive control strategy divides the output timing of HESS and Hydro Power Units through dead zones, determines the output mode and direction based on FD and its rate of change, and modifies the droop and inertia coefficients based on SOC and disturbance type.

4.7 Supercapacitor Control Blocks for Inertial Response

One novel kind of ESS with a very high power density is the supercapacitor. Supercapacitors have the potential to have ten times the power density of batteries and remarkably reduced charging and discharging time constants. These features show that the supercapacitor is appropriate for short-term situations involving high-density energy charging or discharge scenarios. One of these circumstances is the Inertial Response (IR). Figure 4.8 depicts the supercapacitor model for Inertial Response, which is based on [35].

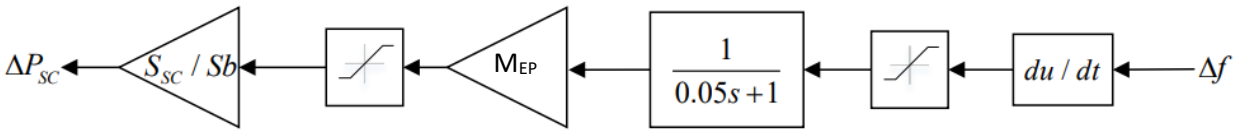

Figure 4.8 *The Supercapacitor Used for IR*

The maximum RoCoF in IR is limited to 0.5 Hz/s. To improve transient stability, the system incorporates Virtual Inertia Control (VIC) to provide synthetic inertia during the critical moments following a disturbance. Within this framework, the derivative element [36] is the primary effective module in the control block; it calculates the rate of change of frequency (RoCoF) to emulate the kinetic energy release of a traditional synchronous machine. To maintain signal quality, the high-frequency sounds and noise inherent to the derivative function are eliminated using a first-order low-pass filter, ensuring a smooth synthetic inertial response. Such a filter also provides a small time-delay, allowing additional assistant generating units from a broader portion of the power system to assist with frequency regulation [37]. In addition, a dead band between -0.001 and 0.001 is incorporated to counteract the impact of minor disturbances. To ensure a power output of the supercapacitor at full capacity when RoCoF is equal to 0.5, M_{EP} is set to 2 because RoCoF should be within 0.5.

The system structure depicted in Figure 4.3 is used to examine the impact of this derivative component. As soon as the IR module is connected in parallel with the original power system model, the transfer function of the power system G(s) = 1/Ms+D looks like this:

$$G(s) = \frac{\frac{1}{Ms+D}}{1+\frac{Ks}{Ms+D}} = \frac{1}{(M+K)s+D} \qquad (4.25)$$

The inertia constant M is changed following the implementation of this module. As was previously said, increasing M can enhance the system's dynamic performance.

4.8 Battery Control Blocks for Primary Frequency Response

One of the most widely used device for storing energy is the battery, which has a comparatively high energy density. Because of this feature, batteries are often utilized in scenarios where power exchange is required over an extended period of time but the immediate demand for energy is not very high. Among these application is PFR. Figure 4.9 displays the battery model utilized for PFR, which is based on the analysis in [38].

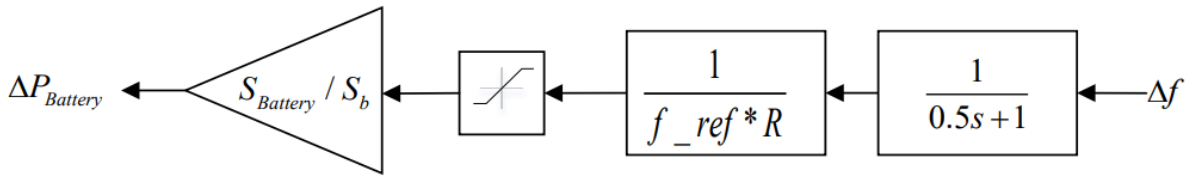

Figure 4.9 *PFR with BESS*

The battery droop coefficient in this model is denoted by R. The frequency deviation limit in this research set at ±0.05 Hz for PFR, meaning that the entire battery capacity must engage in frequency regulation when the frequency deviation reaches 0.05 Hz. Equation (3.3) can be used to determine R = (0.05/50)/(1/1) = 0.001 in order to accomplish this goal.

The mathematical method can be used to illustrate the function of R. G(s) = 1/Ms+D which is the initial system transfer function, is changed to the following after the PFR model and the power system model are connected in parallel:

$$G(s) = \frac{\frac{1}{Ms+D}}{1+\frac{\frac{1}{R}}{Ms+D}} = \frac{1}{Ms+(D+\frac{1}{R})} \quad (4.26)$$

It can be seen that the load damping ratio D has increased in value. According to the discussion above, increasing D can improve the system dynamics.

4.9 Battery for Secondary Frequency Response

The generators are in charge of secondary control in conventional frequency regulation techniques. The battery energy storage system (BESS) can react to rapidly varying signals faster than the generator. Therefore, the filtered ACE technique is the corresponding control method in this research, and the BESS is employed for secondary control enhancement [39]. Figure 4.10 depicts the method's framework. The high-frequency component of the ACE signal can be separated into two components and extracted using a high-pass filter. The BESS receives these signals for additional regulation, and the generator receives the remaining portion for conventional control.

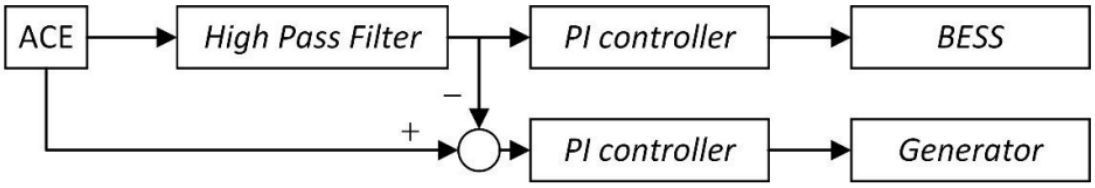

Figure 4.10 *The Filtered ACE Method's Framework*

4.9.1 The Control Blocks of the Battery

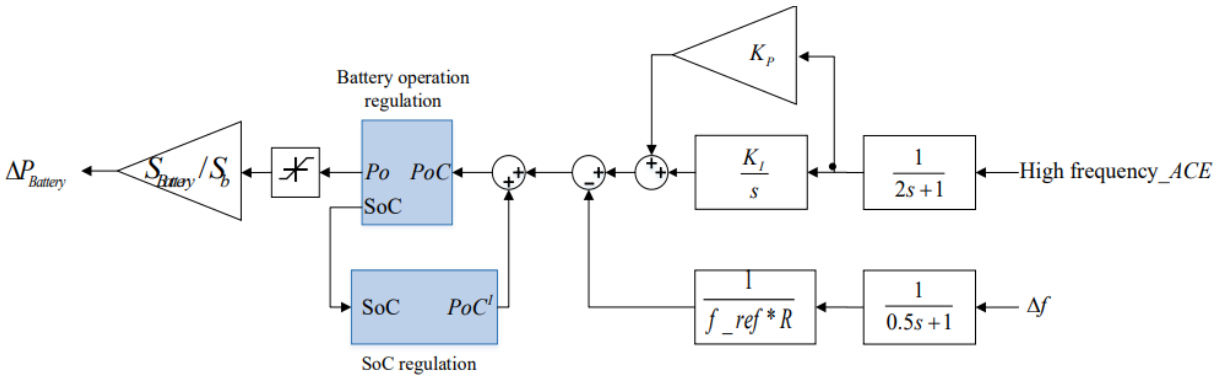

Figure 4.11 *The BESS Control Block*

Figure 4.11 shows the BESS's frequency regulation control block. The high frequency component of ACE signal and frequency deviation serve as the input for this technique.

The Area Control Error signal will be produced in the event of a frequency error. After then, this control block will receive the high frequency portion of the ACE signal. The PI controller begins working to remove this input error signal after a small time delay. The input signal from the secondary control power request plus primary control power command will then be sent to the battery operation regulation block. The total power output within the BESS capacity is then limited by the saturation module. The frequency error will then be eliminated by combining the generator's output with the power output of this battery control block to compensate for the power imbalance.

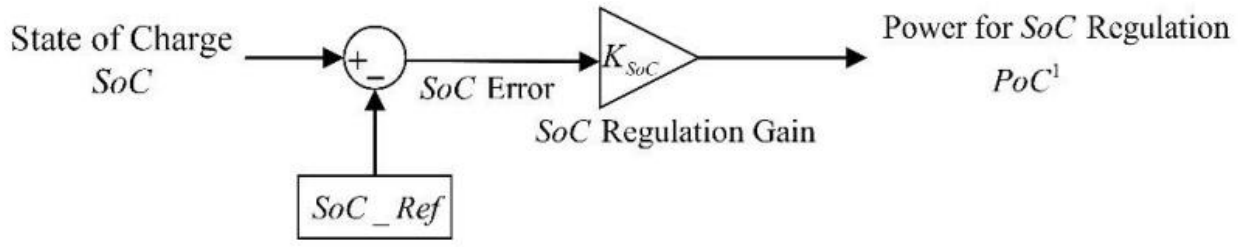

(a) SoC Regulation Control Block

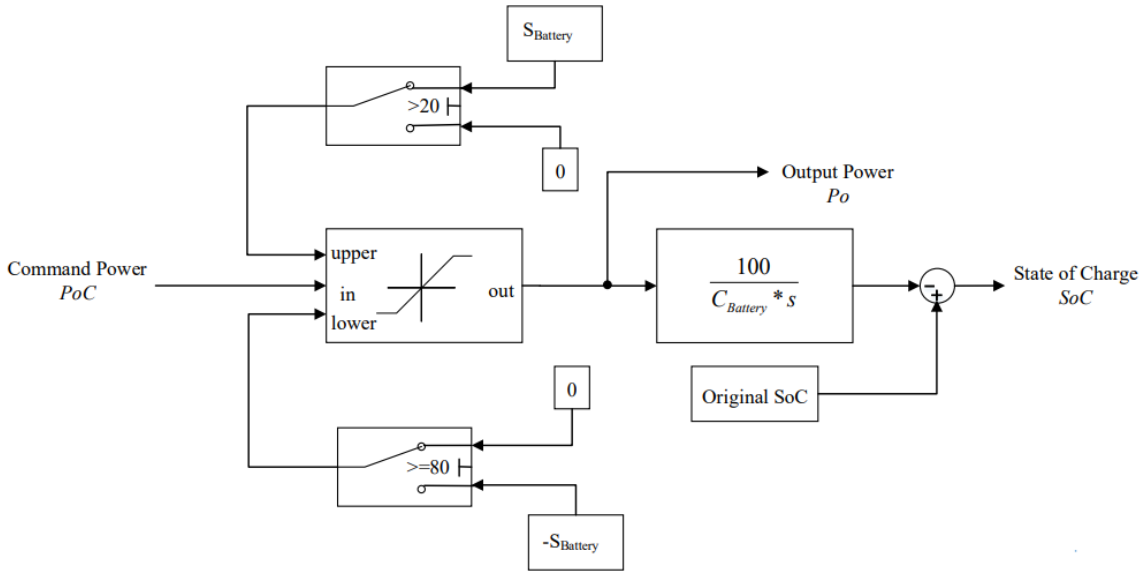

(b) SoC Calculation and Battery Operation Regulation Control Block

Figure 4.12 *The Control Blocks for Battery Regulation*

Figure 4. 12 (b) depicts the control block for battery operation regulation. The input signal is the power command, which is the total of the power requirements from the primary control, secondary control, and SoC regulation. Two switches on the left side of this control block can give operation constraints based on the values of the input signals in addition to the SoC calculation function. This block operates on the following principle:

The upper bound is set to 0 when the SoC is equal to or less than 20%, which indicates that the battery cannot react to the input signal until a negative value is transmitted. The battery's charging condition, shown by the negative value, allows the SoC to be raised. In contrast, the lower bound is set to 0 when the SoC is equal to or more than 80. In this scenario, the battery can only react to positive input signals, which represent the battery's discharging status. As a result, the SoC value may drop.

4.10 Hybrid Energy Storage System Sizing

The suggested HESS sizing approach is primarily based on determining the necessary power scale for the battery and supercapacitor in order to attain the appropriate dynamic response under particular load contingencies.

The system inertia constant H_{areai} can be computed using equation (4.4) as follows:

$$H_{areai} = \frac{\Delta P_L}{S_{sys}} X \left(\frac{df}{dt}\right)^{-1} X \frac{f_0}{2} \qquad (4.27)$$

It should be mentioned that the df/dt in this case equals the highest RoCoF value across the entire dynamic frequency change procedure.

Similarly, the target value of the system inertia constant H_{target} can be calculated by keeping the maximum RoCoF within 0.5 Hz/s, and the equivalent value of df/dt is 0.5. Additionally, the supercapacitor H_{SC} inertial contribution can be described as follows:

$$H_{SC} = P_{SC} X \left(\frac{df}{dt}\right)^{-1} X \frac{f_0}{2} \qquad (4.28)$$

where the supercapacitor's output is P_{SC}.

Consequently, the supercapacitor P_{SC} predicted capacity can be found as [31]:

$$P_{SC} = S_{sys} X \frac{H_{target} - H_{area}}{H_{SC} - H_{target}} \qquad (4.29)$$

Furthermore, the goal of PFR, which is to get the steady-state frequency adjusted to 49.5 Hz, is used to determine the battery's size. The target frequency characteristic λ_{target} can be computed as follows using equation (4.6):

$$\lambda_{target} = -\frac{\Delta P_L}{\Delta f_{ss}'} \qquad (4.30)$$

where ΔP_L is the load demand increase. The target steady-state frequency deviation is 0.5 Hz, denoted by $\Delta f'_{SS}$.

Likewise, the power system's frequency characteristic, λ_{areai}, can be obtained by:

$$\lambda_{areai} = -\frac{\Delta P_L}{\Delta f_{ss}} \qquad (4.31)$$

Where Δf_{SS} denotes the real steady-state frequency deviation.

Typically, λ_{target} is greater than λ_{areai}, and the battery's needed capacity, $P_{battery}$, can be found as [31]:

$$P_{battery} = (R_{battery} \text{ X } f_0) \text{ X } (\lambda_{target} - \lambda_{areai}) \qquad (4.32)$$

4.11 Base Case Data

Important base case data for the Ethiopia grid used for dynamic performance analysis considering only the generating units participating on frequency regulation is shown in Table 4.

Generating Unit	Current Operational Capacity(MW)	Inertial Constant(s)	Speed Damping Constant(%)	Droop(%)	Governor Time Constant(s)	Water Time Constant(s)
GERD	1450MW	3s	1%	4%	8s	1.2s
G. Gibe III	1650MW	3.27s	1%	4%	8s	1.2s
Beles	415MW	3.14s	1%	4%	8s	1.2s

Table 4 *Ethiopian Network Base Case System Data for Dynamic Performance Analysis*

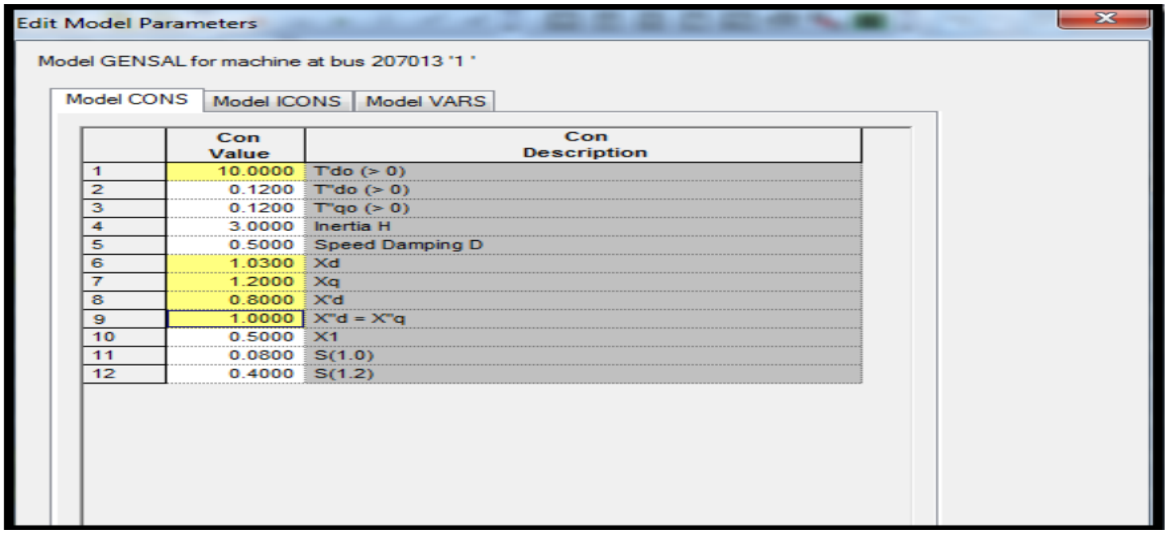

Figure 4.13 *Dynamic Model Data for Sudan Network*

5 Analysis and Outcomes of Simulation

5.1 Power System Under Investigation

The multi-area model in Figure 3.1 can be used with the suggested approach. To validate this approach, the Ethio – Sudan interconnection represented in a two-area interconnected power system model is used in this section. The current operational capacity of the Ethiopian power system from hydro is around 4800 MW, out of these Gilgel Gibe III, Beles and GERD are the power plants which participate on frequency response with a total operational capacity of 3515MW. The inertia constant of Area 2 which is Sudan network is 3, while in Area 1 which is the Ethiopian network, this value is only 2.1, 2.4 and 2.7 due to 30%, 20% and 10% PV penetration respectively. In order to enhance the system dynamic performance, the HESS is installed in Area

To test the effectiveness of the proposed Hybrid Energy Storage System (HESS), this study evaluates a critical operational scenario: the sudden loss of 160 MW of generation. In the context of the Ethiopian National Grid, this is not an arbitrary figure; it represents a high-probability 'N-1' contingency event, such as the unexpected tripping of a major generating unit at the Tana Beles station single 115 MW unit at Tana Beles plus its associated spinning reserve. or two units at the Gilgel Gibe II plant (rated at 107 MW each) operating at partial load,

At t=5s seconds, the simulation initiates this 160 MW deficit to mimic a real-world fault. Without fast-acting intervention, such a loss would cause a rapid drop in frequency (RoCoF). By framing the study around this specific magnitude, we can measure how the HESS acting as a 'virtual shock absorber' provides the necessary millisecond-level response to stabilize the grid and protect local industries from a blackout.

5.1.1 Case Study

A. Case 1

In this instance, the supercapacitor's role in IR enhancement is presented. Two cases are contrasted: 1) Area 1 without any energy storage; 2) Area 1 with only supercapacitor.

As was previously said, RoCoF needs to be kept under 0.5 Hz/s. The Simulation shows that when a generation outage of 160 MW happens the corresponding value of Rate of Change of Frequency is 0.543 Hz/s. Equations (4.27) – (4.29), the nominal power of 3515MW, and a generation outage of 160 MW are used to determine that H_{target} is 2.275 s, H_{SC} is 21.2 s and H_{area1} is 2.093 s and via simulation. Thus, the supercapacitor PSC's capacity may be calculated using:

$$P_{SC} = 3515 * (2.275 – 2.093) / (21.2 – 2.275) = 33.8MW \quad (5.1)$$

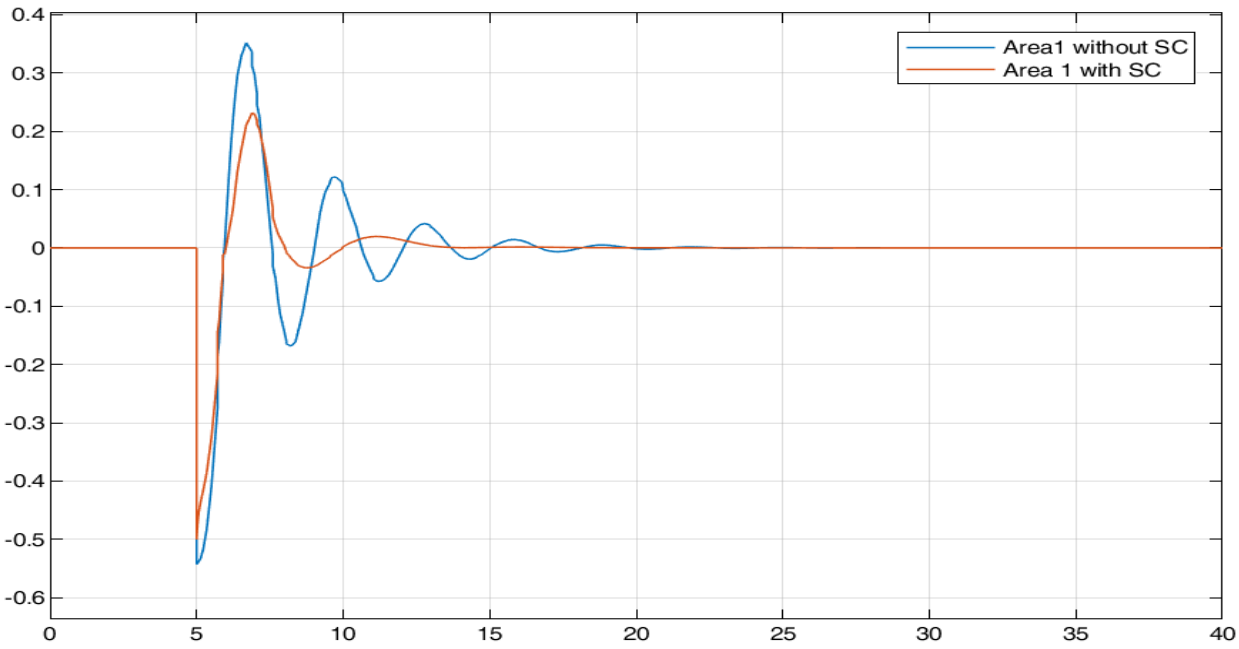

(a) RoCoF

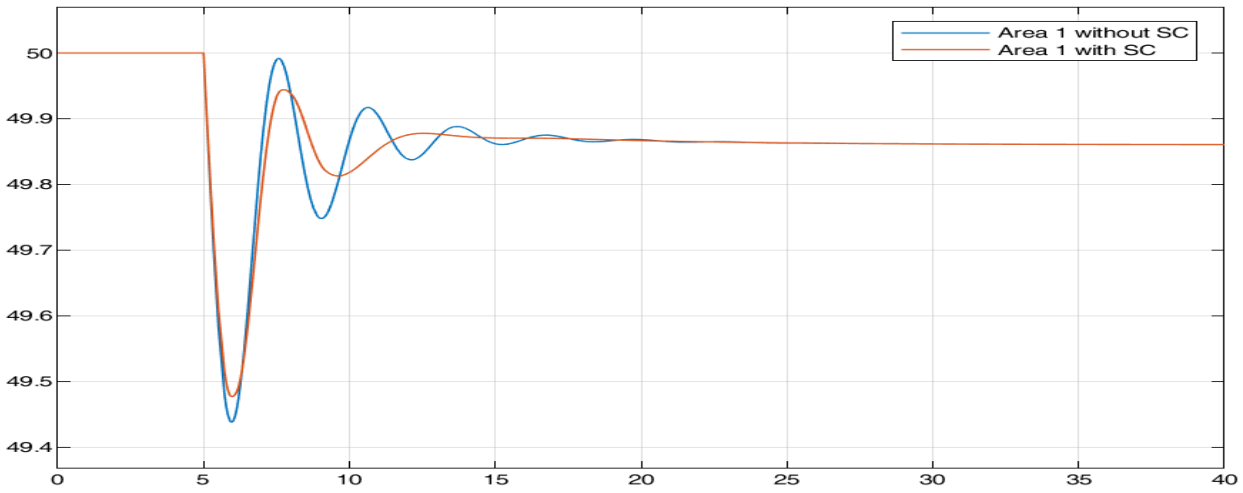

(b) Frequency Response

Figure 5.1 *Area 1's Dynamic Behavior With and Without SC for 30% PV Penetration.*

Figure 5.1 shows the system frequency and RoCoF dynamic performance. During a generation outage, Area 1's frequency nadir without HESS is approximately 49.44 Hz, as shown in Fig. 5.1(b). Following the supercapacitor's implementation, this value is changed to 49.47 Hz, and the supercapacitor provide a 0.03 Hz improvement.

The required capacity of the supercapacitor is determined using the RoCoF's absolute value which is 0.543 Hz/s as shown in Fig. 5.1(a), when dealing with a generation outage of 160 MW. The corresponding value can be adjusted to 0.5 Hz/s after the supercapacitor is employed. As a result, the impact of the lower inertia constant is shown. Moreover, the dynamic performance of IR can be effectively enhanced by the supercapacitor.

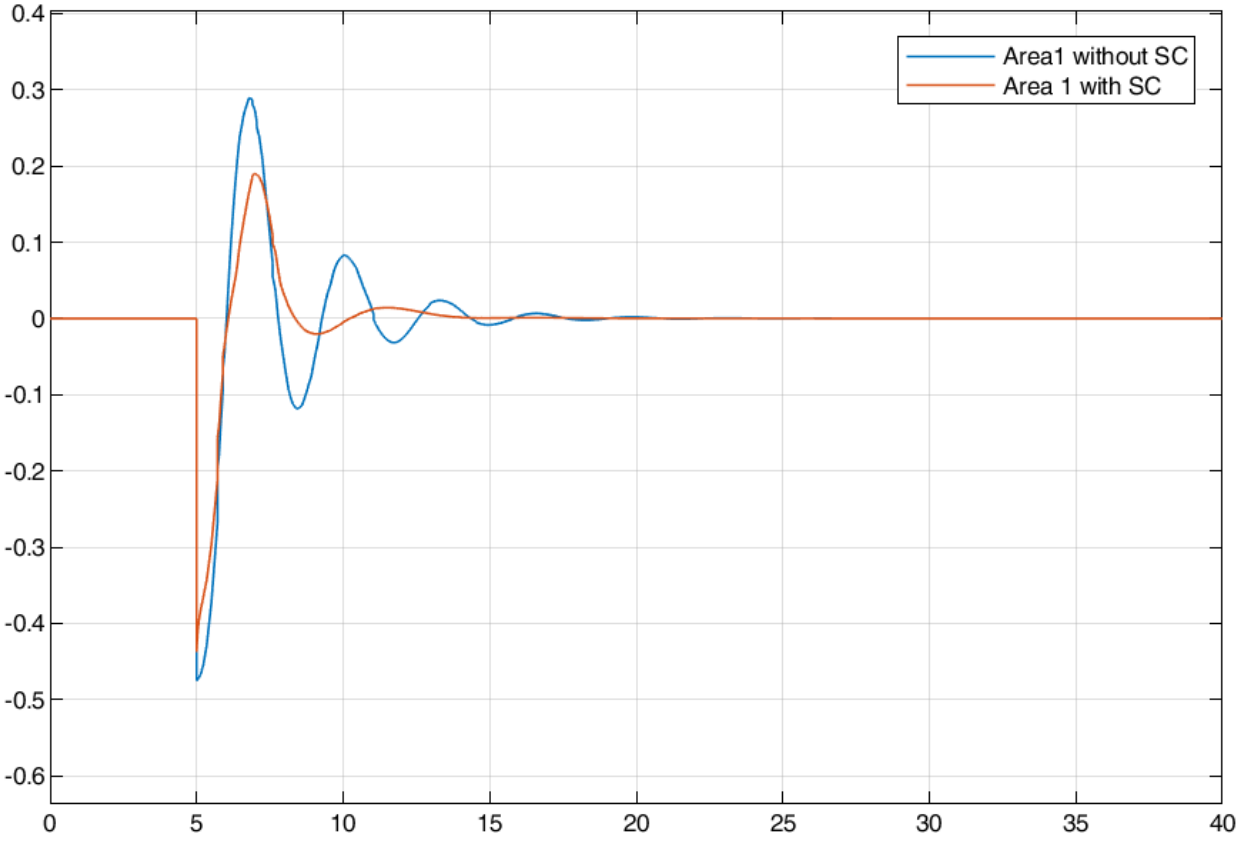
Area1 without SC
Area 1 with SC
0.4
0.3
0.2
0.1
0
-0.1
-0.2
-0.3
-0.4
-0.5
-0.6
0
5
10
15
20
25
30
35
40

(a) RoCoF

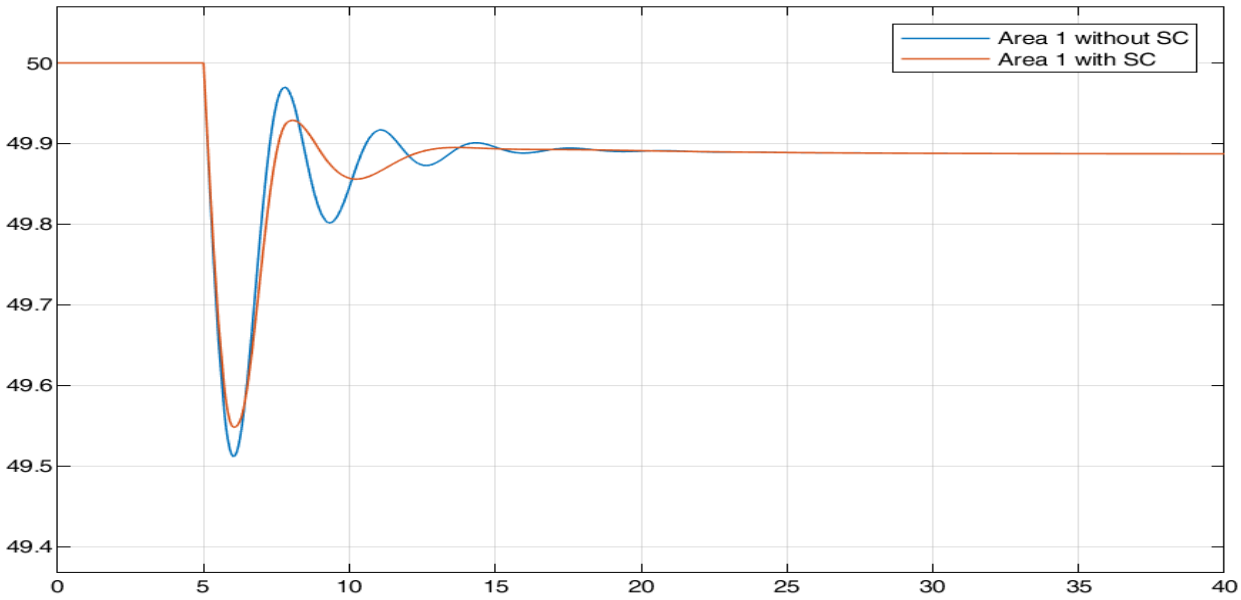

(b) Frequency Response

Figure 5.2 *Area 1's Dynamic Behavior With and Without SC for 20% PV Penetration.*

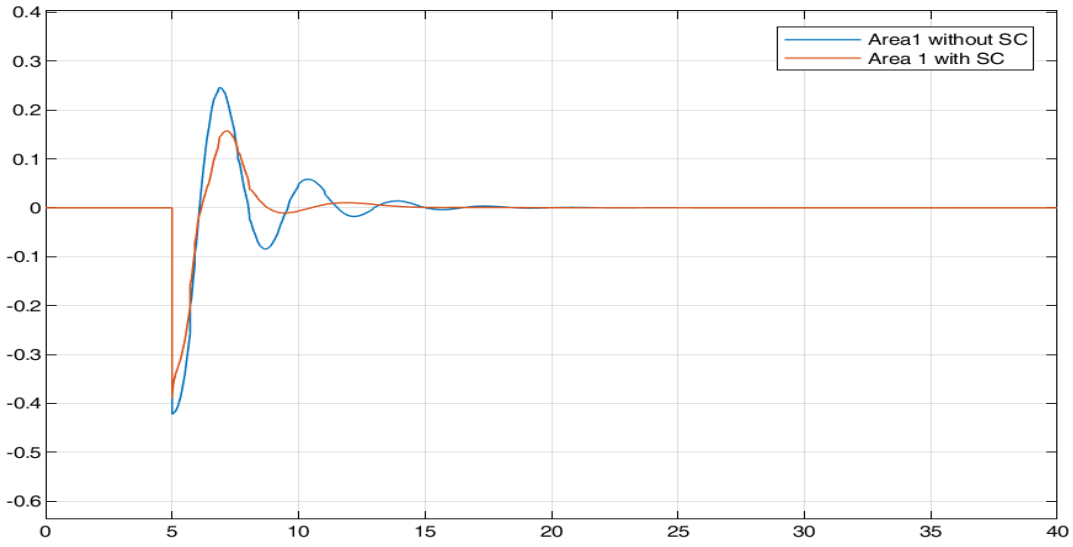

(a) RoCoF

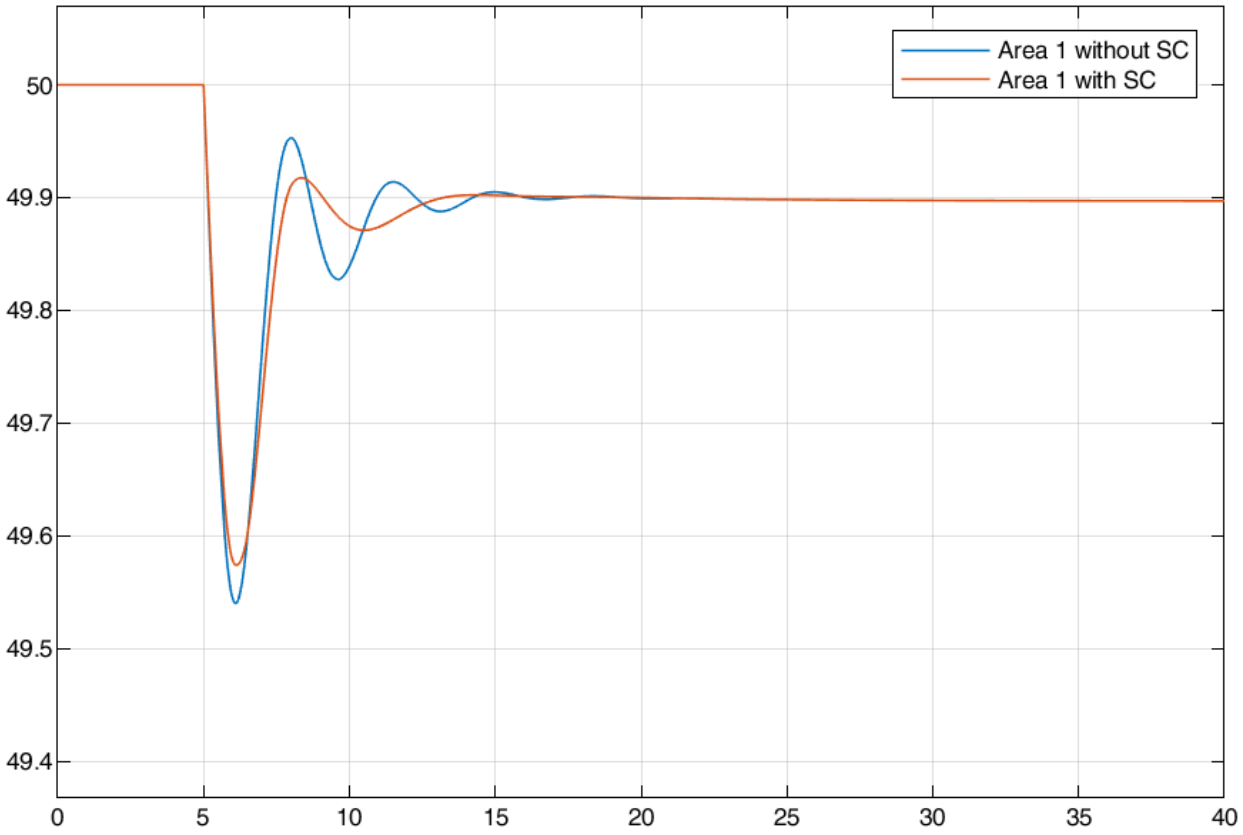

(b) Frequency Response

Figure 5.3 *Area 1's Dynamic Behavior With and Without SC for 10% PV Penetration.*

B. Case 2

In this instance, the battery's role in enhancing PFR is examined. Two situations are examined:

1) Area 1 with only supercapacitor (without battery)
2) Area 1 with both supercapacitor and battery (HESS)

In this research, the steady-state frequency deviation limit is established at ±0.05 Hz. The Simulation shows that, with a 160 MW generation outage, the actual steady-state frequency is 49.87 Hz. Equations (4.30) – (4.32) can be used to implement these values, yielding the results that λ_{area1} is 1230.77MW/Hz and λ_{target} is 3200 MW/Hz. Consequently, the battery's capacity $P_{Battery}$ can be determined by:

$$P_{Battery} = 0.001 \times 50 \times (3200 - 1230.77) = 98.46MW \qquad (5.2)$$

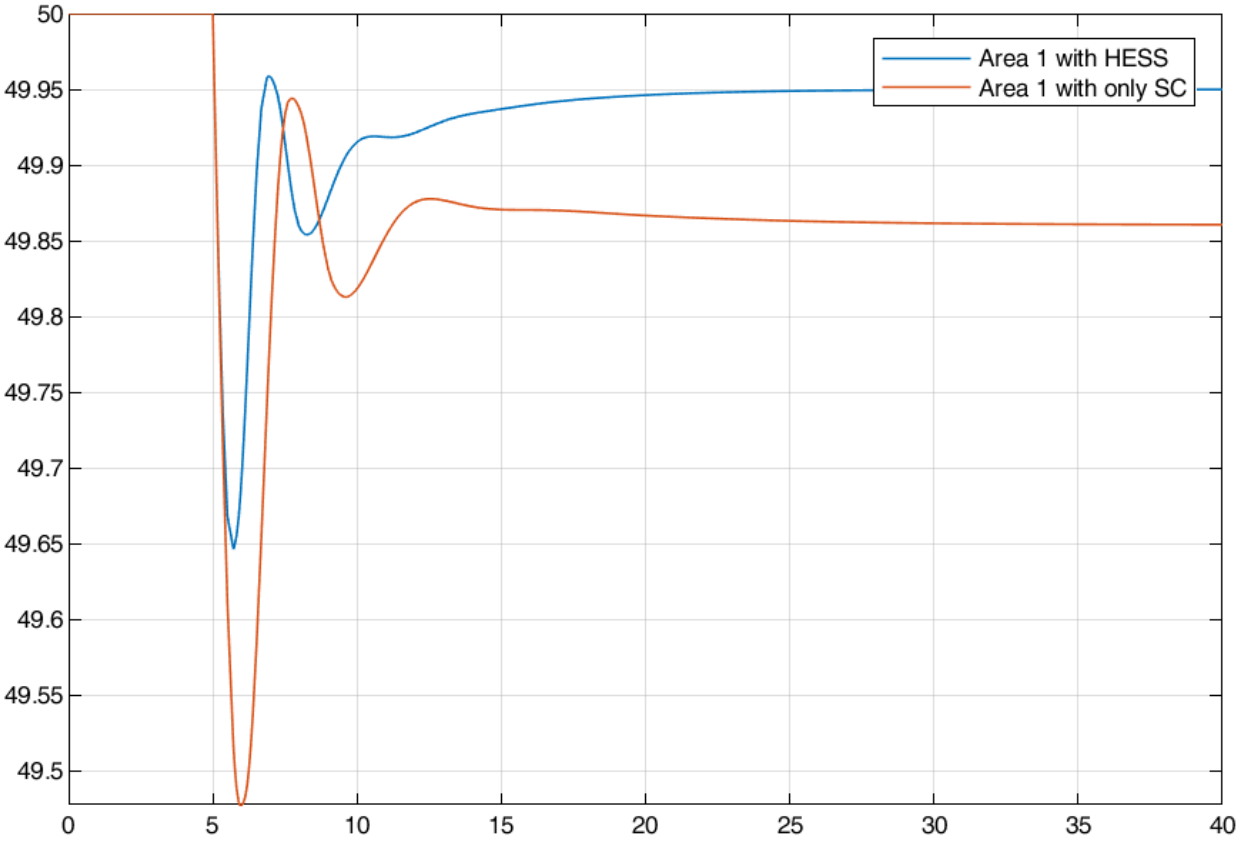

Figure 5.4 *Frequency Response of Area 1 for 30% PV Penetration With Supercapacitor (SC) Alone and Area 1 With Both SC and Battery.*

Figure 5.4 displays frequency response of Area 1 with the HESS and Area 1 with only SC. It has been noted that the sized battery allows the steady-state frequency to be adjusted up to 49.95Hz. Additionally, dynamic performance is enhanced during the process of adjustment. The frequency

nadir is changed from 49.47 Hz to 49.65 Hz during the generation outage. As a result, employing the battery enhances PFR performance.

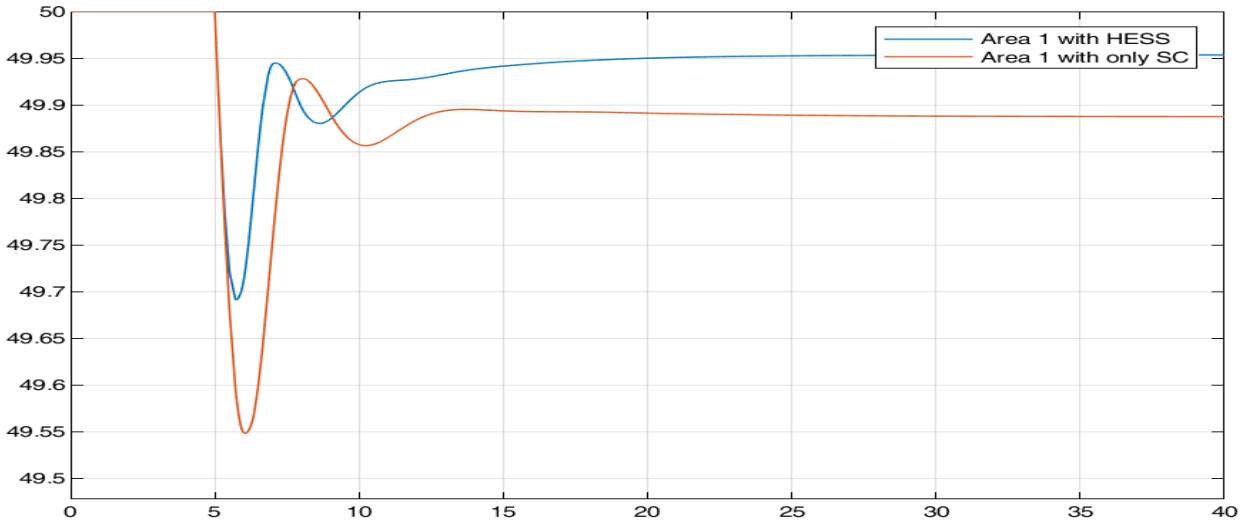

Figure 5.5 *Area 1's Frequency Response With HESS and Area 1 With Only the Supercapacitor (SC) for 20% PV Penetration.*

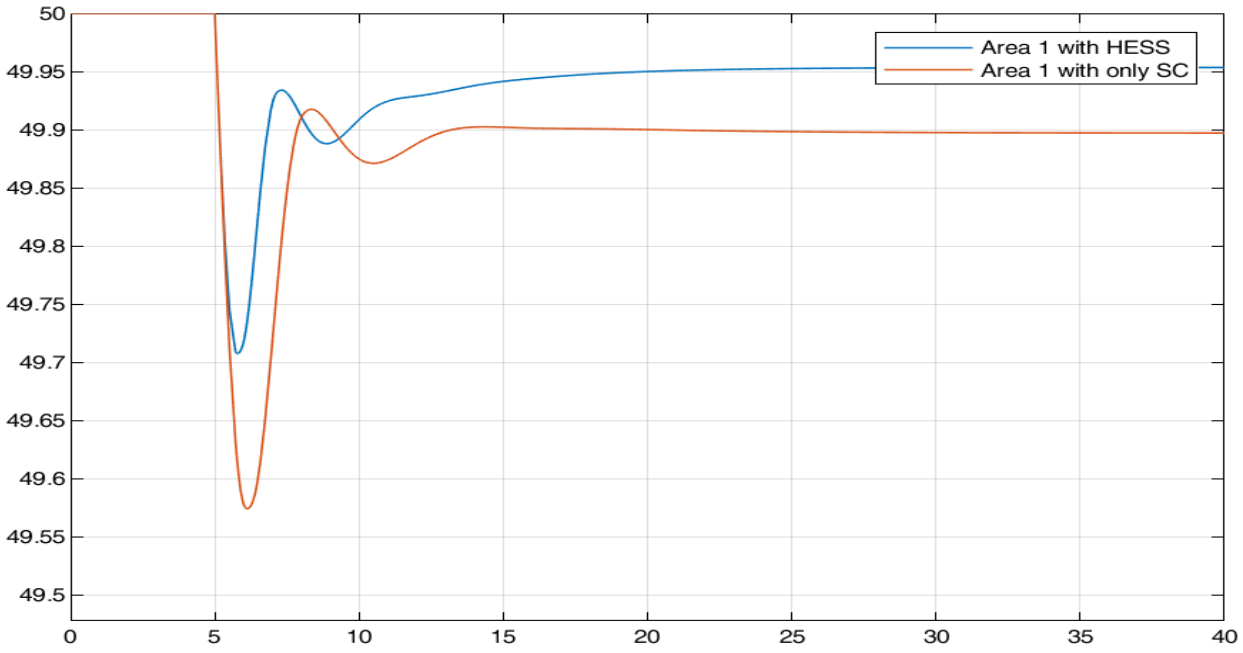

Figure 5.6 *Area 1's Frequency Response With HESS and Area 1 With Only the Supercapacitor (SC) for 10% PV Penetration.*

C. Case 3

In this instance, the HESS's contribution to a power system with secondary control improved dynamic response is examined.

Two situations are contrasted:

1) Area 1 with Hybrid Energy Storage System (HESS);

2) Area 1 without Hybrid Energy Storage System (HESS).

The P controller amplifies the input signal, while the I controller integrates it. As a result, as the P/I gain values grow for the identical input signals, the PI controller's output will also increase. This raises the power compensation that the battery offers.

Controller tuning							
Time Constant of the high pass filter				30s			
Low-frequency part				High- frequency part			
PI controller				PI controller			
K_p	0.5	K_I	0.5	K_P	1	K_I	0.5
Time constant of delay		2s		Time constant of delay		2s	

Table 5 *Adjusting the Controller for the Filtered ACE Technique*

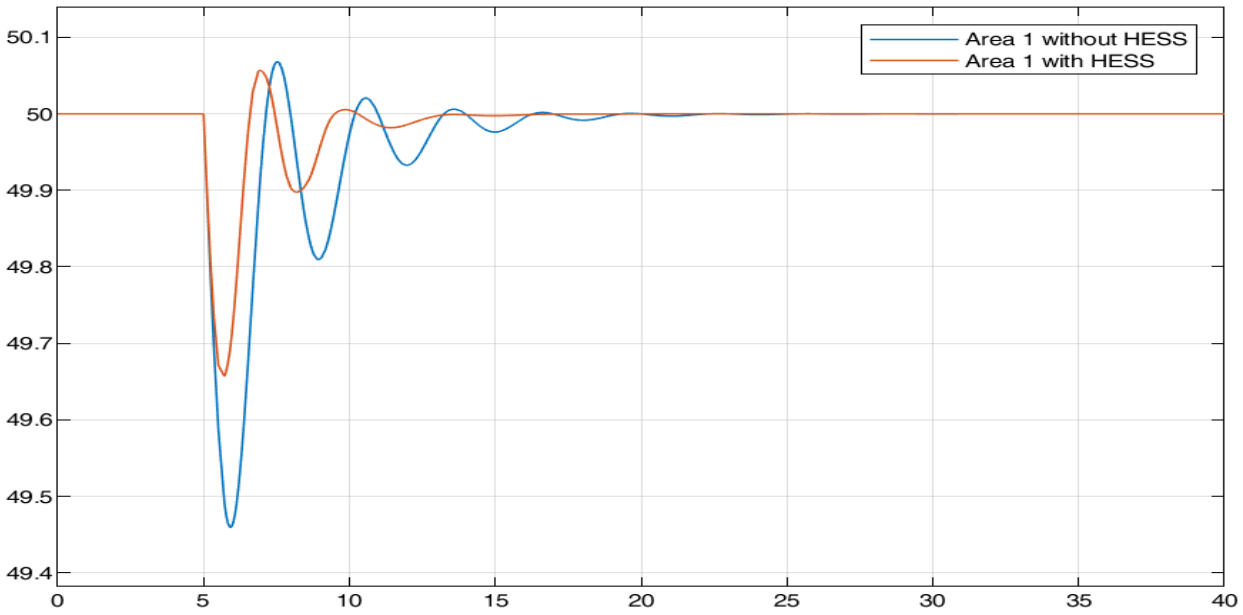

(a) Frequency Response

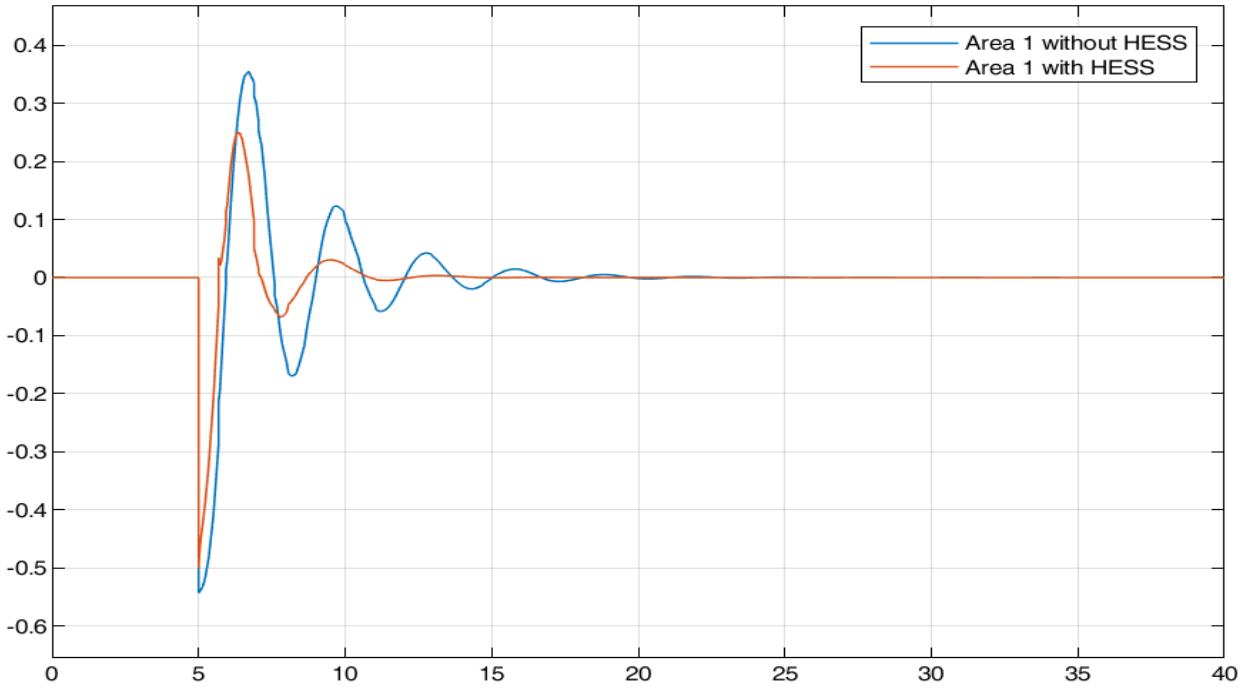

(b) RoCoF

Figure 5.7 *Frequency Response of Filtered ACE Control of Area 1 Without/With HESS for 30% PV Penetration.*

Figure 5.7 displays Area 1 frequency responses with and without the HESS. Following the application of the filtered ACE control approach, the steady state frequency is adjusted to 50 Hz. Furthermore, the lowest extreme value of frequency variation in Area 1 without the HESS is 49.44 Hz as shown in Fig. 5.7(a). These value is raised to 49.68 Hz with the use of the HESS. Additionally, it takes approximately 25 seconds in scenario 1 to recover from the disturbance, whereas in scenario 2 only 13 seconds were used. Furthermore, during the course of change, a notable decrease in frequency deviations is seen. Furthermore, the stability of this system is improved and the maximum value of RoCoF is lowered from Fig. 5.7(b). As a consequence, the HESS significantly improves the system's LFC.

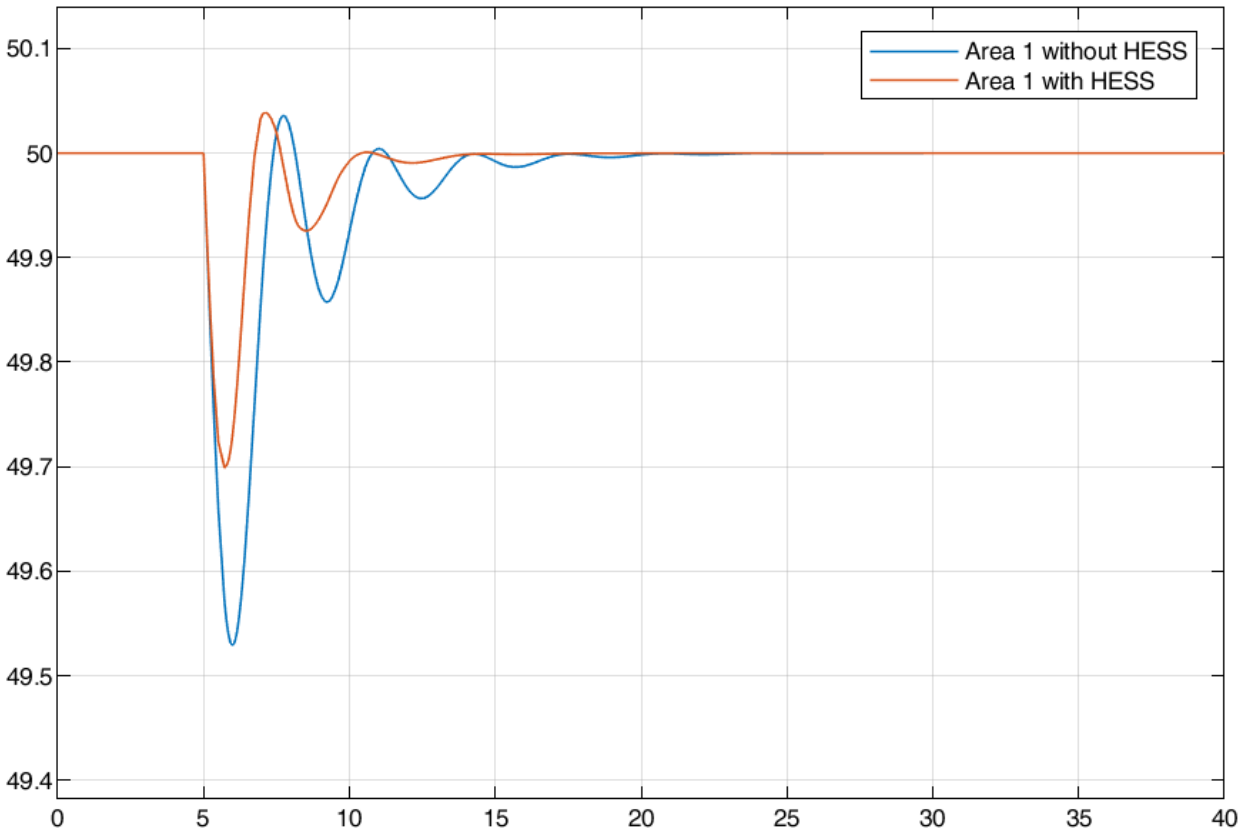

(a) Frequency Response

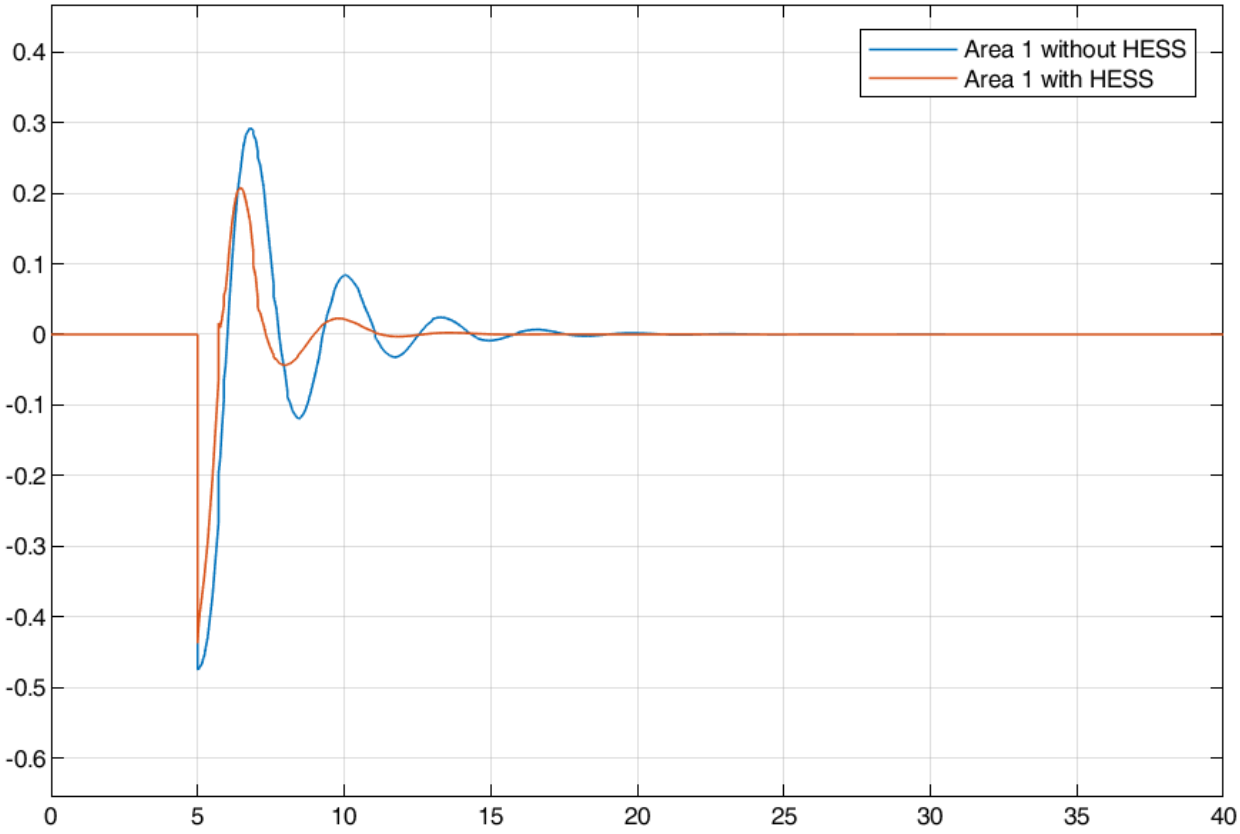

(b) RoCoF

Figure 5.8 *Frequency Response of Filtered ACE Control of Area 1 Without/With HESS for 20% PV Penetration.*

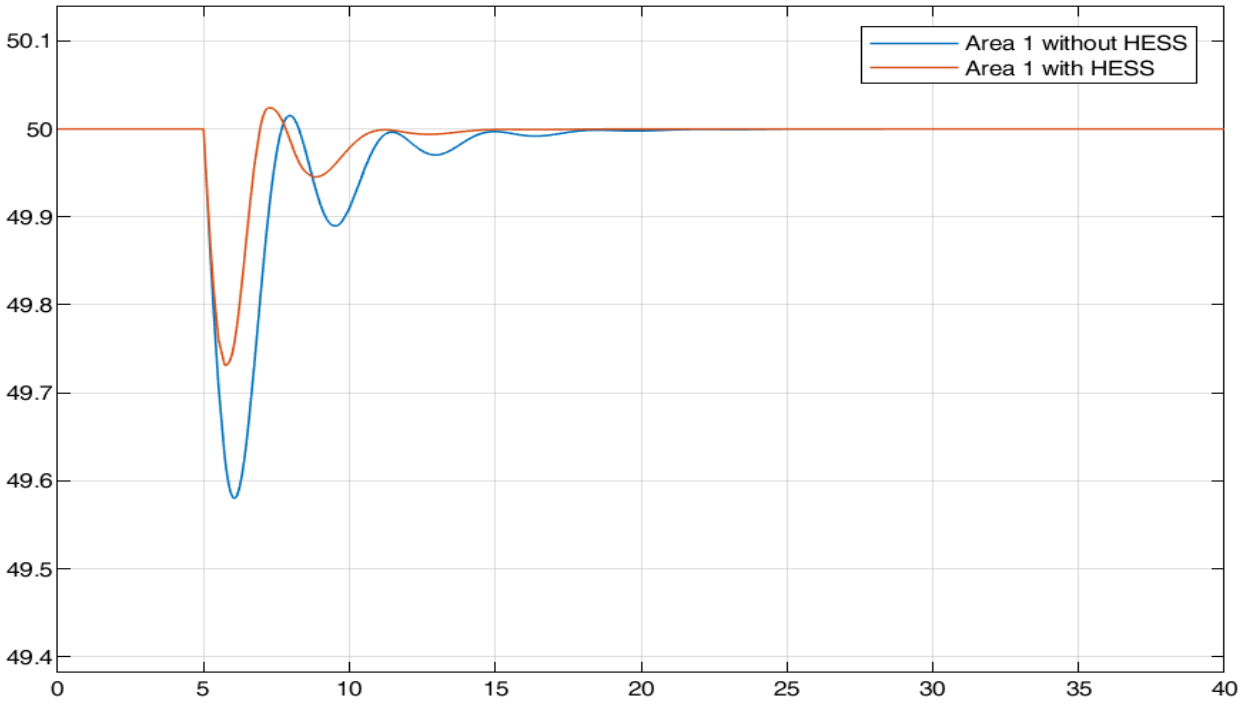

(a) Frequency Response

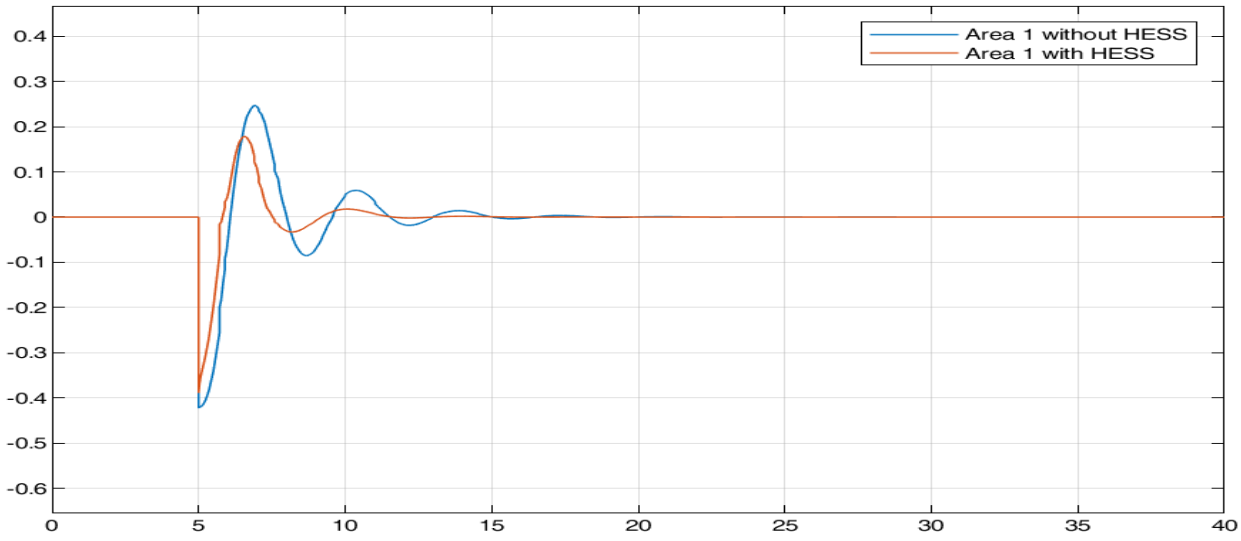

(b) RoCoF

Figure 5.9 *Frequency Response of Filtered ACE Control of Area 1 Without/With HESS for 10% PV Penetration.*

5.2 Mitigating Over Frequency Events Using a Supercapacitor- Battery Hybrid Energy Storage System

In power systems, frequency stability is a key indicator of the balance between generated power and consumer demand. While much attention is often given to load increase scenarios and under frequency events, sudden load decreases can be equally disruptive, causing a rapid rise in system frequency. This over frequency condition occurs when the generation momentarily exceeds the reduced demand, resulting in excess energy within the system. If not quickly mitigated, it can lead to serious consequences such as generator tripping, equipment damage, or system instability.

To address this challenge, Hybrid Energy Storage Systems (HESS) which combine supercapacitors and batteries offer a highly effective solution. The supercapacitor component provides a fast-acting response, capable of absorbing sudden bursts of excess energy within milliseconds, while the battery offers deeper energy absorption over a longer time frame. Together, they ensure both rapid frequency containment and sustained stabilization.

A. Case 1

In this instance, the supercapacitor's role in IR enhancement is discussed. Two scenarios are contrasted: 1) Area 1 without supercapacitor; 2) Area 1 with supercapacitor.

As was previously said, RoCoF needs to be kept under 0.5 Hz/s. The Simulation shows that when the load decreases by 160 MW happens the value of RoCoF is 0.543 Hz/s.

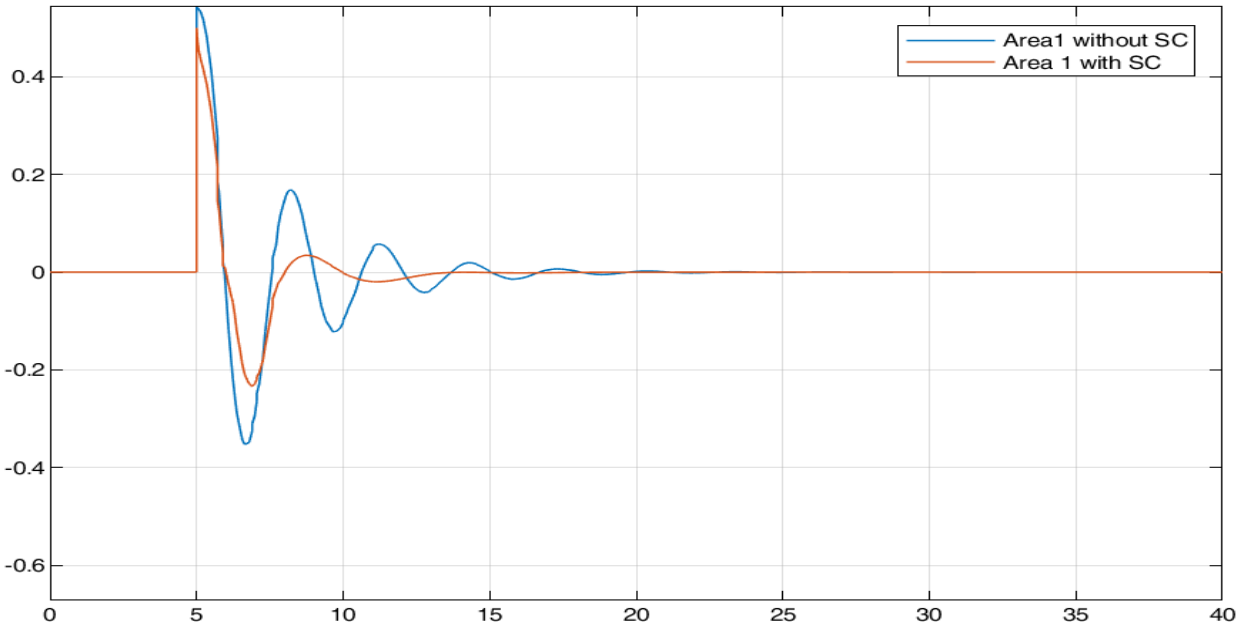

(a) RoCoF

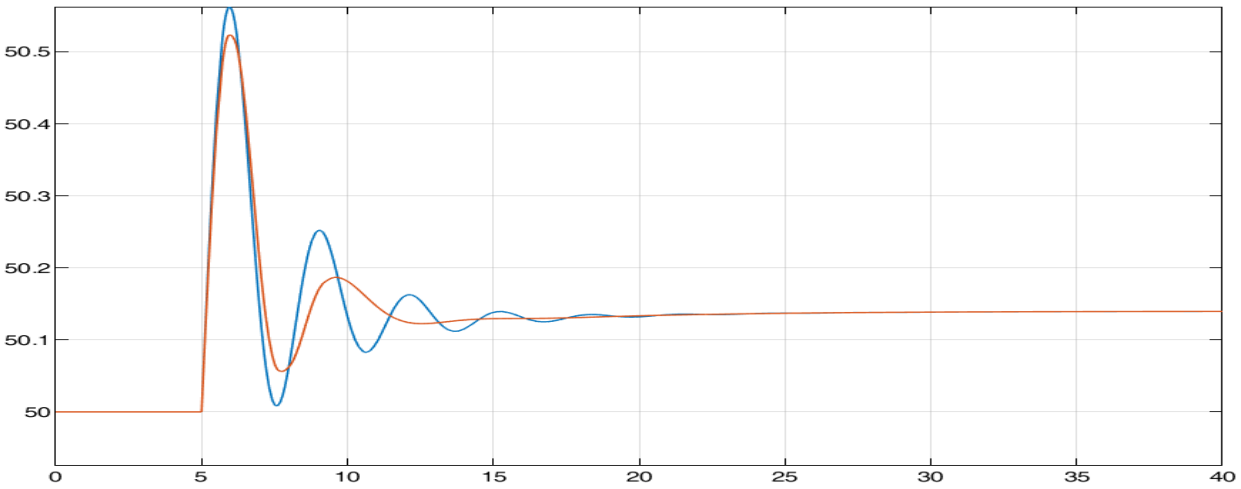

(b) Frequency Response

Figure 5.10 *Area 1's Dynamic Response Without/With SC for 30% PV Penetration.*

Figure 5.10 shows the system frequency and RoCoF dynamic performance. The upper frequency of Area 1 without HESS during the load disturbance is approximately 50.56 Hz, as shown in Fig. 5.10 (b). Following the supercapacitor's implementation, this value is changed to 50.53 Hz, and the supercapacitor provide a 0.03 Hz improvement.

The required capacity of the supercapacitor is determined using the absolute value of RoCoF, which is 0.543 Hz/s, as shown in Fig. 5.10(a), when dealing with load decrease of 160 MW. Once the supercapacitor is used, the associated value can be changed to 0.5 Hz/s. As a result, the impact of the lower inertia constant is shown. Furthermore, it can be said that the supercapacitor can successfully improve IR's dynamic performance.

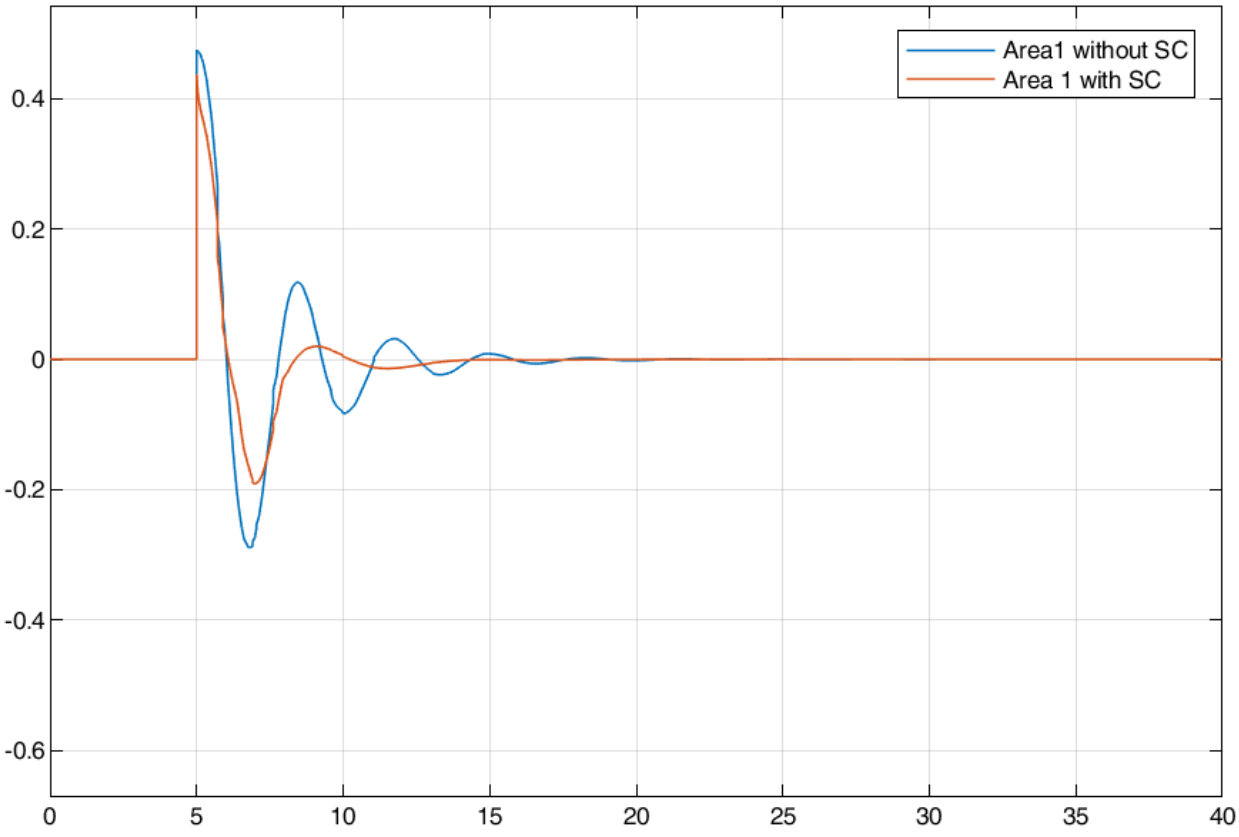

(a) RoCoF

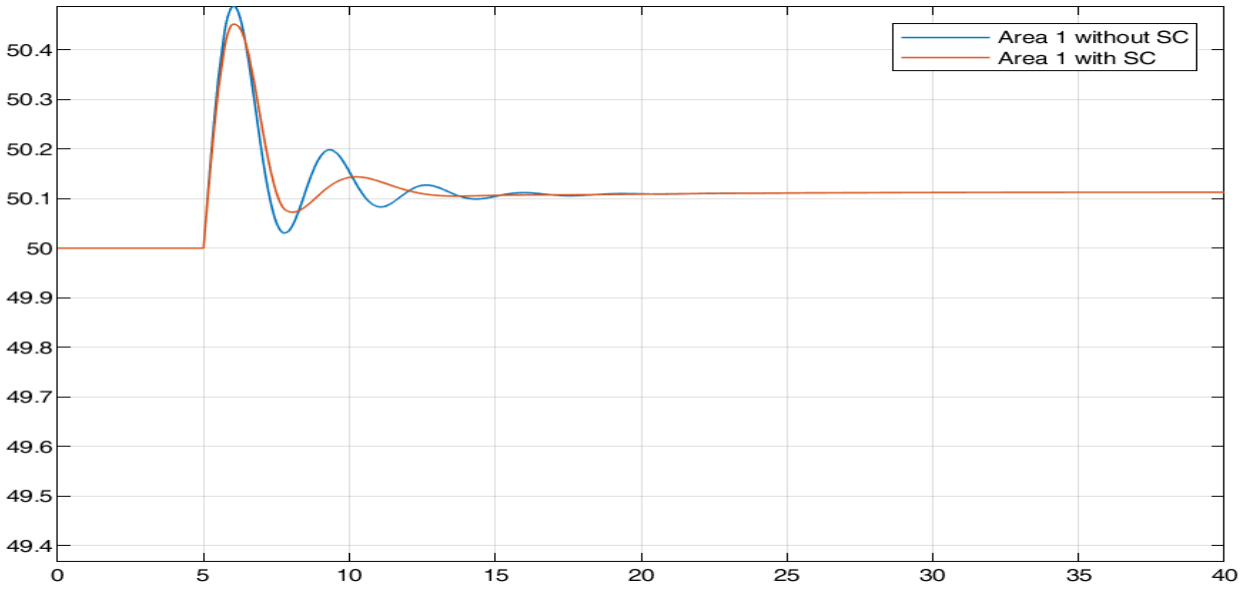

(b) Frequency Response

Figure 5.11 *Area 1's Dynamic Response Without/With SC for 20% PV Penetration.*

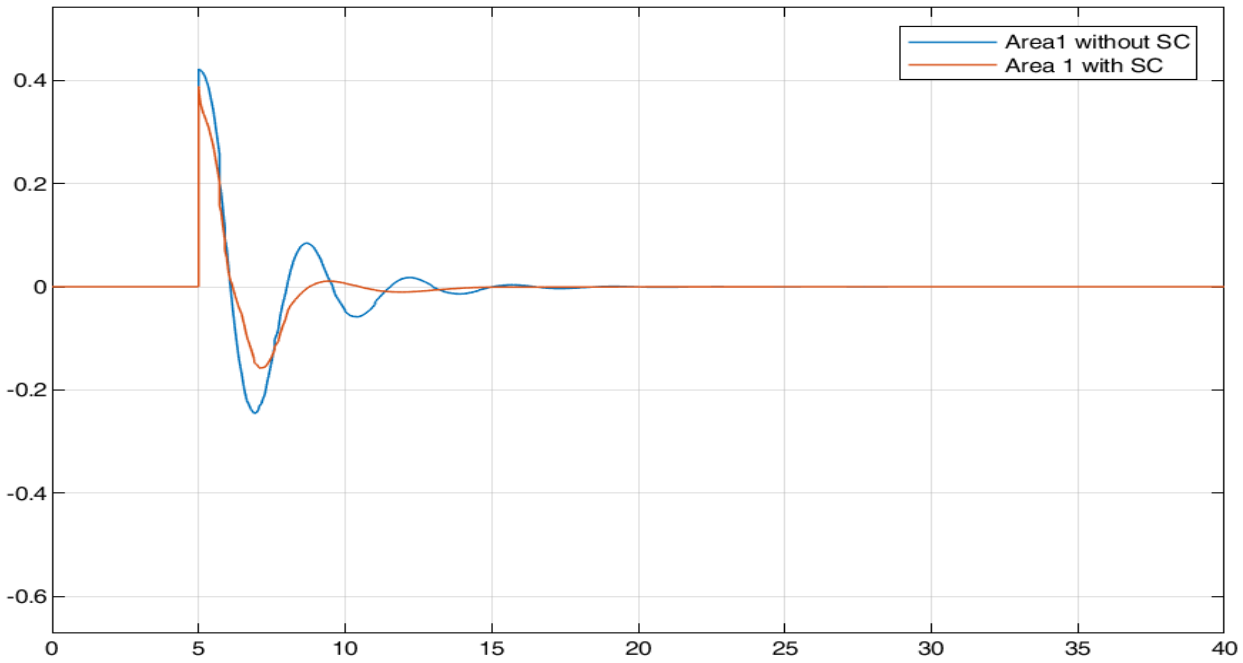

(a) RoCoF

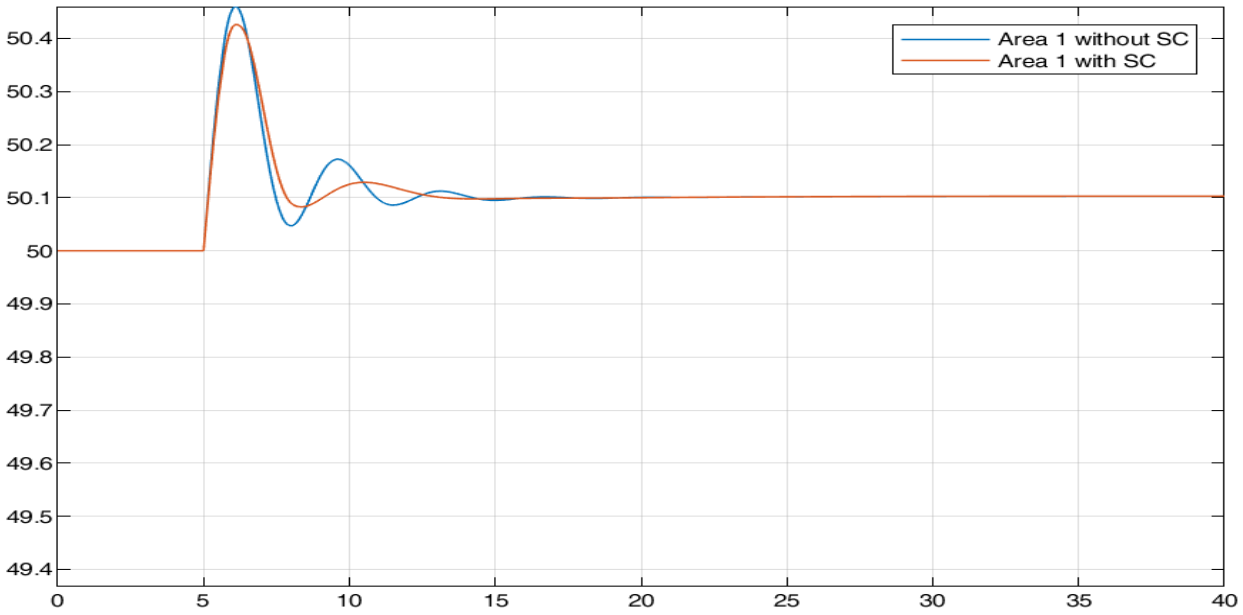

(b) Frequency Response

Figure 5.12 *Area 1's Dynamic Response Without/With SC for 10% PV Penetration.*

B. Case 2

In this instance, the battery's role in enhancing PFR is examined. Two situations are examined: 1) Area 1 without the battery (with the supercapacitor only); 2) Area 1 with the HESS

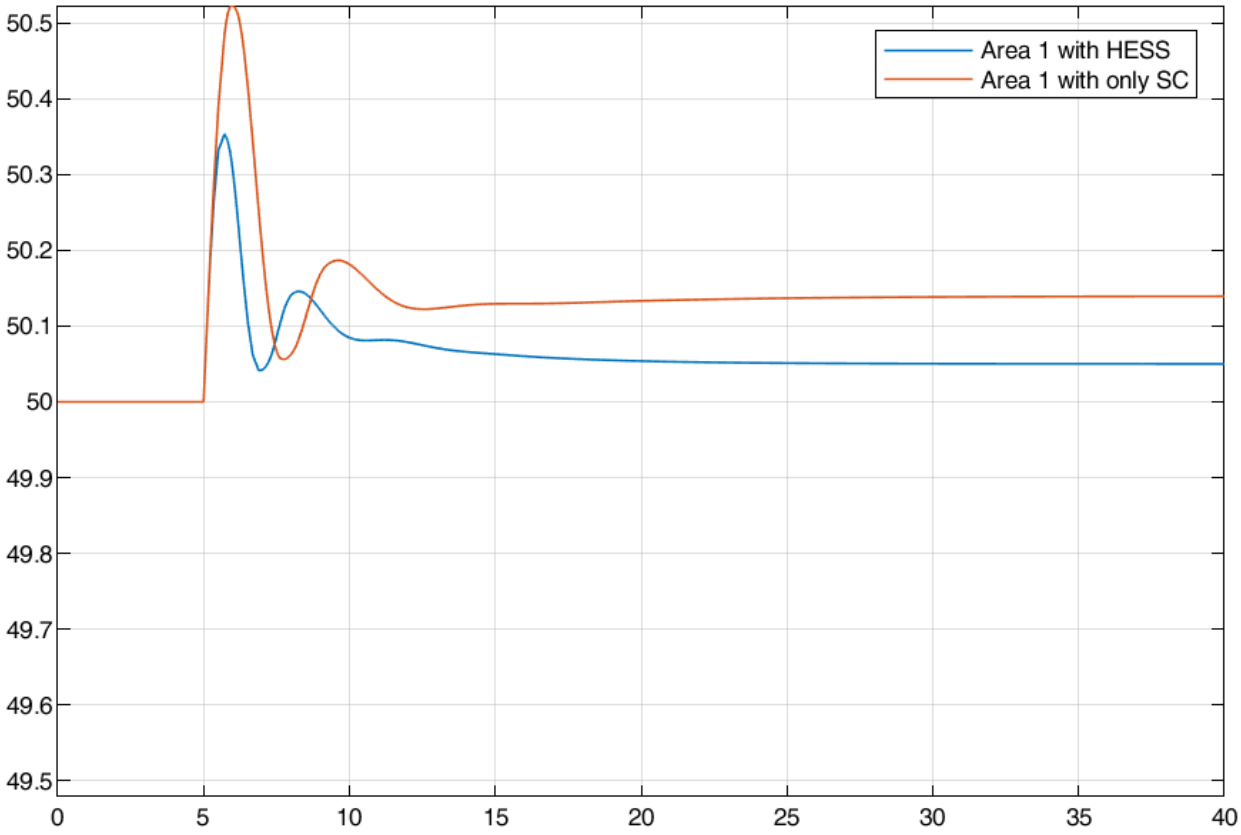

Figure 5.13 *Area 1's Frequency Response With Only the Supercapacitor (SC) and With the HESS for 30% PV Penetration.*

In this research, the steady-state frequency deviation limit is established at ±0.05 Hz. The Simulation shows that, with a 160 MW decrease in total load demand, the actual steady-state frequency is 50.13 Hz.

Figure 5.13 displays the frequency responses for Area 1 with only SC and Area 1 with the HESS. It has been noted that the sized battery allows the steady-state frequency to be adjusted up to 50.05Hz. Additionally, dynamic performance is enhanced during the process of adjustment. The frequency peak is changed from 50.53 Hz to 50.35 Hz during the load demand rise. As a result, employing the battery enhances PFR performance.

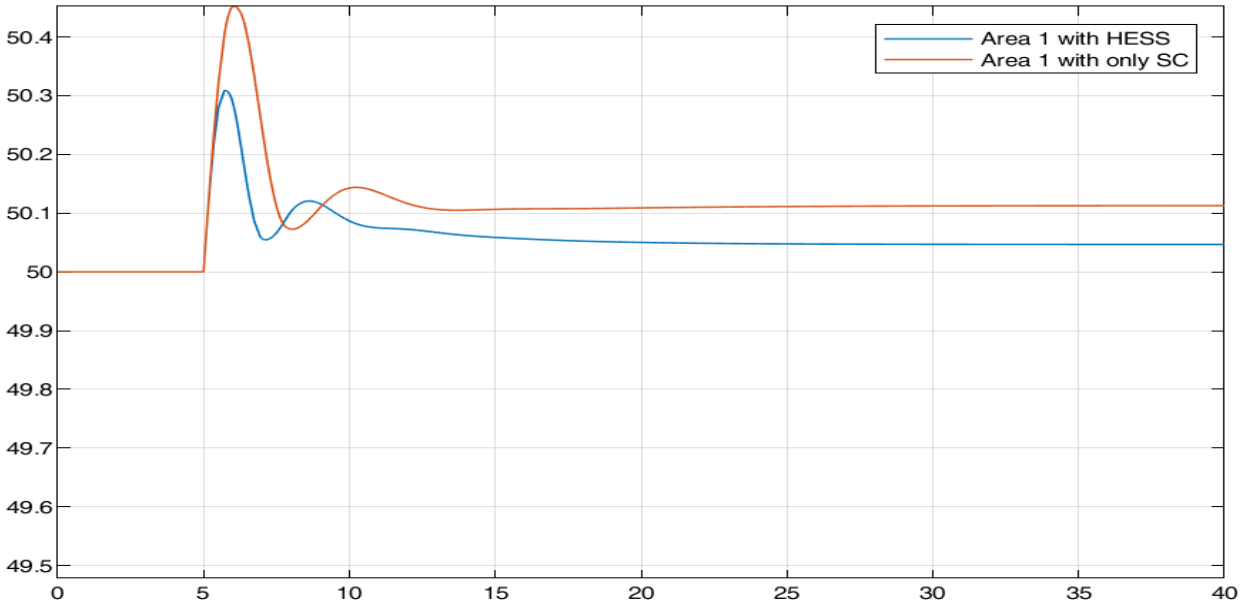

Figure 5.14 *Area 1's Frequency Response With Only the Supercapacitor (SC) and With the HESS for 20% PV Penetration.*

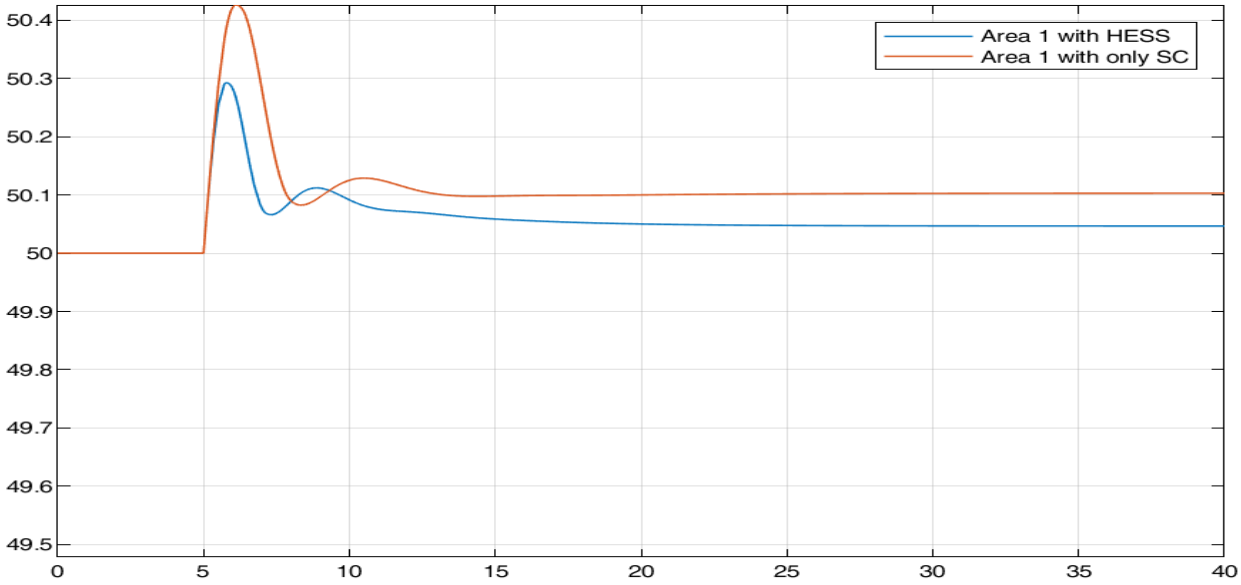

Figure 5.15 *Area 1's Frequency Response With Only the Supercapacitor (SC) and With the HESS for 10% PV Penetration.*

C. Case 3

In this instance, the HESS's contribution to the system with secondary control improved dynamic response is examined. Two situations are contrasted: 1) Area 1 without the HESS; 2) Area 1 with the HESS.

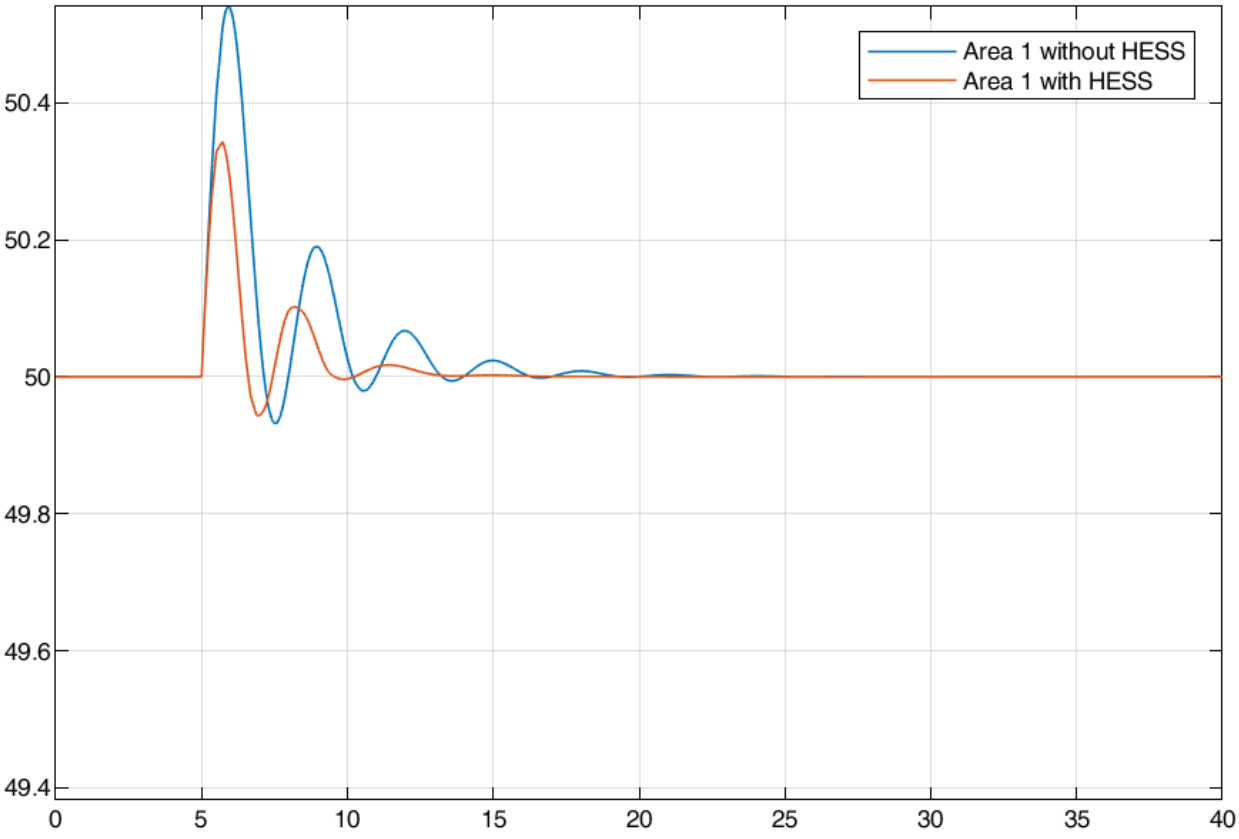

(a) Frequency Response

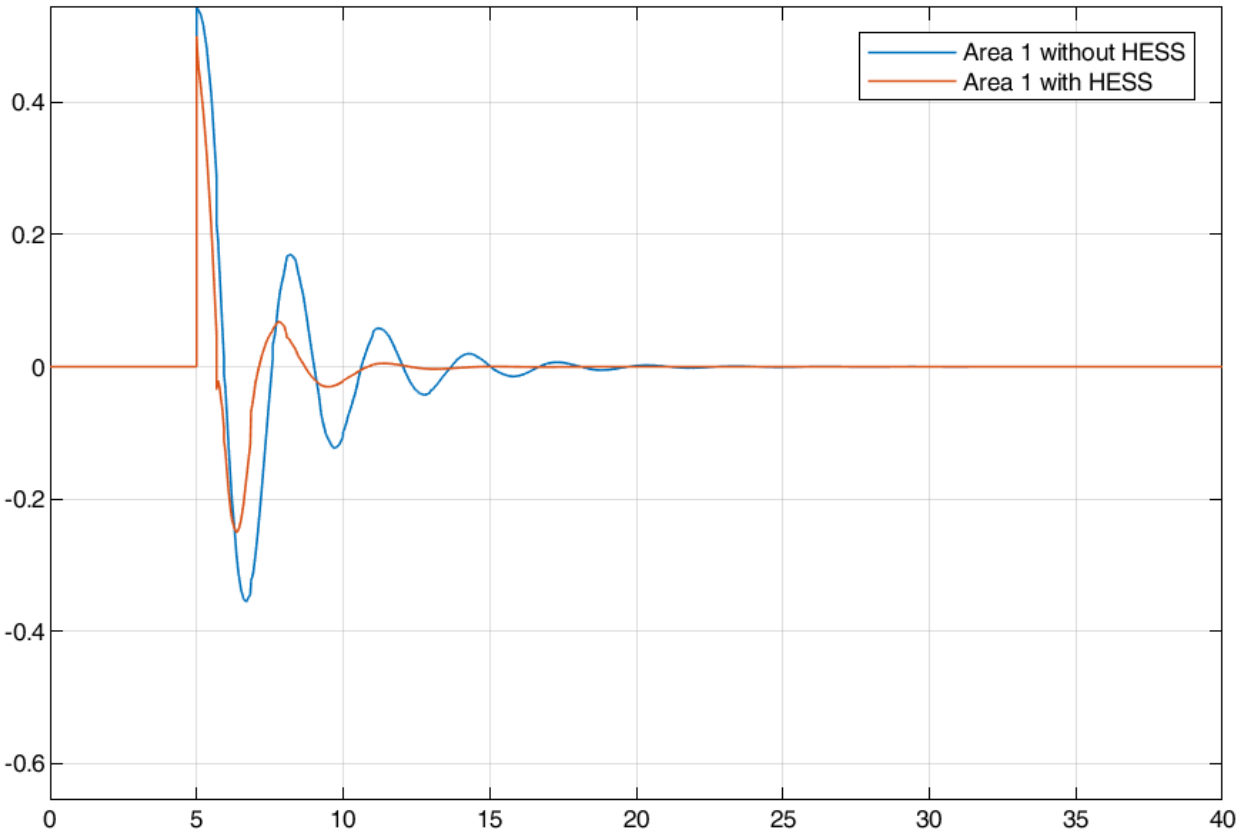

(b) RoCoF

Figure 5.16 *Frequency Response of Filtered ACE Control of Area 1 Without/With HESS for 30% PV Penetration.*

Figure 5.16 displays Area 1 frequency responses with and without the HESS. Following the application of the filtered ACE control approach, the steady state frequency is adjusted to 50 Hz. Furthermore, the upper extreme value of frequency variation in Area 1 without the HESS is 50.56 Hz as shown in Fig. 5.16(a). These value is lowered to 50.32 Hz with the use of the HESS. Additionally, it takes approximately 25 seconds in scenario 1 to recover from the disturbance, whereas in scenario 2 only 13 seconds were used. Furthermore, during the course of change, a notable decrease in frequency deviations is seen. Furthermore, the stability of this system is improved and the maximum value of RoCoF is lowered from Fig. 5.16(b). As a consequence, the HESS significantly improves the system's LFC.

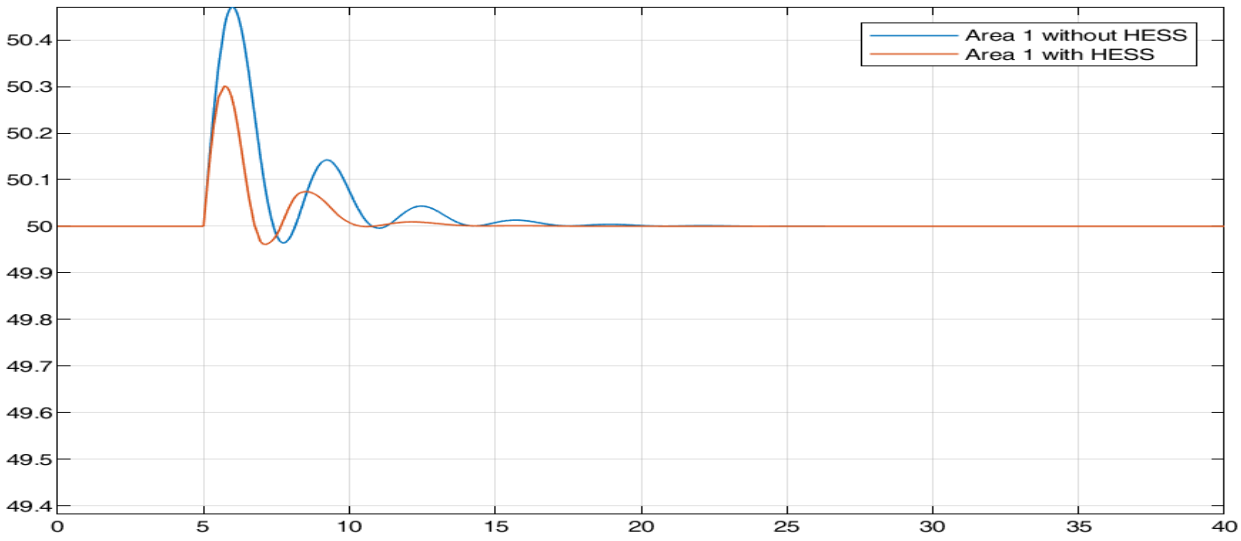

(a) Frequency Response

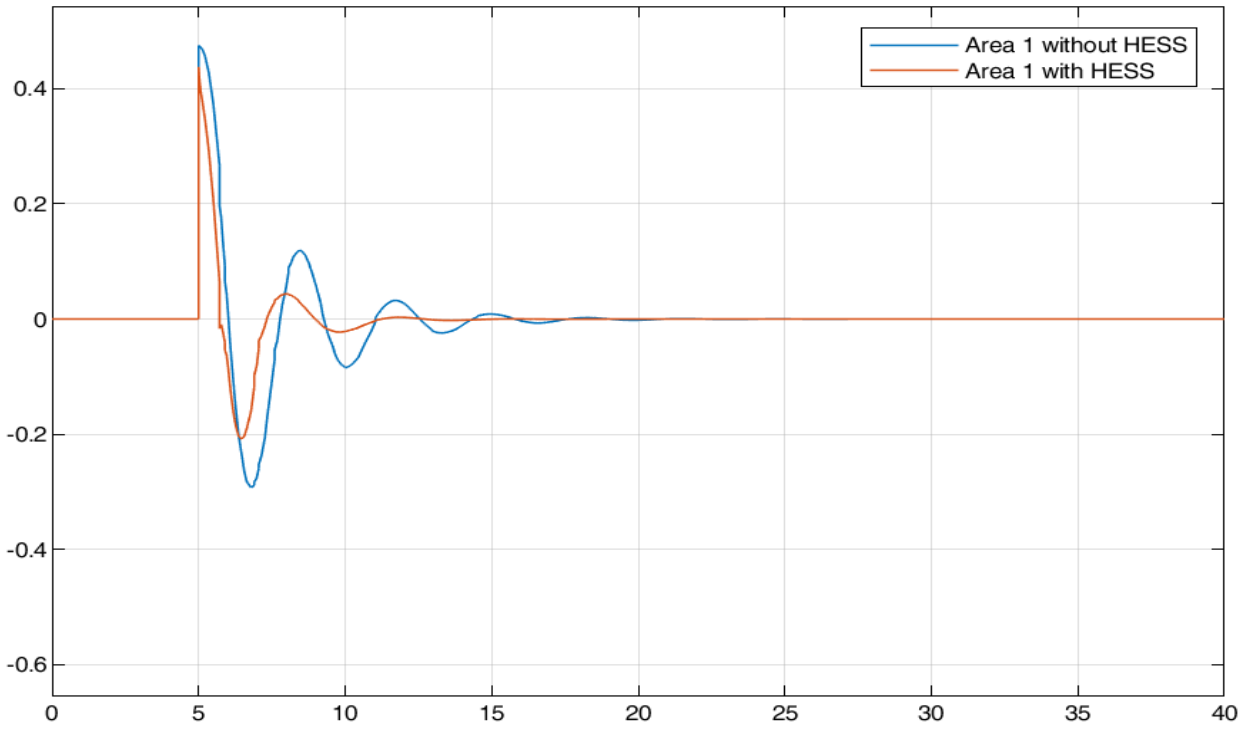

(b) RoCoF

Figure 5.17 *Frequency Response of Filtered ACE Control of Area 1 Without/With HESS for 20% PV Penetration.*

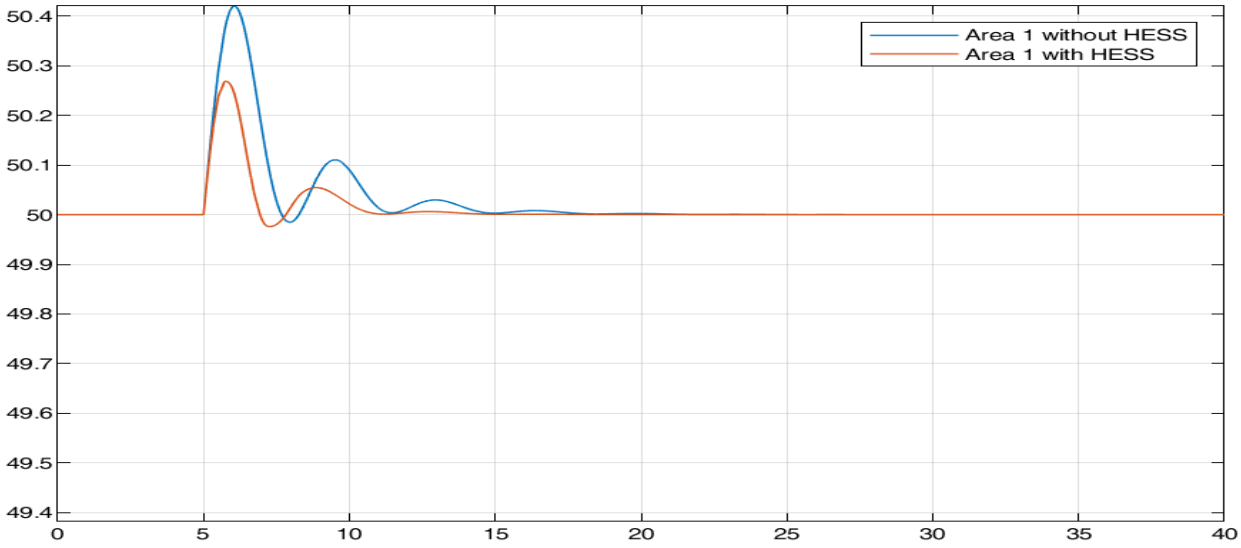

(a) Frequency Response

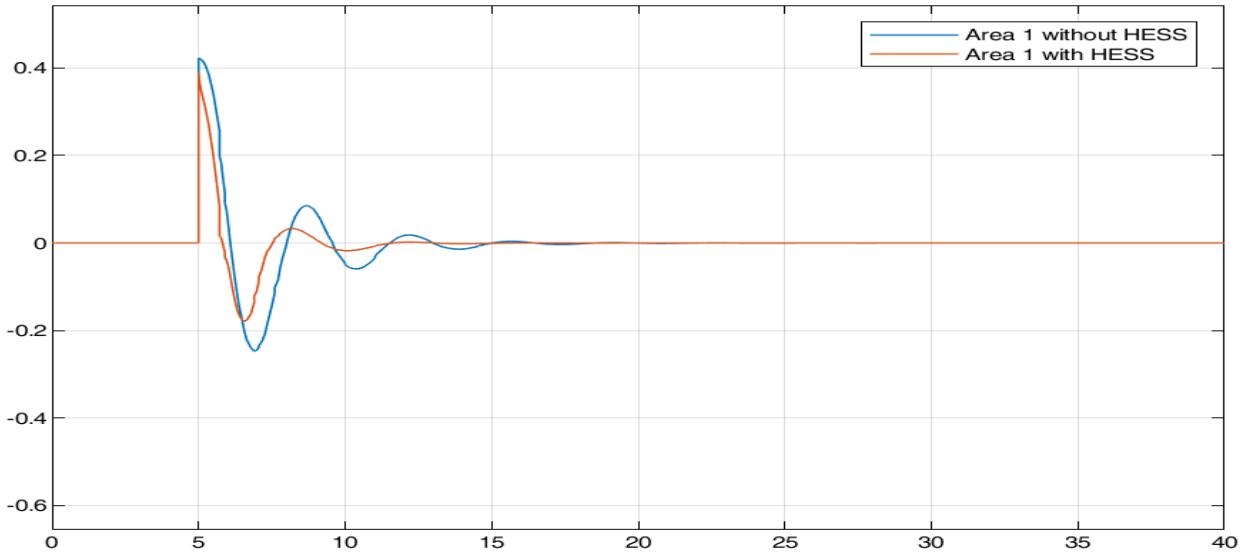

(b) RoCoF

Figure 5.18 *Frequency Response of Filtered ACE Control of Area 1 Without/With HESS for 10% PV Penetration.*

6 Conclusion and Recommendation

6.1 Conclusion

The problems caused by less system inertia are examined in this research. In this scenario, system stability is at risk and system dynamics will be compromised when power fluctuations occur. The supercapacitor and battery were utilized together in a HESS to provide the inertial response and primary frequency control respectively, in order to enhance load frequency control performances and comply with the applicable operation standards.

First, using the mathematical techniques discussed in this research and the application of the HESS sizing approach, the role of the suggested Hybrid Energy Storage System control structure employed for IR and PFR is examined under system contingencies. It is shown that the suggested Hybrid Energy Storage System approach can greatly enhance Load Frequency Control (LFC) performances, and simulation results illustrate the impact of the reduced inertia constant.

The filtered ACE approach is then applied in the Hybrid Energy Storage System (HESS) to improve secondary frequency control performance under typical power variation conditions. The suggested HESS method is confirmed to be highly successful in improving system frequency dynamics based on the previously mentioned works.

6.2 Recommendations

Based on the findings of this study, the integration of Hybrid Energy Storage Systems is strongly recommended as a practical and effective solution for enhancing frequency regulation in renewable-rich power systems. System operators, particularly in hydropower-dominated grids with increasing photovoltaic penetration, should consider deploying HESS to compensate for reduced inertia and improve frequency resilience.

It is also recommended that HESS control strategies explicitly differentiate between fast and slow frequency support requirements. Assigning inertial and primary frequency control tasks to supercapacitors and battery respectively and secondary frequency regulation to batteries ensures

efficient utilization of storage resources, reduces stress on battery systems, and improves overall control performance.

In addition, adopting filtered ACE-based secondary control strategies can further enhance system performance by minimizing unnecessary control actions and reducing frequency oscillations. This approach offers a more stable and coordinated response, especially under typical operating conditions with continuous power variations.

6.3 Future Work

This research was conducted using a two-area interconnected power system model, which provides valuable insights but also presents opportunities for further investigation. Future studies should extend the proposed HESS framework to more complex multi-area power system models in order to validate its scalability and robustness under diverse network configurations.

Moreover, the current study employed a generic energy storage model. Future research should incorporate detailed technology-specific models for batteries and supercapacitors, including degradation effects, efficiency variations, and hydro constraints. This would enhance the practical relevance and accuracy of the results.

The battery sizing methodology adopted in this research focused primarily on system contingency scenarios. Future work should investigate optimal battery sizing strategies under prolonged power fluctuations and sustained frequency regulation requirements. Incorporating state-of-charge (SoC) constraints into the control design will be essential to ensure reliable long-term operation and prevent excessive battery degradation.

Finally, further studies should explore parameter sensitivity analysis for key HESS design variables such as battery capacity, power rating, and energy sharing ratio between the battery and supercapacitor. The development of adaptive and intelligent control algorithms capable of responding to real-time grid conditions and SoC dynamics will play a crucial role in advancing the deployment of HESS in large-scale interconnected power systems.

7 References

1. A. Oudalov, D. C. (2007, August). Optimizing a Battery Energy Storage System for Primary Frequency Control. *IEEE Trans. Power Syst., 22*, 1259-1266.
2. A. Oudalov, D. C. (2007., August). Optimizing a Battery Energy Storage System for Primary Frequency Control. *IEEE Trans. Power Syst., 22*, 1259-1266.
3. C. L. (1995, September). Effect of battery energy storage system on load frequency control considering governor deadband and generation rate constraint. *IEEE Transactions on Energy Conversion*, 555-561.
4. D. K. (1993, September). Battery energy storage for frequency regulation in an island power system. *IEEE Trans. Energy Convers., 8*, 455-459.
5. F. D.-G. (2012, May). A review of energy storage technologies for wind power applications. *Renewable and Sustainable Energy Reviews, 10*, 2154-2171.
6. G. D. (2012, October). Dynamic frequency control support by energy storage to reduce the impact of wind and solar generation on isolated power system's inertia. *IEEE Trans. Sustain. Energy, 3*, 931-939.
7. H. I. (2008, June). Energy storage systems characteristics and comparisons. *Renewable and sustainable energy reviews, 12*, 1221-1250.
8. H. K. (1975, September). An optimal tracking approach to load-frequency control. *IEEE Trans. Power App. Syst., 94*, 1635-1643.
9. H. S. (1994). *Power System Analysis.* New York, NY, USA: McGraw-Hill Education, .
10. M.-u.-d. M. (2009, January). Super-capacitor based energy storage system for improved load frequency control. *Electric Power Systems Research, 79*, 226-233.
11. O. I. (1970., April). Optimum megawatt-frequency control of multiarea electric energy systems. *IEEE Trans. Power App. Syst.,*.
12. P. K. (1994). *Power Systems Stability and Control.* New York, NY, USA.

13. S. K. (2012). Load frequency control using battery energy storage system in interconnected power system. *2012 Third International Conference on Computing, Communication and Networking Technologies.*

14. V. K. (2014, June). Grid inertial response with lithium-ion battery energy storage systems. *IEEE Int. Symp. Ind. Electron. (ISIE)*, ,1813-1818.

15. Amano, H. e. (2012). Utilization of battery energy storage system for load frequency control toward large-scale renewable energy penetration. *Innovative Smart Grid Technologies (ISGT Europe).* 3rd IEEE PES International Conference and Exhibition on. IEEE.

16. Cohn, N. (1957. , Feb.). Some aspects of tie line bias control on interconnected power systems. *IEEE Trans. Power App. Syst, 75* , 1415-1436.

17. Dan Zhou, Z. Z. (2025, February). *An Integrated Strategy for Hybrid Energy Storage Systems to Stabilize the Frequency of the Power Grid Through Primary Frequency Regulation*.

18. Das, I. P. (2016, May). Fractional Order Fuzzy Control of Hybrid Power System with Renewable Generation Using Chaotic PSO. *ISA Transactions*, Pages 19–29.

19. Das, S. K. (2001). Battery energy storage for load frequency control of an interconnected power system. *Electric Power Systems Research, 58*, 179-185.

20. Das, S. K. (2003., January). Design of Load Frequency Controllers Using Genetic Algorithm for Two Area Interconnected Hydro Power System. *Electric Power Components & Systems,, 31*.

21. Deng, X., Sun, W., & Xiao, H. (2018,). Integrated Control Method of Battery Energy Storage Participating in Primary Frequency Regulation. *High Volt. Eng.* , 44, 1157–1165.

22. Dhivya, S. K. (2020., September). Improvement of transient response in grid-tied photovoltaic systems using virtual inertia. *IEEE smart grid., 22*, 1259-1266.

23. Elkasem, A., Kamel, S., Khamies, M., & Nasrat, L. (2024). Frequency regulation in a hybrid renewable power grid: An effective strategy. *Sci. Rep.* , 14, 33.

24. A. P. (2008, June). Energy control of supercapacitor/fuel cell hybrid power source. *Energy Conversion and Management, 49*, 1637-1644.

25. Ewart, N. N. (1975., August). Automatic generation control - performance under normal conditions. *Proc. IEEE*.

26. Feliachi, D. R. (2003). Decentralized load frequency control using LMI control toolbox. *Proceedings of the 2003 International Symposium on Circuits and Systems.*

27. Feng Zhu, X. Z. (2021, November). A Load Frequency Control Strategy Based on Disturbance Reconstruction for Multi-Area Interconnected Power Systems with Hybrid Energy Storage System. *7*, 8849–8861.

28. Gaber Magdy, E. A. (2018, December). Optimized Coordinated Control of LFC and SMES to Enhance Frequency Stability of a Real Multi-Source Power System Considering High Renewable Energy Penetration. *Protection and Control of Modern Power Systems, 3*.

29. H. H. Chen et al. (1995, September). Effect of battery energy storage system on load frequency control considering governor deadband and generation rate constraint. *IEEE Trans. Energy Convers., vol. 10*, 555-561.

30. Huang, J., Li, X., Chang, M., Li, S., & Liu, W. (2017,). Capacity Allocation of Battery Energy Storage System in Primary Frequency Regulation Considering Its Technical-Economic Model. *High Volt. Eng.*, 32, 112–121.

31. Kirchmayer, C. C. (1953, Jan). Tie line power and frequency control of electric power systems - Part I. *IEEE Trans. Power App. Syst., 72*, 562-572.

32. Kirchmayer, C. C. (1954., January). Tie line power and frequency control of electric power systems - Part II. *IEEE Trans. Power App. Syst., 73*, 133- 146,.

33. Kirchmayer, L. (1959.). *Economic Control of Interconnected Systems.* John Wiley & Sons.

34. Li, J., Guo, Z., Yang, H., Li, L., Sun, B., & Fan, X. (2021). Primary Frequency Regulation Control Strategy of Energy Storage Based on Dynamic Droop Coefficient and SOC Reference. *Power Syst. Prot. Control*, 49, 1–10.

35. Li, J., Tao, H., Mu, G., Yan, G., Li, C., & He, D. (2020,). Primary frequency regulation strategy with energy storage system based on weight factors and state of charge recovery. . *Autom. Electr. Power Syst.* , 44, 63–72.

36. Li, P., Fu, Y., Liu, X., Tan, Z., Yang, B., & Han, J. (2019,). Control Strategy for Energy Storage Battery Participating in Primary Frequency Regulation of Power Grid Considering Ultra-short-term Load Forecasting. Autom. *Electr. Power Syst.* , 43, 87–93.

37. Liu, J. (2022.). Hybrid Energy Storage for Frequency Modulation Cooperative Control of Power Grid. . *Master's Thesis, North China Electric Power University, Baoding, China,* .

38. Liu, Y., Chen, M., Xie, B., & Ban, M. (2024,). Integrated control strategy of BESS in primary frequency modulation considering SOC recovery. *IET Renew. Power Gener.*, 18, 875–886.

39. Liu, Y., Tian, S., Liang, H., Xie, Y., Huo, Q., & Tang, X. (2022,). Control Strategy of a Battery Energy Storage System Considering SOC in Primary Frequency Regulation of Power Grid. . *Power Syst. Prot. Control* , 50, 107–118.

40. Ma, Z., Li, X., Tang, Z., Huang, J., & Li, H. (2019,). Integrated Control of Primary Frequency Regulation Considering Dead Band of Energy Storage. . *Trans. China Electrotech. Soc.*, 34, 2102–2115.

41. Marinescu, I. S. (2014, September). Control strategy of three-phase battery energy storage systems for frequency support in microgrids and with uninterrupted supply of Local loads. *IEEE Trans. Power. Electr., 29*, 5010-5020.

42. Mufti, S. Z.-u.-d. (2017). Load frequency control in a two-area power system with supercapacitor energy storage system. *2017 International Conference on Intelligent Computing, Instrumentation and Control Technologies.*

43. Shirai, G. (1979, October). Load frequency control using Lyapunov's second method: Bang-bang control of speed changer position. *Proc. IEEE, 67*, 1458-1459.

44. Sluis, P. S. (2008). *Electrical Power System Essentials.* New York, NY,, USA: Wiley.

45. T. K. Nagsarkar, a. M. (2007). Power system analysis. *Oxford University Press,*.

46. Tarnowski, P. W. (2011.). Inertial for wind power plants-State of the art review-Year 2011. *Proc. 10th Int. Workshop Large-Scale Integration of Wind Power into Power Systems.* Aarhus, Denmark.

47. Teshome Hambissa, G. B. (2023, December 14). mitigating impact of photovoltaic penetration in Ethiopia–Kenya HVDC link in mitigating impact of photovoltaic penetration in Ethiopia–Kenya HVDC link. *International Journal of Electrical Power and Energy Systems*.

48. Umer Akram, R. S. (2019, November). Hybrid Energy Storage System for Frequency Regulation in Microgrids with Source and Load Uncertainties. *IET Generation, Transmission & Distribution, 13*, 5048–5057.

49. V. Knap et al. (2016., September). Sizing of an energy storage system for grid inertial response and primary frequency reserve. *IEEE Trans. Power Syst., , 31*, 3447-3456.

50. Wakihara, M. (2001, January). Recent developments in lithium-ion batteries. *Materials Science and Engineering*, 109-134.

51. Wang, Y., Yang, M., Xue, H., Zhang, Y., & Mi, Y. (2021,). Adaptive Integrated Control Strategy for Battery Energy Storage System Considering SOC in Primary Frequency Regulation. . *Electr. Power Autom. Equip.* , 41, 192–198, 219.

52. Willems, J. L. (1974, September). Sensitivity analysis of the optimum performance of conventional load frequency control. *IEEE Trans. Power App. Syst, PAS-93*, 1287- 1291.

53. Wollenberg, A. W. (1984). *Power Generation, Operation, and Control.* John Wiley & Sons.

54. Xavier, A. (2022, March). *https://www.quora.com/*.

55. Xinshou Tian, Y. C. (2024, JULY). Optimal frequency response coordinated control strategy for hybrid wind-storage power plant based on state reconstruction. *IET Renewable Power Generation, 18*, Pages 2892–2906.

56. Xu, Y., Li, H., Qin, J., Wang, K., & Han, J. (2023,). Frequency Control of Hybrid Energy Storage Assisted Thermal Power Units Based on SOC State. *Autom. Appl.* , 64, 78–83.

57. Y. Mi, X. H. (2019, July). Frequency control strategy of multi-area hybrid power system based on frequency division and sliding mode algorithm. *IET Generation, Transmission & Distribution, 13*, 1145–1152.

58. Yan, L., Shui, T., Xue, T., Wang, M., Ma, N., & Li, K. (2022, 15). Comprehensive Control Strategy Considering Hybrid Energy Storage for Primary Frequency Modulation. . *Energies* , 4079.

59. Zhou, D., Zou, Z., Dan, Y., Wang, C., Teng, C., & Zhu, Y. (2025,). An Integrated Strategy for Hybrid Energy Storage Systems to Stabilize the Frequency of the Power Grid Through Primary Frequency Regulation. . *Energies* , 18, 246.